Performance Analysis of PEM Fuel cell incorporating Enhanced Cross-flow Split Serpentine Flow Field Design- Computational Study

Submitted in partial fulfillment of the requirements for the award of the degree of

DOCTOR OF PHILOSOPHY

IN

CHEMICAL ENGINEERING

By

ABDULLA SHEIKH

(Roll No.714145)

Under the supervision of

Dr. Venkata Suresh Patnaikuni
Associate Professor

DEPARTMENT OF CHEMICAL ENGINEERING

NATIONAL INSTITUTE OF TECHNOLOGY WARANGAL

WARANGAL - 506004, TELANGANA INDIA.

OCTOBER 2020

DECLARATION

This is to certify that the work presented in the thesis entitled **"Performance Analysis of PEM Fuel Cell incorporating Enhanced Cross-Flow Split Serpentine Flow Field Design – Computational Study"** is a bonafide work done by me under the supervision of Dr. VenkataSuresh Patnaikuni and was not submitted elsewhere for award of any degree.

I declare that this written submission represents my ideas in my own words and where others' ideas or words have been included, I have adequately cited and referenced the original source. I also declare that I have adhered to all principles of academic honesty and integrity and have not misrepresented or fabricated or falsified any idea/data/fact/source in my submission. I understand that any violation of the above will be a cause for disciplinary action by the Institute and can also evoke penal action from the sources which have thus not been properly cited or from whom proper permission has not been taken when needed.

S. Abdulla.

ABDULLA SHEIKH

(Roll No.714145)

NATIONAL INSTITUTE OF TECHNOLOGY- WARANGAL
Warangal – 506004, Telangana, INDIA.

CERTIFICATE

This is to certify that the thesis entitled **"Performance Analysis of PEM Fuel Cell incorporating Enhanced Cross-Flow Split Serpentine Flow Field Design – Computational Study"** being submitted by **Mr. ABDULLA SHEIKH (Roll No.714145)** for the award of the degree of Doctor of Philosophy (Ph.D) in Chemical Engineering to the National Institute of Technology, Warangal, India is a record of the bonafide research work carried out by him under my supervision. The thesis has fulfilled the requirements according to the regulations of this Institute and in my opinion has reached the standards for submission. The results embodied in the thesis have not been submitted to any other University or Institute for the award of any degree or diploma.

Date: 05-10-2020

Dr. Venkata Suresh Patnaikuni
Associate Professor
Supervisor
Department of Chemical Engineering
National Institute of Technology
Warangal 506004, Telangana State
INDIA

Acknowledgements

I take this opportunity to express my sincere gratitude to my respected supervisor ***Dr. Venkata Suresh Patnaikuni***, Associate Professor, Department of Chemical Engineering, National Institute of Technology, Warangal, India for giving me an opportunity to pursue doctoral thesis work under his esteemed supervision. His outstanding guidance, constant support, patience, motivation and immense knowledge extremely helped me in all the time of research and writing of this thesis. I could not have imagined having a better advisor and mentor for my PhD study.

I am grateful to ***Prof. N.V. Ramana Rao***, Director, NIT Warangal for providing me institute fellowship for completing the Ph.D. I am thankful to ***Prof. Shirish H Sonawane***, Head of the Department, Chemical Engineering for providing necessary facilities in the department and for his valuable suggestions. I am also thankful to earlier HODs, ***Prof. A. Sarat Babu, Prof. K. Anand Kishore*** and ***Prof. A. Venu Vinod***.

I would like to express my sincere gratitude to all my Doctoral Scrutiny Committee members ***Dr. A. Seshagiri Rao, Dr. S. Murali Mohan*** Department of Chemical Engineering and ***Dr. G. Naga Srinivasulu,*** Department of Mechanical Engineering for their valuable time, patience, attention, insightful comments and helpful advices during the review presentations of this research work.

I would like to express heart-felt thanks to ***Dr. T. Sunil Kumar***, Associate Professor, Department of Chemical Engineering, Indian Institute of Technology Tirupati for his suggestions, support and encouragement.

I wish to express my profound thanks to the entire Faculty, Scholars, Non-teaching staff and all others in the Chemical Engineering Department and in the Institute who directly and indirectly helped me during the course of my research work at NIT Warangal

I wish to express sincere thanks to my beloved friends and lab mates ***D. Surywanshi Gajanan, Snigdha Saha*** and ***Shailesh Singh Shikarkar*** for their constant encouragement and help acquired during my research period at NITW.

I wish to express my gratitude to ***Dr. P. Dorca R J Chandrika*** for her sisterhood affection, constant support and encouragement throughout my research work.

My heartfelt gratitude to my friends ***Dr. Shaik Liyakhath Ahmed***, ***Dr. A. Divya Priya, P. Aruna, Dr. Pathan Ameer Khan and B. Basant Kumar Pillai*** for all the technical discussions we had that helped me in approaching newer insights of research, for being supportive in all situations, for all the joyful and memorable moments we had during my stay at NIT Warangal.

My sincere thanks to my fellow scholars ***Dr. Shabana Shaik, Semal Sekhar, Sheik Abdul Gaffar*** and ***Dr. D. Y. Sasidhar*** for their timely help and support in completion of my research work.

I would like to express my profound gratitude to my family members: my parents ***Mr. Ram Lal Sheikh*** and ***Mrs. Nurjahan Sheikh***, my sister ***Mrs. Sheikh Vahida begum*** and other members of my family for their support and continuous encouragement throughout my years of study and through process of researching and writing this thesis.

Also I take this opportunity to thank all my relatives, friends, ***Teachers***, well-wishers who are part of this journey directly and indirectly. Thank You.

Abdulla Sheikh

Abstract

Most generally used flow channel designs in a polymer electrolyte membrane fuel cells (PEMFCs) are serpentine flow designs as single channels or as multiple channels due to their advantages over parallel flow field designs. But these flow fields have inherent problems of high pressure drop, improper reactant distribution, and poor water management, especially near the U-bends. The problem of inadequate water evacuation & improper reactant distribution become more severe as these designs become worse at higher current loads (low voltages) and higher active areas. A novel flow field layout named as 'enhanced cross-flow split serpentine flow field (ECSSFF) having unique feature of induced cross-flow at preferential locations was proposed by Suresh et al. (2011) to address the above problems. Its advantages of less pressure drop and more cross-flow in the flooding prone regions leading to better reactant distribution were computationally demonstrated by considering only hydrodynamics without reactions on one half of the cell. A detailed full-scale performance study of the PEMFC with this potential ECSSFF using electrochemistry, multi-component and multi-phase phenomena are not available in the literature. A systematic analysis of effect of channel to rib width ratio of ECSSFF design on the cell performance and parametric study of different operating conditions was also not done. This forms the basis for the current study.

In the present work, a detailed performance analysis of ECSSFF design for both rectangular and square cross-sectional PEMFCs has been conducted using a three-dimensional (3-D) multiphase, steady state, computational fluid dynamic (CFD) model. The ECSSFF design is used on cathode side of the cell because of the sluggish oxygen reduction reaction kinetics and a parallel flow field is used on the anode side of the cell. Air and pure hydrogen are used as reactants on cathode and anode side respectively. The performance of PEMFC with 3-channel ECSSFF has been compared with the performance of single serpentine and parallel triple serpentine flow designs on cathode side by keeping all other parameters and anode side flow field design similar. The best ratio of channel width to rib width for the flow fields are also found. The performance is evaluated in terms of their polarization curves. A detailed parametric study is also carried out by varying different operating conditions, viz, reactant flow rates, cell operating temperature, pressure and

reactant humidities. The effectiveness of the ECSSFF design has also been evaluated for higher active areas.

It has been shown that the ratio of channel to rib widths of 2:1 gives the best results for rectangular shaped ECSSFF layout. The performance displayed by ECSSFF design is found to be on-par with that of single serpentine flow field design for the same flow rates with almost 30 times lesser pressure drop. ECSSFF has exhibited superior performance in terms of offering high currents and low pressure drops compared to both single serpentine flow field design and triple serpentine flow field design. The percentage increase in the net power output with ECSSFF design over triple serpentine flow field design increases from 4.5% to 13.5% with increase in cell area from 50 cm^2 to 200 cm^2. The percentage drop in net power density with increase in active area for ECSSFF design is almost 55% less compared to that with triple serpentine design.

Finally, the concept of ECSSFF channel layout is extended to a square cross-sectional PEM fuel cell to find its applicability. A detailed parametric study including the channel and rib width dimensions for square shaped ECSSFF channel design is carried out. This layout has also been evaluated for its efficacy at higher active areas up to 200 cm^2. The CW to RW ratio of 1:1 resulted in peak performance at cell operating pressure and temperatures of 200 kPa and 70 ^oC for fully humidified anode reactants and 50% humidified cathode reactants. The performance of the square PEMFC with 4-channel ECSSFF design on cathode side is found to be superior to that with five parallel serpentine design and the proposed design is also found to be effective for higher active areas.

This study establishes that the ECSSFF layout is more beneficial when a PEM fuel cell needs to be operated at higher current densities and a potential flow field design to be considered for higher active area cells/stacks for large scale power production.

Table of contents

List of Figures

List of Tables

Nomenclature

AFC	Alkaline Fuel Cell
APU	Auxiliary Power Unit
AR	Aspect Ratio
BCGSTAB	Bi-Conjugate Gradient Stabilize method
BP	Bipolar Plate
BV	Butler –Volmer equation
C_p	Specific heat capacity, J/ kg. K
C_r	Condensation rate constant, s^{-1}
CC	Current Collectors
CESFF	Convection-Enhanced Serpentine Flow Field
CFD	Computational Fluid Dynamics
CHP	Combined Heat and Power
CL	Catalyst Layer
CW	Channel Width, mm
D_i	Gas diffusion coefficient, m^2/s
D_i^o	mass diffusivity at reference pressure (P_o) and temperature (T_o)
D_i^{eff}	Effective gas diffusivity, m^2/s
D_l	Membrane Water Diffusivity
DMFC	Direct Methanol Fuel Cell
ECSSFF	Enhanced Cross-Flow Split Serpentine Flow Field
F	Faraday constant, C/kmol
GDL	Gas Diffusion Layer
GFC	Gas Flow Channel
HSI	Hybrid Serpentine-Interdigitated
IC	Internal Combustion engines
j^{ref}	reference exchange current density per active surface area, A/m^2
K	Ratios of heat capacities (=1.4)
K_{eff}	effective thermal conductivity, W/m.K
k_s & k_f	thermal conductivities of solid and fluid phases in porous media, W/m.K

LBM	Lattice-Boltzmann Method
$\dot{m}$	Mass flow rate, kg/ s
M_m	equivalent weight of the dry membrane
MCFC	Molten Carbonate Fuel Cell
MEA	Membrane Electrode Assembly
MPL	Micro Porous Layer
OCV	Open Circuit Voltage, V
ORR	Oxygen Reduction Reaction
P	Pressure, atm
P^{in} & P^{out}	Air Pressure to and from the compressor, atm
P_{wv}	water vapour pressure, atm
PAFC	Phosphoric Acid Fuel Cell
PEM	Polymer Electrode Membrane
PEMFC	Polymer Electrode Membrane Fuel Cell
PSFF	parallel Serpentine Flow Field
PTBP	Parallel Trapezoid Baffle Plate
q	Flow Rate, m^3/s
R	universal gas constant, J/mole.K
R_{elec} & R_{ionic}	Electronic and Ionic Resistance
R_{mem} & R_{sol}	Membrane and Solid phase volumetric transfer current
r_s	exponent of pore blockage
r_w	condensation rate
R_{an} & R_{cat}	exchange current densities at the anode and cathode
RH	Relative Humidity
RH_a	Anode side RH
RH_c	Cathode side RH
RW	Rib Width
S_a	Anode Stoichiometry
S_c	Cathode Stoichiometry
S_c	species volumetric source
s	Leverett function

SOFC	Solid Oxide Fuel Cell
SSFF	Single Serpentine Flow Field
STBP	Staggered Trapezoid Baffle Plate
T	Operating temperature, K
TPB	Triple Phase Boundary
TSFF	Triple Serpentine Flow Field
TUI	Text User Interface
UDF	User Defined Functions
WSFF	Waved Serpentine Flow Field
$\vec{u}$	velocity vector
κ	Permeability of porous media
η_a & η_c	cathode & anode the over potentials
α	water activity
y_{H2O}	Mole fraction of water
y_{H2}	Mole fraction of Hydrogen gas
y_{o2}	Mole fraction of Oxygen gas

Greek Symbols

μ	dynamic viscosity
η	compressor efficiency
ρ	density
ε	Porosity
ϕ	electric potential (volts)
σ	electrical conductivity (1/ohm-m)
ζ	specific active surface area
α	transfer coefficient,
γ	concentration dependence coefficient
σ_m	membrane conductivity
λ	water content

Chapter 1

Introduction

Introduction

World's population is estimated to rise by 2 billion in next 30 years, from present 7.7 billion to 9.7 billion by year 2050. It is projected that India will overtake China by 2027 making it most populated country in the world [1]. India's percentage in total primary energy demand globally is estimated to be almost doubled by 2040, due to its population growth and economic development. India's net CO_2 emissions are set to be doubled by year 2040 to 5 Gt, meaning its share of global emissions increases from 7% (2018) to 14% by 2040 [2]. Transport sector as a whole was accountable for 24% of overall CO_2 emissions worldwide in 2016, out of which road transport alone is responsible for 72% emission [3]. One of the best alternatives to reduce the CO_2 emissions from road transport is to use fuel cell powered vehicles. The most suitable type of fuel cell, which can be used to power the varying loads of vehicles is polymer electrolyte membrane (PEM) fuel cell. These cells can also be used for stationary power applications.

1.1 Fuel cell as a power generation system – Working principle

Fuel cells are electro-chemical devices which convert stored chemical energy of the fuel into electrical energy by redox reactions. In a typical PEM fuel cells, hydrogen gas as fuel is sent to anode side, which gets oxidized in the presence of a catalyst, releasing electrons and protons. These generated electrons flow through the external circuit doing the work and reach the cathode side. The generated protons will pass through electrolyte reaching the cathode side. The electrolyte will allow only the protons to pass through it. Oxygen is sent on cathode side, where it combines with electrons coming from external circuit and protons coming through electrolyte in presence of catalyst, forming water as final product. This is a exothermic reaction releasing some waste heat. The overall process of power generation from hydrogen gas using PEMFC is shown in Figure 1.1.

Following are the two half-cell reactions taking place in a typical hydrogen based PEM fuel cell.

Anode side reaction:

$$H_2 \rightarrow 2H^+ + 2e^- \qquad E_o = 0\ V$$

Cathode side reaction:

$$\frac{1}{2} O_2 + 2H^+ + 2e^- \rightarrow H_2O + \text{Heat} \qquad E_o = 1.229 \text{ V}$$

Overall Reaction:

$$H_2 + \frac{1}{2} O_2 \rightarrow H_2O + \text{Power} + \text{Heat} \qquad E_o = 1.229 \text{ V}$$

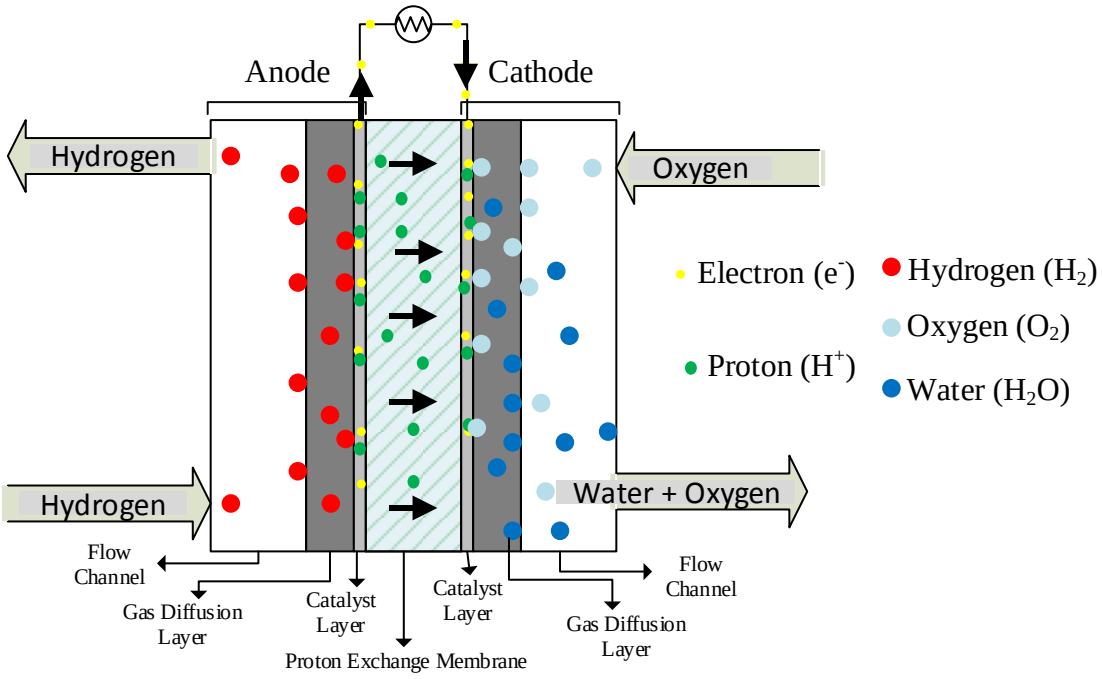

Figure 1.1 Schematic of the functioning of a typical PEM Fuel Cell.

1.2 History and Types of Fuel cells

The idea of a fuel cell had been effectively demonstrated by Humphry Davy in the early 19th century. This was followed by pioneering work on what were to become fuel cells by the scientist Christian Friedrich Schönbein in 1838. The invention of fuel cells are credited to William Grove, a chemist and physicist, who developed the fuel cell in 1839. Grove had conducted a series of experiments, showing the generation of electric current from an electro-chemical reaction between oxygen and hydrogen in presence of platinum catalyst, which he termed as "gas voltaic battery". Charles Langer and Ludwig Mond were the first to propose the term "fuel cell" in 1889, who used coal gas as a fuel for fuel cells [4].

Professor Francis Bacon altered Mond's and Langer's equipment in 1932, to develop first alkaline fuel cell (AFC). It took almost 27 years for the development of, first practical 5 kW fuel cell system by Bacon in 1959. In the same year, Harry Karl Ihrig fitted a modified Bacon cell of 15 kW to an Allis-Chalmers agricultural tractor. NASA partnered with industries in late 1950s and early 1960s for developing fuel cell generators for manned space missions. NASA's partnership with General Electric (GE) resulted in the invention of first Polymer Electrode Membrane Fuel Cell (PEMFC) unit by Willard Thomas Grubb. Another researcher from GE Leonard Niedrach, modified Grubb's PEM Fuel Cell by replacing catalyst with platinum, which is still the best catalyst for PEMFCs. The Grubb-Niedrach cell was further improved in collaboration with NASA, and was used for Gemini space program in 1960s. UTC Power developed an AFC of 1.5 kW capacity for Apollo space mission. This cell provided both electrical power as well as drinking water. UTC Power successively developed AFC of 12 kW to provide power to onboard systems on all space flights.

Commercialization of fuel cells for various applications began in 2007. In particular, direct methanol fuel cell (DMFC) and PEMFC were used as auxiliary power units (APU) in campervans and boats, similarly fuel cell units were also sold in portable sector such as educational kits and toys. These fuel cells were also used for providing power to communications and surveillance equipment for military purposes. The requirement of a reliable off-grid or on-grid stationary power in developing countries, reliable APU units for telecom networks during rescue operations further imputes the usage of fuel cells for stationary power generation. The need of reliable on-grid or off-grid stationary power in developing countries further boosted the fuel cell technology. In late 2000s, PEM fuel cell units powered by natural gas and hydrogen gas were sold in east Africa and India as backup or primary power units of telecom poles.

Fuel cells are also being deployed for transport applications, they are majorly being used in material handling segment in warehouses to arrange the goods. Buses powered by fuel cells were successfully demonstrated but, due to high cost and lack of hydrogen infrastructure made these buses to be available only in limited numbers. Many car manufacturing companies are also

venturing to invest in fuel cell powered cars in the future, which will hopefully reduce the cost of fuel cell powered vehicles [5].

Classification of Fuel Cells:

There are several types of fuel cells that have been developed. They are usually classified on the basis of the type of electrolyte used, as the electrolyte limits the functioning temperature and type of fuel that can be used. Different types of fuel cells are briefly discussed here and various features of these cells are presented in Table 1.1.

Polymer Electrolyte Membrane Fuel Cells (PEMFCs):

These are usually operated at low temperatures i.e., around 50 to 90 ^{o}C due to the limitation on the thermal stability of the polymer membrane electrolyte used in the cell. The PEMFC is highly susceptible to carbon monoxide poisoning which reduces the performance by several percent, if contaminated fuel is used. Because of waste heat generation, these fuel cell systems require cooling systems and also produced water is to be evacuated properly. Efficiencies of 60 percent may be attained with these cells, when used in transportation vehicles.

Alkaline fuel cells (AFCs):

These fuel cells have an aqueous solution of potassium hydroxide or sodium hydroxide as electrolyte. This cell also uses hydrogen gas as fuel with pure oxygen (or oxygen present in air) as oxidizer. AFC operates below 100 °C and are built from metal and plastics. Carbon and metals such as nickel are used for electrodes. The water produced must be removed by evaporation. The efficiencies of these cells vary from 30 to 80 percent, depending on the type of fuel and oxidizer used.

Phosphoric acid fuel cells (PAFCs):

The PAFCs use ortho-phosphoric acid as electrolyte, which allows them to operate up to 200 °C. Because of this high operating temperature, contaminated hydrogen fuel with oxygen cane

be used in PAFC. The electrodes comprise of catalyzed carbon and are organized in pairs, set back-to-back to create a series circuit. The mounting structure for this assembly of cells is made of graphite. These PAFCs were tested for local municipal power generation on a limited scale and also in remote-site power generation. Efficiencies of up to 40 percent may be attained with these cells.

Molten carbonate fuel cells (MCFCs):

The electrolyte of a MCFC is made up of molten carbonate salt suspended in a porous ceramic matrix. Carbonated salts like potassium, lithium and sodium are commonly used. These fuel cells operate at high temperatures around 650 ^{o}C. Because of these high temperatures, the reaction kinetics are high and usage of noble metal catalyst is not required to improve the performance. These fuel cells can also work with varies types of fuels such as methane or natural gas, including coal derived fuels gas, eliminating the pre-reformation of the fuel. Efficiencies of 50 percent may be attained, where fossil fuels are used.

Solid oxide fuel cells (SOFCs):

The Solid oxide fuel cells work at very high temperatures, around 800^{o}C - 1,000°C. The electrolyte of SOFCs is made up of solid ceramic, like zirconium oxide stabilized with yttrium oxide, instead of membrane or liquid. As this fuel cell operates at high temperature, pre-reforming of the fuel is not required. SOFC can also be used with various kinds of hydrocarbon fuels because of high operating temperatures. These fuel cells are also resistant to minor quantities of sulphur impurity in the fuel. SOFCs have an efficiencies of over 60% when used for only electricity generation and when they are used for CHP applications, the efficiency jumps to over 80%.

Table 1.1 Types of Fuel Cell [6].

Fuel Cell Type	PEMFC	AFC	PAFC	MCFC	SOFC
Common Electrolyte	Perfluoro sulfonic acid	Aqueous solution of potassium hydroxide soaked in a matrix	Phosphoric acid soaked in a matrix	Solution of Lithium, sodium, and/or potassium carbonates, soaked in matrix	Yttria stabilized zirconia
Operating Temperature	50 -100 ºC	90 - 100 ºC	150 – 200ºC	600 – 700ºC	600–1000ºC
Efficiency	Transportation – 60% Stationary Applications- 35%	60 %	40 %	50– 60 %	50- 60 %
Applications	• Backup power • Portable power • Distributed generation • Transportation • Specialty vehicles	• Military • Space	Distributed generation	• Electric utility • Distributed generation	• Auxiliary power • Electric utility • Distributed generation
Advantages	• Solid electrolyte reduces corrosion & electrolyte management problems • Low temperature • Quick start-up	• Cathode reaction is faster in alkaline electrolyte, leads to high performance • Low cost components	• High temperature enables CHP • Increased tolerance to fuel impurities	• High efficiency • Fuel flexibility • Can use a variety of catalysts • Suitable for CHP	• High efficiency • Fuel flexibility • Can use a variety of catalysts • Suitable for CHP & CHHP • Hybrid/GT cycle
Challenges	• Expensive catalyst • Sensitive to fuel impurities	• Sensitive to CO_2 in fuel and air • Electrolyte management	• Pt catalyst • Long startup times • Sensitivity	• High temperature corrosion and breakdown of cell component • Long startup time • Low power density	• High temperature corrosion and breakdown of cell component • High temperature operations requires long startup times and limit shutdowns

1.3 Operation and Components of PEM fuel cells

PEM fuel cells consist of several components which are made up of different materials. The main parts of a PEM fuel cell are, the membrane electrode assembly (MEA) which is the heart of PEM fuel cell and consists of membrane and catalyst layers, gas diffusion layers , bipolar plates, current collectors and end plates.

Polymer Electrolyte Membrane (PEM):

The polymer electrolyte membrane also called as proton exchange membrane, is usually poly[perfluorosulfonic] acid with polytetrafluorethylene (PTFE) back bone, which conducts only positively charged ions and blocks the electron`s. The PEM is the most important component of the fuel cell, that creates a potential difference between anode and cathode, which is the driving force for the electron to flow externally from anode to cathode.

Catalyst Layers (CLs):

Catalyst layers are added on both sides of the membrane—the anode layer on one side and the cathode layer on the other. These catalyst layers include high-surface-area carbon in which nanometer-sized particles of platinum are dispersed. This mixture of carbon supported platinum catalyst is mixed with an ionomer and sandwiched between the membrane and the GDLs. On the anode side, hydrogen molecules are split in to protons and electrons in presence of the platinum catalyst. On the cathode side, oxygen is reduced on the platinum surface by reacting with the protons and electrons, producing water. The ionomer mixed in the catalyst layers creates the pathways for the proton to travel through these layers and reach the catalyst sites.

Gas Diffusion Layers (GDLs):

The GDLs lying between the catalyst layers and the bipolar plates on both sides facilitate the transport of reactants into the catalyst layer, as well as removal of produced water from the CLs to the channels of the flow field. GDLs are made up of carbon paper or carbon cloth, in which the

carbon fibers are coated with polytetrafluoroethylene (PTFE). Gases diffuse rapidly through the pores of GDL. The water buildup in the GDL can reduce the quantity of reactants diffused to the catalyst layer. As the GDLs are made up of carbon materials, they have good electrical conductivity allowing the generated electrons to conduct through them.

Bipolar Plates (BPs):

Bipolar plates are generally made up of graphite material and they have good electrical conductivity for electrons and also provide good physical strength to the cell. They also act as flow field plates as flow channels designs are typically grooved on to their surface. These channel designs help in proper distribution of the reactants through the entire cell active area. Figure 1.2 shows the three basic types of flow channel designs - parallel, serpentine and interdigitated. Many more designs are developed based on the variations and / or combinations of these basic designs. Some of these are discussed in the Chapter 2. In stacks, some additional channels are also provided on these plates for the circulation of the coolant.

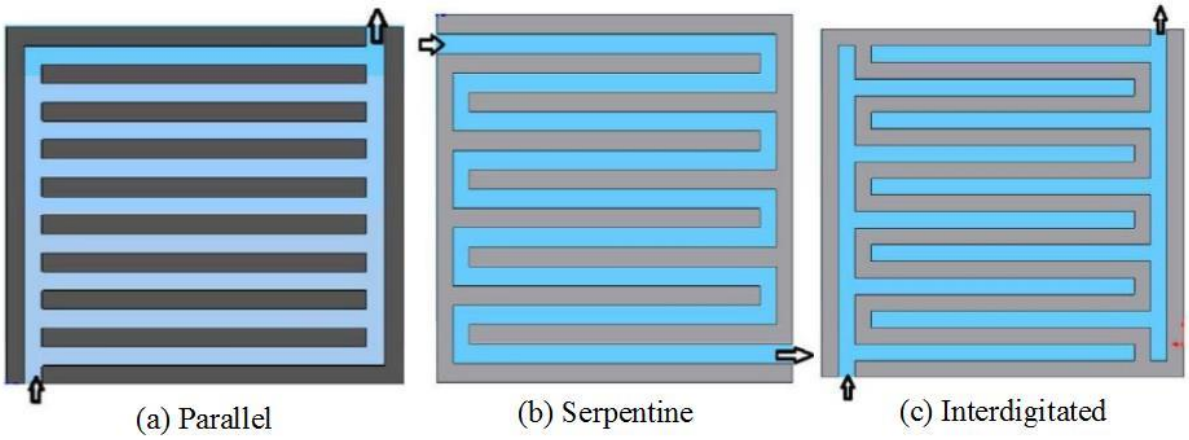

Figure 1.2 Basic types of flow channel designs [7].

Gaskets:

When MEAs in a fuel cell are sandwiched between two bipolar plates, gaskets are required to be added around the edges of the MEA to prevent leakage of the reactant gases. These gaskets are generally made of a rubbery polymer.

Current collectors (CCs):

Current collectors are mostly made up of copper because of its high electron conductivity. The electrons which are generated on anode side pass through catalyst layer, GDL and bipolar plates to reach the current collectors. On the other hand the electrons pass from the current collectors to catalyst layer via bipolar plates and GDL on cathode side. These current collectors on anode and cathode sides are connected externally to close the circuit and helps in the flow of the generated electrons from anode to cathode.

End Plates:

End plates which are kept at the back end of the anode and cathode sides help in keeping all the fuel cell components in place. These plates are mostly made up of aluminum, because of its good thermal conductivity. These plates help in the dissipation of the waste heat generated during the operation of the fuel cell to the surroundings.

1.4 Performance of PEM fuel cells (Polarization losses and IV curve)

The output voltage of a single fuel cell is dependent on working conditions such as applied load, temperature and reactant flow rates. The standard measure for performance of a fuel cell is the polarization curve, which shows the behavior of voltage against current density. Even though the theoretical potential of a single fuel cell is 1.229 V, the open circuit voltage (OCV) drops to a lower value during the actual operation of the fuel cell due to the thermodynamic limitations. The polarization curve shows the drop in output voltage with current density. Polarization curves are typically obtained with a galvanostat/potentiostat, which draws current and measures the output voltage of the cell. A representative polarization curve is shown in Figure 1.3.

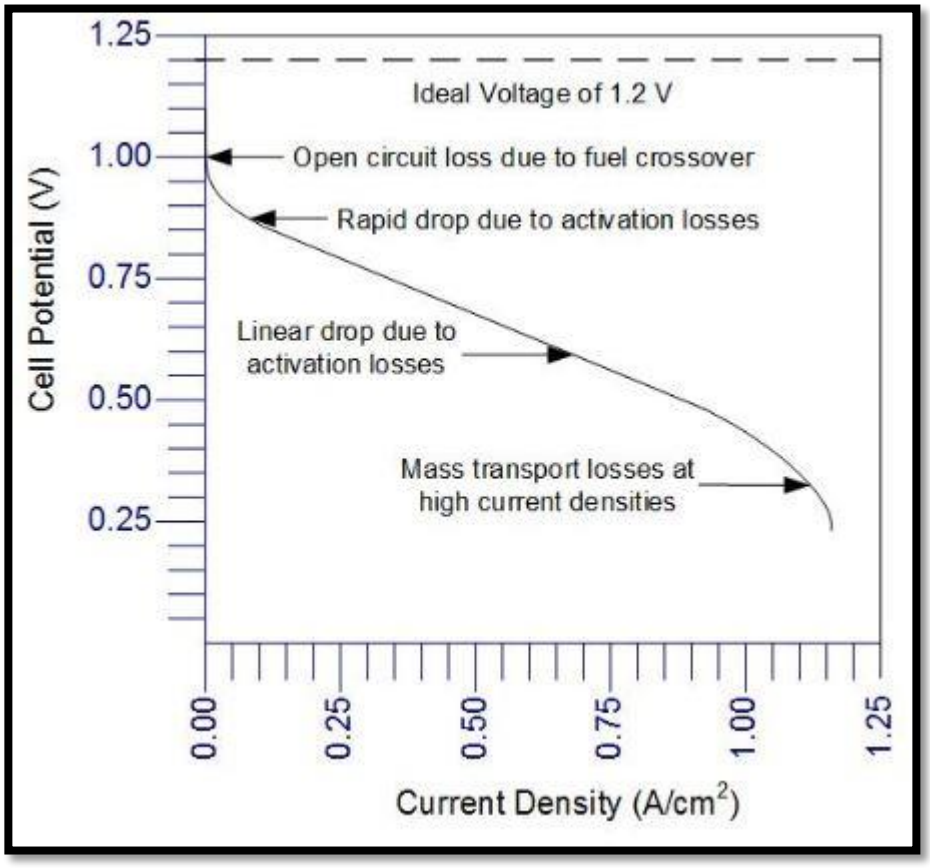

Figure 1.3 Polarization curve of a PEMFC [8].

In general, three distinct regions can be seen in the polarization curve of the fuel cell:

- In the lower current density region, the drop in cell potential is due to activation polarization.
- In the moderate current density range, the fuel cell potential drops linearly with output current due to ohmic losses.
- In the high current density or at low voltage region, the drop in potential is more drastic mainly due to concentration polarization.

Activation Polarization:

Activation polarization is the voltage over-potential required to overcome the activation barrier for the electro-chemical reaction to happen on the surface of catalyst. The reactions involve

complex 3-phase issue, as gaseous fuel, solid catalyst and electrolyte must make a contact. The voltage loss happens in both anode and cathode sides however, oxygen reduction requires much higher over-potential, because of sluggish electrode kinetics than hydrogen oxidation. The total activation over-potential reduces almost 0.1 to 0.2 V from the theoretical voltage making the OCV below 1 V. At low current densities activation polarization is predominant.

Ohmic Polarization:

Conductors have an intrinsic property to resist the flow of charged particles, which results in reduction of cell voltage. This phenomenon is called "ohmic polarization," and it constitutes of two resistances, one is electronic (R_{elec}) resistance and other is ionic (R_{ionic}) resistance. The electronic (R_{elec}) resistance occurs due to the resistance to the electron flow in the cell components. The cell components which contribute for the electrical resistance are catalyst layer, gas diffusion layer, bipolar plates, interface contacts and terminal connections. The ionic (R_{ionic}) resistance mainly occurs due to the resistance to the flow of protons through the membrane. This over-potential increases almost linearly with voltage and is more predominant in moderate voltage range. The ohmic losses are mostly dependent on the material properties.

Concentration Polarization:

In a fuel cell, reactants must be supplied continuously to produce electricity and the formed products should also be removed continuously to run the fuel cell at maximum efficiency. The concentration of the reactant and product on the catalyst surface determines the conversion of fuel to products. Concentration polarization occurs when the reactant concentration is not replenished at the catalyst surface as fast as the reactants are consumed, which happens due to mass transport limitation. This results in the drop in the output voltage. The mass transport in fuel cell electrodes is dominated by diffusion. To minimize the concentration loss, mass transport in fuel cell electrodes should be improved. One of the best way is to optimize the flow filed structure. The concentration losses are strongly dependent on the operating conditions of the cell. The drop in output voltage can also occur because of fuel cross-over and electric short-circuit if there are any punctures in the membrane and leaks in the assembly.

1.5 Technical challenges and targets

Many research groups and companies are working hard to develop better, more efficient and safe hydrogen based fuel cells so that they can become viable alternative to fossil fuels. However, Hydrogen fuel cells are facing the following challenges which are delaying their release on full scale into the energy market.

Quite Expensive:

Due to utilization of platinum catalyst and Nafion membrane (benchmark membrane as of today) in hydrogen fuel cells, the cost of the power production is still high compared to that from the fossil fuels. Even though in long run this high expense will be paid of, it is becoming difficult to scale up for commercialization due to this high upfront cost.

Not Very Robust:

Compared to coal, oil and gas, hydrogen fuel cells are not robust due to delicate electrolyte and intricate workings of the fuel cell. Fuel cells are more sensitive to environment, fuel contamination and temperature. Due to these limitations, fuel cells cannot be used in very hot or very cold conditions.

Safety:

The major application of hydrogen fuel cells is to replace internal combustion (IC) engines in cars. Real problem is the issue of safety with hydrogen gas. This gas is highly flammable and is harder to contain than oil. This means that cars fitted with a hydrogen fuel cells need to have extra layer of protection for hydrogen gas compared to conventional fuels. This safety issue is one of the major problem to have fuel cells powered cars as on today.

Fuel Flexibility:

Fuel cells must be developed to be capable of variations in fuel composition and operate without harmful impact to the environment or cell itself. The capability of using renewable and waste fuels is critical to capture market opportunities for fuel cells. The primary fuel used in a fuel cell is hydrogen, which is obtained from natural gas, gasoline, coal-gas and other fuels having hydrocarbons. Increase in the fuel flexibility of the fuel cells will make it possible to use them with the existing fuel infrastructure.

Innovative break-Through:

Fuel cell industries need to find break-through in key areas like, finding alternative catalyst for expensive platinum, finding better materials to reduce the intrinsic losses, increase the utilization of the fuel.

Targets:

Targets set by Department of Energy (DOE), USA specifically for integrated PEM fuel cell power systems operating on direct hydrogen for light duty transportation applications are listed in Table 1.2. DOE targets for hydrogen based PEM fuel cell backup power systems of range 1-10 kWe are listed in Table 1.3.

Table 1.2 DOE Targets for 80 kW_e integrated transportation PEM fuel cell power systems with hydrogen [9].

Characteristic	Units	2015 Status	2020 Targets	Ultimate Targets
Cost	$/$kW_{net}$	53	40	30
Durability in automotive drive cycle	hours	3900	5,000	8000
Start-up/shutdown durability	cycles	-	5,000	5000
Peak energy efficiency	%	60	65	70
Power density	W/L	640	650	850

Table 1.3 DOE Targets for 1–10 kW_e range hydrogen based fuel cell backup power systems [9].

Characteristic	Units	2015 Status	2020 Targets
Cost	$/kW	6100	1000
Durability	hours	8000	10000
Lifetime	years	10	10000
Energy efficiency	%	50	60
Ambient temperature range	^oC	-20 to 40	-50 to 50
Start-up time	Seconds	60	15

1.6 Motivation for the study

Although the PEM fuel cell technology has seen noteworthy progress over the last two decades, its commercialization with low cost and high performance is not yet seen. Major issues affecting the performance of the low temperature PEM fuel cells are improper water management and maldistribution of the reactants in the flow channels and on the catalyst layer. One of the most effective solutions to address these issues is found to be the suitable design of the flow field. To make the technology more cost-effective, it is essential to use flow designs which allow the fuel cells to operate at as high current/power densities as possible and effective for large active area cells. Hence, the present study is aimed to identify a suitable flow field design to address the above issues and conduct a systematic full scale three dimensional computational simulations to establish the advantages and efficacy of the selected flow field design for different operating conditions and higher active areas. The detailed study can be used as basis for the design of fuel cell as well as scale up of the cell for large scale power production.

1.7 Organization of thesis

The overall thesis is organized as follows.

Chapter 1 explains the theory, types, working principle and major losses in a fuel cells. It also includes the challenges in the present field.

Chapter 2 presents the extensive literature review based on the works available on the important modeling and experimental aspects on PEM fuel cells. It presents status of the research in the field of flow field designs development and the experimentation. This chapter concludes by highlighting some gaps in the literature and formulating the objectives and scope of the study, which have guided the definition and conduct of the present research work.

The problem formulation and detailed modeling methodology are presented in the Chapter 3. The governing equations solved, boundary conditions applied and the simulation strategy used along with the model validations are detailed in this chapter.

The results obtained from the present work are detailed and discussed in Chapters 4, 5, 6 and 7. Chapter 4 presents the performance comparison of the rectangular cross-sectional PEM fuel cell with ECSSFF design against that with triple serpentine flow field. A detailed parametric study on the rectangular shaped ECSSFF is also presented. Chapter 5 discusses fuel cell performance simulation results obtained with single serpentine flow field in comparison with ECSSFF. A parametric study and best ratio of channel to rib widths of the flow field design of the fuel cells is also presented in this chapter. The performance evaluation of ECSSFF design for higher active area cells is discussed in Chapter 6 with detailed discussion of the results. The extension of concept of ECSSFF to square shaped PEM fuel cells is carried out and the cell performance predicted with the proposed ECSSFF design for square cross-sectional cells is detailed in chapter 7.

Finally, Chapter 8 presents the overall conclusions drawn from the present study along with scope for future work. At the end, the research publications based on the thesis are listed.

Chapter 2

Literature Review

Literature Review

Polymer electrolyte membrane fuel cell technology is a potential alternative for energy needs of automobiles and portable electronic appliances because of its lower operating temperature range between 50 ^{o}C to 90 ^{o}C, quick start-up and ability to work well under varying load conditions. These are also eco-friendly as the by-products are only water and heat along with electricity, if hydrogen gas is used in pure form as the fuel. It has the potential to satisfy the ever-increasing demand especially in automotive sectors [10]. Because of these reasons, large research interest is going on to boost the efficiency of the PEM fuel cell systems. Among all the parts in a PEM fuel cell, bipolar plate is a crucial component because of its multi-functional capability -such as delivering oxidant and fuel to the reactive sites, removal of products like unreacted reactants and water, transferring generated current, and providing mechanical support to the cells. Moreover, the BP contributes up to 88% in the total weight of the PEMFC. Therefore, designing the BP with optimum dimensions not only improves performance greatly but also reduces cost and weight [11]. The main objective of optimizing the BP design is to improve reactant distribution and reduce flow channel pressure drop [12]. This chapter presents a systematic review of the important works on different types of flow field layouts and variants in serpentine design available in the literature. Studies on the optimization of the channel dimensions, effect of operating conditions on the cell performance and the studies on higher active area cells are also reviewed in this chapter.

2.1 Studies on flow field designs

In general, there are four desirable properties of the gas flow channel (GFC) [13]. It has to (i) distribute reactants uniformly to the catalyst sites to minimize hot spots, (ii) remove excess water to prevent flooding and also to keep the membrane hydrated, (iii) provide a large contact area between the GDL and BP for transport of produced electrons and (iv) offer less pressure drop to reduce parasitic losses. The land area between channels is used for the transmission of generated electrons to the current collector. It also conducts the heat produced in the catalyst layer (CL) due to the electrochemical reactions to the end plates, where it is dissipated to the surroundings. Higher channel width helps in improving water removal and delivery of reactants, it also results in less pressure drop thereby reducing the parasitic losses [14]. On the other hand, broad land area results

in better electrical and thermal conduction and also increases mechanical stability [15]. There are quite a few numerical studies on the optimization of channel width-to-land width ratio.

Modelling has been widely used in addition to experimental approach in exploring different designs and understanding the effect of various parameters on the performance of the fuel cells. Among various modelling approaches and tools existing, computational fluid dynamics (CFD) is especially interesting, because of its powerful capability to optimize and evaluate fuel cell performance [16]. Numerical modelling is a cost-effective and efficient way to optimize the design and operating parameters of a PEMFC, as it reduces significantly the time and cost which are associated with trial-and-error approach of experiments [17]. Designing a bipolar plate having innovative and variant layouts with optimized channel dimensions experimentally is tedious as it requires plenty of time and resources, whereas computational methodology is an effective approach to optimize the flow channel design to acceptable accuracy [18]. The cathode half reaction is the limiting reaction in a PEMFC, so better distribution of the oxygen will aid the conversion. Cathode flow channel helps in evacuating the water produced besides supplying air to the reaction sites. Hence, proper design of the cathode flow channel is important to maintain proper water management by keeping the membrane sufficiently hydrated and removing the excess water. It should also offer less pressure drop, which effects the compressor power consumption and thereby effecting the overall efficiency of the fuel cell system [19]. Uneven water management and high pressure drop along the channel will lead to poor performance of PEMFC [20]. The non-uniform distribution of reactants will result in non-uniform production of water and current [21]. These non-uniformities in the distribution of current density create local hot-spots, which effect the durability and longevity of the membrane in the PEMFC. Flooding of the cell and membrane dehydration both have a great impact on the lifespan of PEMFCs [22]. Kerkoub et al. [23] analysed the influence of channel design and flow field dimensions on fuel cell performance. Serpentine, interdigitated and parallel designs were considered in their study. Ghanbarian et al. [24] experimented on various parameters viz., rib width between two neighbouring channels, height and width of the channel, numbers of serpentine turns and parallel channels to examine the transport characteristics in PEMFC. Wang et al. [25] numerically and experimentally studied the impact of varying channel cross-section area and rib to channel width ratio of parallel-serpentine flow design on PEMFC

performance. They concluded that, the channel dimensions have a profound effect on the water removal and cell performance. El- Carcadea et al. [17] developed a comprehensive multiphase, 3- D and non-isothermal model to examine the outcome of parallel flow design on the power output of a PEM fuel cell. Improvement in the fuel cell performance was noticed with decrease in the size of the channel. This is due to increase in reactant velocity with smaller channel widths, which aided in the oxygen availability at the catalyst layer and liquid water removal. Chowdhury et al. [26] concluded that, current density generated from a PEM fuel cell was influenced by both channel width and rib width. Zeng et al. [27] developed a non-isothermal 3-D model along with a genetic algorithm to optimize the flow channel configuration. Cooper et al. [28] experimented on interdigitated flow design by varying channel aspect ratio (AR). Their findings indicated that net power density improved with decreasing AR when pump losses were considered.

Manso et al. [29] studied the influence of channels design on power output of PEMFC and concluded that homogeneous distribution of reactant gases in the flow fields provide uniform current density distribution across the cell active area. Uniform distribution of temperature in PEMFC reduces the mechanical stresses on the membrane electrode assembly (MEA) and increases life-time of PEMFC. Ferng et al. [30] examined different flow filed designs to study their impact on the PEMFC performance. They concluded that the modified parallel channel having step-wise depth significantly improved the PEMFC performance. Henriques et al. [31] experimentally and numerically investigated the fuel cell performance with a parallel transversal channel layout. The utilization of this channel layout has improved the efficiency by 26.4%. Khazaee and Ghazikhani [32] experimented on a triangular channel design at different reactant and operating temperatures. Their results showed that the performance was improved by 20 % with the increase in reactant gases temperature from 40 to 65 ^{o}C and the improvement in performance was 18 % with increase in cell temperature from 45 to 65 ^{o}C. Wan et al. [33] designed an M-like channel for cathode bipolar plate in a PEM fuel cell and compared its performance with wave-like channel computationally. The results showed that the maximum power density of the cell with M-like channel was 21.3 % higher compared to that of cell with wave-like channel. Kuo et al. [34] computationally studied the effect of wave- like surface on the gas flow characteristics, the electrochemical reaction efficiency, the temperature distribution and the electrical performance of

the PEM fuel cells. They found that this channel design provided an improved convective heat transfer performance, a more uniform temperature distribution and a higher gas flow velocity compared to those in a straight flow channel.

Roshandel et al. [35] proposed a flow layout inspired by biological pattern and matched its performance with conventional serpentine design. The pressure distribution and reactant concentration were found to be more homogeneous in this flow field, compared to conventional serpentine design. Badduri et al. [36] investigated the fuel cell performance with triple serpentine, lung and leaf flow channel designs numerically and experimentally. Their study showed that, the leaf channel design performed better than the other channel layouts. Monsaf et al. [37] studied the geometrical factors to analyze their effect on the performance of a PEMFC with spiral flow filed. From the analysis, they reached to a conclusion that, reactant distribution was better in wider channels. The obtained results showed that the performance of PEMFC was enhanced due to induced centrifugal motion of the reactants in a spiral design. Atyabi and Afshari [38] designed a cathode channel layout similar to honey comb and named the new design as honeycomb flow filed. The numerical results showed that this flow field displayed uniform local current density and less pressure drop across the channel. Zhang et al. [39] designed a constructal tee-shaped mini-channel network pattern, which contains two branches having channels with shrinking cross-sectional area at a fixed rate, and observed lower pressure drop and power consumption of the pump compared to those with serpentine pattern. Dong-Hui et al. [40] suggested a new flow design named as novel intersectant flow field using bionics, fractal theory, and Murray's law to reduce the drag force for product and reaction medium. They showed improved performance with their design against single serpentine design. Damian-Ascencio et al. [41] computationally developed four different tree-like channel design configurations based on the veins of the leaves of various trees for PEM fuel cell. Their results showed that the configuration having two levels of bifurcation at an angle of 37^{o} was more efficient at removing water and resulted in improved current density. It was also observed that with the increase in the number of bifurcations, the PEM fuel cell performance improved. Kang et al. [42] conducted a study to investigate the performance of PEM fuel cell of $25\ cm^2$ active area using the bipolar plate having a flow field design that mimics the leaf veins. They also studied the fuel cell performance with serpentine, parallel, and net leaf flow fields mimicking ginkgo and

dicotyledonous leaves. The results showed that the maximum power density was 7% lower with ginkgo design when compared to serpentine design, but they showed almost 40% higher performance than that with parallel design.

Dosoky et al. [43] proposed a corrugated gas channel design to improve the removal of condensate water droplets that are formed on the channel walls. They modelled different types of corrugated designs such as semicircle, rectangular dent, and saw-tooth corrugation for the removal of sessile droplets from channel walls. They showed that the condensate removal time was much smaller in a corrugated channel when compared to an un-corrugated channel. This type of flow design was shown to be more advantageous at low inlet velocities. Zehtabiyan et al. [44] studied the influence of cross-section area by using divergent and convergent channels in parallel channel design. Their findings showed that two adjacent divergent channel were fed by a single convergent channel due to the pressure difference. This effect increases the utilization of the catalyst under the rib portion, thereby improving the overall power output. Xing et al. [45] presented a novel single channel design on cathode side featuring multi- inlets and outlets along the channel to mitigate the effect of flooding and enhance the cell power output. Wang et al. [46] designed a cathode flow channel with three sub-channel inlets in parallel flow field and experimentally analyzed the new channel layout in PEM fuel cell. The proposed design effectively eliminated water from the fuel cell and increased the maximum power density by 13.2% compared to the conventional parallel design. Fan et al. [47] designed two innovative cathode channel designs with multi-plates structure channel & integrated structure channel and investigated them using numerical model. The results showed that cell with 30° angle, 0.5 mm width and 6.0 mm distance of air-guide plates displayed the best performance. Compared with the conventional channel design, the novel designs were found to be more capable of forcing oxygen towards CL which improved the electrochemical reaction rate. In addition, they also displayed higher liquid water removal capability from the cell, thereby effectively avoiding the water flooding. The simulation results showed that, the maximum improvement of PEM fuel cell net power densities for the multi-plates structure and integrated structure were 4.7% and 7.5%, respectively. Dehsara and Kermani [48] investigated a 3-D configuration of flat, semi-circular and wavy shaped channel beds. They showed an improvement up to 18–22% in fuel cell performance due to increase in the reactant gas penetration in to the catalyst layer. Wang et al. [49] studied a 3-D multiphase fuel cell model with Forchheimer's inertial

effect in the porous electrode to better simulate the convective flow induced due to baffle plates. They analysed conventional parallel flow field, staggered trapezoid baffle plate and parallel trapezoid baffle plate in this study. The staggered trapezoid baffle plate and parallel trapezoid baffle plate designs resulted in the peak net power enhancements of 6.39% and 2.54%, respectively compared to the parallel flow design.

Heidary et al. [50] studied the effect of staggered and in-line blockage configurations within a parallel flow field and compared the results with the parallel design. Their results indicated that, with staggered blockage the cell performance was improved by 28% over the baseline case, and about 18% when compared with in-line blockage. Perng and Wu [51] numerically investigated the effect of baffles of trapezoid shape placed in single channel on PEMFC performance. Their study showed an improvement of 90% in net power with 60° angle and 1.125 mm height baffles. Heidary et al. [52] analysed numerically the performance of a PEM fuel cell with four corrugated channel beds configuration which include trapezoidal, rectangular, triangular and wavy (sinusoidal) shape for PEMFC and direct methanol fuel cell. They analysed the effects of Reynolds number, shape boundaries, triangle block number and amplitude on the fuel cell performance. Thitakamol et al. [53] developed a mid-baffle interdigitated flow field, which is a variation of interdigitated flow field for PEM fuel cells. Their experimental results indicated that the modified interdigitated flow field produces about 1.2 to 1.3 time's higher power than the conventional flow field. However, its high flow resistance due to baffles resulted in large parasitic losses. Figure 2.1 shows some of the different flow field designs studied by various groups in the literature.

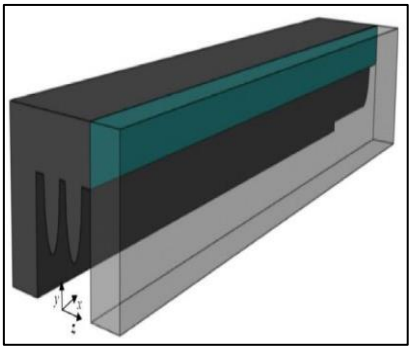

(a) M like Channel [33]

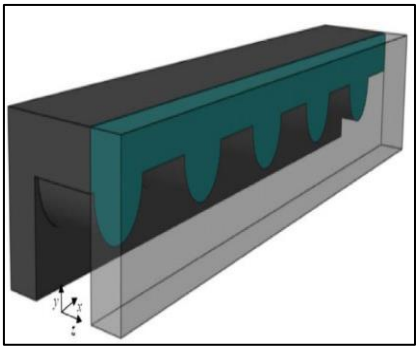

(b) Wave like Channel [34]

(c) Leaf Channel [36]

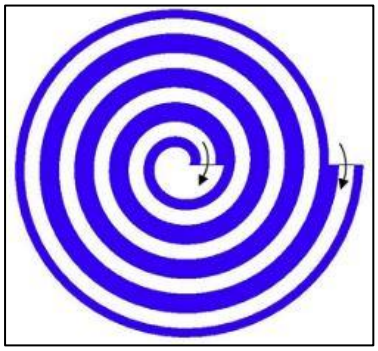

(d) Spiral Channel [37]

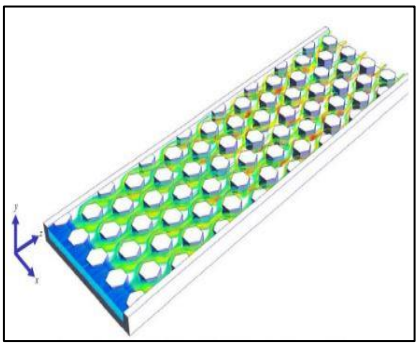

(e) Honey Comb Channel [38]

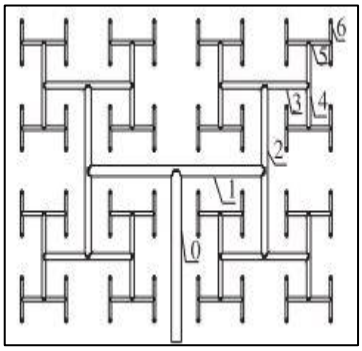

(f) Contractual Tree-Shaped Channel [39]

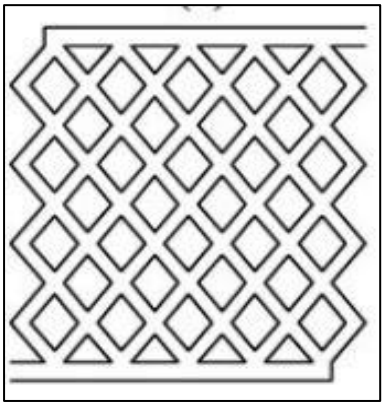

(g) Novel Intersection Channel [40]

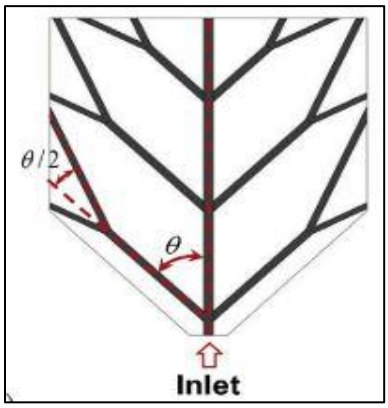

(h) Tree like Channel [41]

(i) Staggered Trapezoidal Baffle Channel [49]

Figure 2.1 Different Flow Field Designs available in the literature.

2.2 Studies on variants in Serpentine flow field designs

The serpentine flow channel design was introduced to improve the non-uniform distribution of reactants and water management in PEMFCs. Reactant gas is forced to flow through a single or multiple channel paths that are skewed to the edge of the entire active area. A serpentine flow field has a higher pressure drop than parallel channels due to the friction of the wall and the turning channel, and the increased pressure drop enhances the purging of accumulated water from the channel. This enhances the uniform distribution of the reactant over the entire active area, leading to uniform distributions of current density and water [54]. Consequently, PEMFCs have longer life spans due to decreased mechanical stress on the MEA [55]. Taccani and Nicola [56] examined parallel and serpentine channel designs. Their findings showed that serpentine design offered

higher presser drop than parallel but it showed better power density. Liu et al. [57] experimented on different flow field configurations such as serpentine, interdigitated, parallel and pin-type. They concluded that out of all these flow channel designs, serpentine flow design is the best for PEMFC. Wang et al. [58] analysed the impact of design parameters such as number of channels, number of bends and channel width of a serpentine channel design on the fuel cell performance. Khazaee and Sabadbafan [59] developed a 2-phase 3-D model of PEMFC with 1-serpentine and 4-serpentine channels to analyze the effect of direction of flow and humidity of reactant gases for water management. Their results showed improvement in performance with increasing relative humidity at low voltages for 4-serpentine channel design and for all voltages in case of 1-serpentine. When both the fuel cells were operated at ideal conditions 4-serpentine channel showed better performance than 1-serpentine.

Rostami et al. [20] numerically investigated the effect of U bend size in a serpentine channel on the fuel cell performance. They considered the bend sizes of width 0.8 mm, 1 mm and 1.2 mm. Their results showed that the power density of the fuel cell increased by 1.78% with 1.2 mm bend compared to the cell having channels with 0.8 mm bend size. Kang et al. [60] suggested a novel way to supply air in a triple serpentine channel design. They examined the fuel cell with dual air supply and compared with the cell with single air supply. The maximum power of the fuel cell with dual air supply was found to be increased by 8% compared to that of fuel cell with conventional single air supply. Alizadeh et al. [61] proposed a cascade type serpentine flow field for PEMFC and numerically investigated the cell performance at various channel widths & depths and rib widths. They concluded that the cascade type serpentine flow field displayed uniform local stoichiometry and current density as well as an improved water management at optimized channel dimensions of 1.2, 0.8 and 0.8 mm of channel width, rib width and depth respectively.

Baz et al. [62] modified single serpentine flow field design into 5 different configurations by varying the location of inlet and outlet, to increase the power output of the fuel cell. Their numerical studies showed that convection-enhanced serpentine flow field (CESFF)-4- 3 showed an improvement of 22.6 % in power density compared to conventional single serpentine design. Han et al. [63] compared the performance of a 300cm^2 active area PEMFC with serpentine, parallel

and branch designs in a CFD environment. Their analysis showed that, parallel design performance is greatly affected, when the active area is increased due to flooding. Fuel cells with serpentine and branch design performed almost similar but the pressure drop of branch layout is less, giving this design advantage over serpentine, when net power output is considered. Li et al. [64] designed a novel cathode channel named Waved Serpentine Flow Field (WSFF) to improve the water management compared to conventional parallel serpentine flow field. The modelling studies revealed that WSFF design is better in removing liquid water and promoting oxygen transport though the diffusion layer than the conventional serpentine channel. Experimental studies have shown an improvement of 17.8% in peak power density with WSFF compared to conventional serpentine design.

Vazifeshenas et al. [16] proposed a compound channel layout by combining the parallel and serpentine layouts and studied the performance in a PEMFC numerically. The study demonstrated superior water evacuation capabilities of the compound design. The power output of the PEMFC with compound layout was higher compared to parallel layout but not much difference was observed when compared with cell having serpentine design. Limjeerajarus et al. [65] conducted a numerical investigation on hybrid serpentine-interdigitated (HSI) design and compared the performance with the single serpentine design. The cell with HSI design showed higher performance compared to the cell having single serpentine at 0.6 V. Number of inlets and outlets for HSI were also analyzed and concluded that, 2 inlet and 2 outlet HSI had shown the best performance with less pressure drop and uniform reactant distribution. Esbo et al. [66] investigated various modified parallel serpentine designs to reduce the chances of flooding in the terminal region of the channel. Their studies showed that, 2-1serpentine design has improved local stoichiometry at the terminal region. This effect reduced the possibility of flooding and slug flow in flow channels. This design outperformed other channel designs at low operating voltages.

A variation of serpentine design named as Enhanced Cross-flow Split Serpentine Flow Field (ECSSFF) was proposed by Suresh et al. [67,68] This field design was developed based on the splitting of the channel with enhanced cross-flow in selected regions that are more prone to localized flooding. The layout was designed in such a way that all the U-bends of the split

serpentine channels were taken care by the nearest feeder channels. Its principal hydrodynamic features were demonstrated using CFD analysis in their study. It showed lower pressure drop, enhanced cross-flow along with better reactant distribution. However, the full scale fuel cell performance simulation study with the ECSSFF design was not performed. Saco et al. [69] numerically analyzed the performance of 225 cm^2 active area PEMFC with the straight parallel, serpentine parallel, straight zig-zag, and serpentine zig-zag paths. The study revealed that, straight zig- zag design had better reactant consumption with uniform distribution of water on the electrolyte improving the proton conductivity. This design also offered less pressure drop compared to other designs used in their study. Chowdhury and Timurkutluk [70] modified the conventional single serpentine flow field into convergent and divergent design and investigated numerically. The modified convergent serpentine design was found to be superior compared to the divergent serpentine and conventional serpentine due to its ability to offer uniformity in current density, pressure distribution & oxygen transport and also showed reduced water concentration in the CL. Their study indicated an increase of 2% better oxygen mass fraction and 3.3% reduction of water content at CL for the modified convergent serpentine flow field compared to conventional single serpentine.

Belchor et al. [71] compared the performance of fuel cell having parallel-serpentine with and without baffle channels experimentally. They concluded that the better performance was exhibited by the fuel cell having parallel-serpentine with baffle because of higher water retention, when the cell is operated at low RH conditions. Karthikeyan et al. [72] experimented on the effect of Zig-zag positioned porous carbon inserts in a serpentine flow channel on cathode flow plate. The results showed an improvement of 11.5% and 7% in power density and current density respectively with the zigzag positioned porous (80 - 90% porosity) inserts in the flow channel when compared to the conventional serpentine flow channel. Ebrahimzadeh et al. [73] studied the effect of different obstacle sizes (with 0.5, 1, 1.5 and 2 mm heights & 0.9, 1.8, 2.7 and 3.6 mm widths) and shapes (including square, triangular, trapezoidal and cylindrical) in a serpentine channel design. Their simulation results showed that the width of 3.6 mm and the height of 1.5 mm had the highest impact on the fuel cell performance in terms of species consumption, current density and pressure drop. Out of the four obstacle shapes, triangular and square obstacles were found to

perform better in improving the cell performance. The experimental results showed that the current density was increased with triangular obstacle by more than 50% compared to unobstructed channel. Figure 2.2 shows some of the variants proposed in serpentine flow field in the literature.

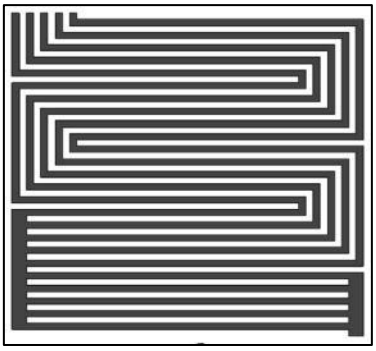

(a) Compound Channel [16]

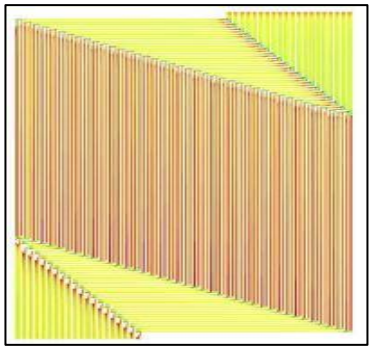

(b) Branch type Channel [63]

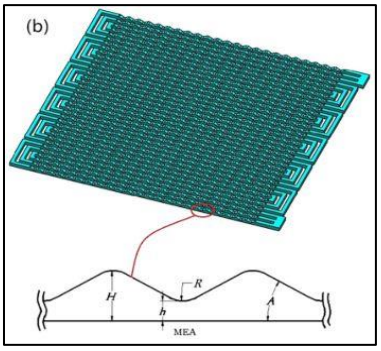

(c) Waved Serpentine Channel [64]

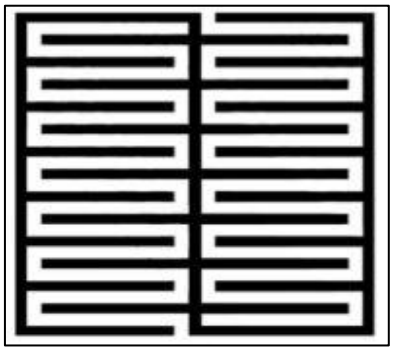

(d) Hybrid Serpentine-Interdigitated Channel [65]

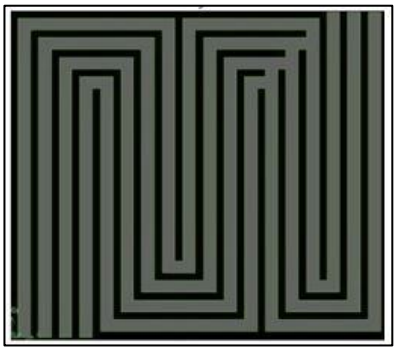

(e) 4-3 Serpentine Channel [66]

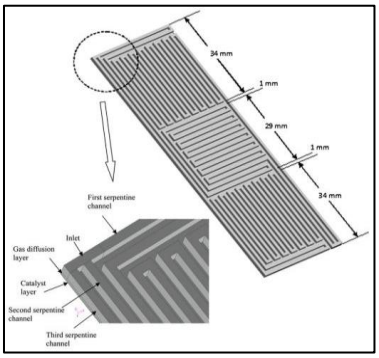

(f) Enhanced Cross-flow Split Serpentine Channel [68]

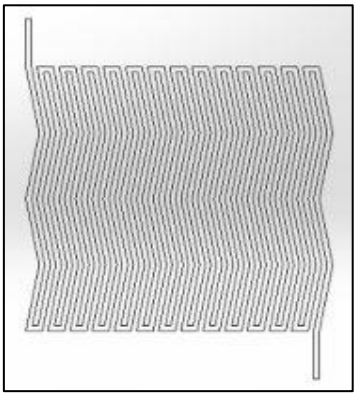

(g) Serpentine zig-zag Channel [69]

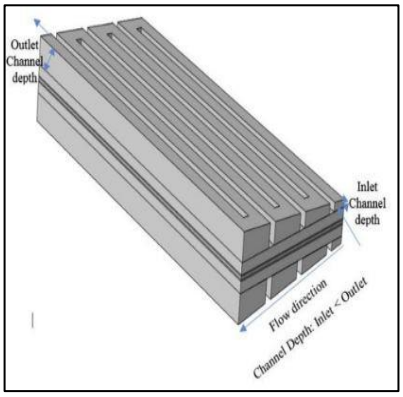

(h) Serpentine Divergent Channel [70]

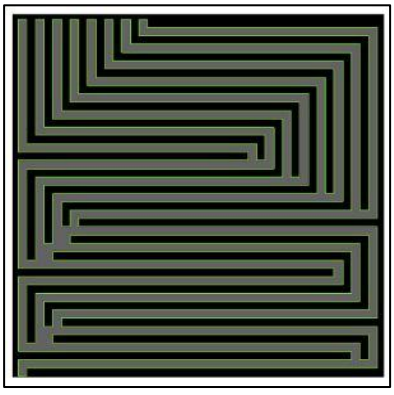

(i) Cascade type Serpentine Channel [61]

Figure 2.2 Variants in Serpentine design from literature.

As can be seen above, most of these works try to mitigate the inherent problems of serpentine channel designs such as high pressure drop, improper reactant distribution and poor water management. Out of the several studies on different channel designs available, a particular design proposed by Suresh et al. [68] named as Enhanced Cross-flow Split Serpentine Flow Field is appealing because of its quadruple advantages over serpentine channels. The special arrangement of the single serpentine channels in the ECSSFF design has resulted in uniform reactant distribution over the entire cell active area; low overall pressure drop, thereby reducing the parasitic power losses; effective liquid water evacuation in the U-bends; and more oxygen replenishment in the oxygen-deficient portions. This design is more promising than other designs like bio-inspired design and other variations in serpentine designs because of its simplicity & can mitigate most of the draw backs of serpentine design. Hence, ECSSFF has been chosen as the flow field design on the cathode side in this study.

2.3 Features of ECSSFF design

The ECSSFF design shares the advantages of the serpentine design and mitigates its disadvantages. Following are some of its important features [74]:

(i) Different serpentine channels in different layouts with a common inlet and outlet are arranged on the flow field plate, instead of a single channel running throughout the plate. This arrangement offers lower pressure drop because of the lower flow rate through each flow path.

(ii) These split serpentines are arranged in such a way that the pressure drop in each serpentine channel is almost same as in the others. This results in almost uniform flow split among the channels.

(iii) The channels are placed in such a manner that most of the U-bends in the serpentines get fed from the adjacent feeder channel via cross-flow through the porous diffusion layer. This reduces the possibility of localized flooding.

(iv) The feeder channels are planned in such a way that higher cross-flow occurs in the tail-end channels, which generally suffer from the lower reactant concentrations. This selective replenishment of the reactant to the more oxygen-depleted areas will improve the cell overall performance.

Figure 2.2(f) shows the arrangement of the three split serpentine channels arranged in ECSSFF fashion on a rectangular bipolar plate. It can be seen that all the U-bends could derive the benefit of induced cross-flow through the GDL/CL underneath the rib.

2.4 Studies on effect of operating parameters on the cell performance

This section reviews important studies available in the literature on the effect of various operating parameters such as RH and stoichiometry of the reactant gases, temperature and pressure on the performance of the fuel cell. HSing and Futerko [75] worked on a 2-D model by considering mass transport, fluid flow and electrochemistry in PEMFC. The model also considered the alterations in membrane water diffusion coefficient. Kim [76] studied the effect of percentage relative humidity (%RH) of the reactants and stoichiometry on the PEM fuel cell performance using a 2-D model taking the effect of formed liquid water on reactant transport into consideration. His results indicated that at a fixed anode RH of 100%, lower cathode RH was sufficient enough for better cell performance. Further, he reported that a low anode side RH not only provides more hydrogen but also increases water back diffusion from the cathode side reducing the possible flooding chances. Xing et al. [77] designed a 2-D model to explore the impact of RH, channel length and flow ratio on the power output of PEMFC. Peclet number was used, for evaluating the contribution of diffusion and advection on liquid water & heat transfer. They concluded that higher RH on anode side is required for improved fuel cell performance. Zhang et al. [78] investigated the effects of cathode RH on the fuel cell at various loads. They also simulated the fuel cell start-up process and concluded that an increase in the cathode inlet humidification improved the start-up performance and reduced the time required to reach steady state of a PEM fuel cell.

In general, studies have shown that the PEMFC performance largely depends on the reactants RH and their variation may show a negative or positive influence on the fuel cell power

output depending on the operational parameters [79]. The work of Kim et al. [80] has shown that, the decrease in the reactants humidity level can increase or decrease the fuel cell power output depending on the Nafion ionomer content of the MEA. The studies of Iranzo et al. [81] showed that the fuel cell performance is mainly effected by the cathode RH when compared to anode humidification. The studies of Neyerlin et al. [82] on the effect of RH on oxygen reduction reaction (ORR) kinetics, revealed that, when the reactants RH is above 50 %, the ORR kinetics is independent of RH. If the reactants RH is below 30%, a loss of 20 mV is observed in ORR kinetics. Wang et al. [83] numerically studied the effect of reactant RH's on the local transport phenomena in a PEM fuel cell with interdigitated and parallel flow field designs. Their studies showed that, fully humidified cathode and low RH anode or vice versa, the PEMFC power output increases. Kulikovsky [84] investigated the diffusion of liquid water in to the membrane of a PEMFC by means of a quasi-three-dimensional model. Lee and Chu [85] created a 3-D model to spot the liquid-gas interface at different humidity conditions in the cathode GDL. Only cathode side of the cell was simulated in the study to decrease the computational requirement. They showed that the RH has a profound influence on cell performance. Hu et al. [86] concluded that humidification of reactants on cathode is important for an interdigitated channel design to perform better than parallel flow channel design. Janga et al. [87] studied the problem of water management and humidity effect of both reactants on the PEMFC work. The results divulge that, while modelling for lower voltages, liquid water effect is compelling and higher inlet humidity enhances fuel cell performance. Kahveci and Imdat [88] modelled a PEMFC having single serpentine channel using 3-D single-phase steady state model and found that for increasing the performance of the cell, humidity of the reactant gases is important. When the fuel cell is operated at lower voltages, decreasing the RH of cathode side reactants improves cell performance because of mass transport limitations on cathode side. They also examined the influence of GDL porosity and RH on a single-serpentine fuel cell using 3-D modelling [89]. Modelling results proved that higher GDL porosity is preferable for better cell performance. As RH on anode side increased there was an improvement in the cell performance but the performance was found to be deteriorated with increase in cathode RH. Sun et al. [90] studied the influence of humidification of reactants and concluded that, humidified reactants are to be used for achieving the best cell performance. Too low or too high humidification may cause irregular spreading of current density locally.

Chen et al. [91] studied the consequence of clamping pressure and humidification temperature on the cell performance. They proposed that, when the cell is operated above 0.65V, humidification temperature should be 5 ^{o}C above cell temperature and when operated below 0.65V, temperature should be below 5 ^{o}C of cell temperature. Zhang et al. [92] used a 3-D lattice Boltzmann model to predict oxygen diffusion and water transport in GDL of a PEMFC. This model is used for exploring the influence of micro porous layer (MPL) on cell output. The results evidently showed that the liquid water content diminished with the use of MPL which improved current density. Molaeimanesh et. al. [93] analyzed the water droplet behaviour in the GDL at various cell compression by Lattice-Boltzmann method (LBM). Their results showed that, due to compression, the pore size in CL reduces, resulting in better air velocity in the GDL. This improved air velocity helps in removal of stagnant water from the GDL. Suresh and Jayanti [94] presented detailed analysis of cross-flow in the GDL through CFD simulations and quantified the cross-flow using Peclet Number.

Ozen et al. [95] studied the fuel cell performance at different operating temperature and relative humidities. Their results showed that, the increase in reactant RH and operating temperature have positive effect on fuel cell power output. Song et al. [96] analyzed the power output in a PEM fuel cell with increase in operating temperature. Their results indicated that, the performance of a PEM fuel cell improves with the increment in the operating temperature because of improved reaction kinetics of the reactants. Coppo et al. [97] inspected the effect of operating temperature on a PEMFC. Their findings showed that the transport of liquid water from the GDL surface plays a vital role in determining the appropriate operating temperature of the fuel cell. Santarelli and Torchio [98] experimented on single PEMFC at varies operating conditions. They have concluded that the increase in cell temperature improves the fuel cell performance when both the reactants streams are sufficiently humidified. Yan et al. [99] analysed the PEM fuel cell behaviour at different operating conditions. The results showed that, when all other parameters are constant, the fuel cell performance improved till operating temperature of 75 ^{o}C and from there it reduced.

Several studies [12,99–102] have shown that, the increase in the reactant stoichiometry have positive effect on the PEM fuel cell performance. Higher flow rates will not only increase the reactant concentration on the catalyst layer but also, will improve the water evacuation capabilities. Wang et al. [103] studied the effect of cross-flow in sub-rib in single and parallel serpentine designs on the power output of PEMFC using a 3-D model. They established that at high current densities, the increased gas velocity at low aspect ratio of flow channel helped in the elimination of liquid water, thereby improving the cell performance. Morin et al. [104] examined the impact of reactant flow direction on water management in a fuel cell. Their studies showed that, the counter current flow is more preferable over co-current flow as, counter flow has shown good membrane hydration, which increases the proton conductivity thereby improving the cell performance. In the literature, there are various studies available [17,105–108] on the effect of operating pressure on the fuel cell performance. The increase of operating pressure increases the overall performance of the fuel cell. In general, to send the air at higher pressures, air blower or compressor are used. These utilities increase the system power consumption greatly, reducing net power output [109]. Hence, optimizing the operating pressure reduces the system's power consumption, effectively increasing the overall system efficiency.

2.5 Studies on higher active area cells

For large scale power applications like decentralised power production, hydrogen powered buses, UPS systems etc., the use of stack made of small active area PEM fuel cell make them bulky and difficult to maintain due to more number of single cells. In such cases, it is effective to use less number of higher active area cells for large scale power production.

Shimpalee et al. [110] presented a study showing the performance and reactant transport in a large area PEMFC of 200 cm^2 with serpentine layout. They concluded that local issuance of current density, temperature and water content became more uniform when shorter channel lengths were used. A numerical study was conducted by Wang et al. [111] on the effect of active areas on the PEMFC performance with parallel, interdigitated and serpentine channel designs. They observed that the performance of fuel cell with parallel flow field decreased with increase in active

area, whereas that with serpentine channel improved. In case of PEMFC with interdigitated flow design, increase in active area had little influence on the performance. The areas considered in their study were only 11 × 11 mm^2 and 41 × 41 mm^2. Li et al. [112] analyzed five different fuel cells of active areas 50, 100, 200, 300 and 441 cm^2 for checking the possibility of scaling up of the PEMFC. Their results showed that, the serpentine design could be used in higher active area fuel cells without much flooding of the channel. Shimpalee et al. [113] modelled a PEM fuel cell of active area 480 cm^2 using parallel computing. They considered J.A. Rock patented flow-field as cathode channel design. Their modelling results showed that by using dry cathode reactant in this flow design, the pressure drop was reduced by 30% without effecting the performance. They also concluded that with proper combination of flow-field design and operating conditions, PEMFC can give a high performance with optimization of water management.

2.6 Gaps identified in the literature

From the above literature review, the following gaps are observed on the identified potential flow field design, ECSSFF.

(i) Though enhanced cross-flow split serpentine flow field has got lot of potential to be an efficient flow field design for PEM fuel cells, it is not well explored. Only one study [68] is available on this rectangular cross-sectional flow field layout. It is also limited to hydrodynamic considerations as the reaction chemistries and proton/electron transport phenomenon were not considered. Detailed full-scale performance study of the PEM fuel cell with ECSSFF is not available in the literature. The effect of various operating parameters on the cell performance with ECSSFF is not explored. Full scale fuel cell performance comparisons among ECSSFF and other flow fields such as parallel serpentine and single serpentine are also not available.

(ii) The reactant distribution, water evacuation and pressure drop in flow channel are dependent on the ratio of channel width to rib width. This best ratio of the channel and rib widths is not found for the ECSSFF design.

(iii) The work of Suresh et al.[68] on ECSSFF was limited to a small active area cell. Whether the ECSSFF layout is effective for higher active areas when compared to standard parallel serpentine designs is not explored. This information will be useful when designing a scaled up fuel cell stack for commercial purposes.

(iv) As the ECSSFF design was originally developed for rectangular cross-sectional cells, it will be interesting to see whether ECSSFF layout is also effective for square cross-sectional PEM fuel cell, as square shaped fuel cells are also being widely used.

These gaps lead to the formulation of the following objectives of the present study.

2.7 Objectives and scope of the present work

The overall objective of this study is to conduct a detailed computational performance analysis of the PEM fuel cell with Enhanced Cross-flow Split Serpentine Flow Field on the cathode side and establish the efficacy of the flow field by comparing the cell performance with other serpentine flow field designs. Towards this, following are identified as the sub-objectives of the present work.

1) To simulate and compare the performance of a rectangular cross-sectional fuel cell with ECSSFF design against that with Triple Single Serpentine Flow Field design by considering all the multi-physics involved including the reaction chemistries in a typical PEM fuel cell.

2) To study the effect of channel width to rib width ratio of the ECSSFF design layout on the performance of the rectangular type PEM fuel cell.

3) To compare the performance of PEM fuel cell with ECSSFF layout against that with Single Serpentine Flow Field design.

4) To study the efficacy of ECSSFF layout for higher active area PEM fuel cells.

5) To propose ECSSFF channel layout for square cross-sectional PEM fuel cells and compare its performance with regular parallel serpentine design.

The above stated objectives are achieved by developing a three dimensional, multiphase, isothermal steady state model for solving the multi-physics associated with the PEM fuel cell.in CFD environment using academic version of ANSYS®17.2. The computational domains are discretized into small hexahedral cells which do not form highly skewed cells. The flow, electrochemistry and species balance equations are solved using in-build Fuel cell add-on module. The scope of the study is limited to the computational analysis of the fuel cell having ECSSFF design for rectangular and square cross-sectional PEM fuel cells with different active areas. The detailed modelling equations and solution strategies used to simulate the PEM fuel cell performance are described in the next chapter.

Chapter 3

Modelling Methodology

Modelling methodology

The main objective of the present study is to evaluate the PEM fuel cell performance by employing ECSSFF, an unconventional flow channel design on cathode side. The study aims to simulate the performance of a rectangular cross-sectional PEM fuel cell with a 3-channel ECSSFF design and compare against the performance obtained with triple serpentine flow field design and single serpentine flow field design. It is also aimed to extend the ECSSFF layout to square cross-sectional cell and evaluate its performance. Another objective of the study is to evaluate the efficacy of this design to higher active area cells for large scale power applications. Computational analysis is performed in this study to achieve the above objectives (also mentioned in section 2.7 of Chapter 2). For computational analysis, a PEM fuel cell is required to be simulated completely including the hydrodynamics, reaction chemistries, multi-component, two-phase flow and electron and ion transport. This is carried out systematically in a simulation environment using Academic version of ANSYS®17.2. The detailed description of the modelling equations and solution strategies along with the computational domains are discussed in this chapter.

3.1 Problem formulation and Modelling equations

The PEM fuel cell comprises of different physics involving coupled phenomena, which include mass transport of species such as hydrogen, oxygen, water and nitrogen, heat transfer, electrochemical reactions and fluid flow. These phenomena are modelled as partial differential equations describing species, energy, mass conservation, electrical charges and momentum. A three dimensional, multi-phase, multi-component, laminar flow through the computational domain containing different parts of the PEM fuel cell is studied using an inbuilt fuel cell module in ANSYS®17.2 to analyse the cell performance. A rigorous 3-D computational fluid dynamic modelling methodology, which solves species transport equations, Navier-Stokes equations, mass and energy conservation equations and electrical potential equations coupled with the Butler – Volmer (BV) equations to define electro-chemical reactions on the surface of catalyst is used in this study. The effect of various operating parameters on the cell performance is studied. The effect of pressure drop is also realized in present work to make the results more relevant to actual operating conditions.

Governing equations

The following steady state transport equations are solved in this computational study:

- Continuity equation

$$\nabla.(\rho\varepsilon\,\vec{u}) = 0 \qquad (1)$$

- Momentum conservation equation

$$\nabla.(\rho\varepsilon\vec{u}\vec{u}) = -\varepsilon\nabla P + \nabla.(\mu\varepsilon\nabla\vec{u}) + \frac{\varepsilon^2\mu\vec{u}}{k} \qquad (2)$$

where, μ is dynamic viscosity (Pa.s), $\vec{u}$ is velocity vector (m/s), P is pressure (Pa), ε and k are porosity & permeability (m^2) of porous media and ρ is mixture density (kg/m^3).

In the flow channel, ε and k are set as 1 and ∞, respectively, and the assumptions of laminar gas flow and incompressible are used. Darcy term is exempted in Navier- Stokes and continuity equations. Darcy source term is applied for the flow of reactants through porous media such as GDL, CL and membrane layers. The Darcy drag force is imposed on the fluid by the pore walls which leads to pressure drops across the porous layers.

- Species conservation equation

The species equation which defines the mass transfer in the PEM fuel cell is given by:

$$\nabla.(\varepsilon\rho\vec{u}Y_i) = \nabla.\left(\rho D_i^{eff}\nabla Y_i\right) + S_c \qquad (3)$$

where, Y_i is the mass fraction of the i^{th} species

$$\sum_i Y_i = 1 \qquad (4)$$

$$D_i^{eff} = \varepsilon^{1.5} D_i \qquad (5)$$

where, D_i^{eff} is the effective gas diffusivity (m^2/s). The effect of the tortuosity and porosity of the porous media on the gas diffusion coefficient (D_i) is given by Bruggeman correlation [114].

Gas phase species diffusion coefficient is computed by

$$D_i = (1-s)^{r_s} D_i^0 \left(\frac{P_o}{P}\right)^{\gamma_p} \left(\frac{T}{T_o}\right)^{\gamma_t} \qquad (6)$$

where, D_i^o is the mass diffusivity at reference pressure (P_o) and temperature (T_o). These reference values and the exponent of pore blockage (r_s) as well as the exponents (γ_p and γ_t)

are taken as T_o = 300 K, P_o=101325 Pa, r_s =2.5, γ_p =1 and γ_t =1.5 and are defined in user defined functions (UDFs).

The species volumetric source terms S_c (kg/m^3.s) for species conservation are obtained from Equations 7 and 8 for hydrogen and oxygen respectively. Equation 9 is used for finding the total water content that can be generated if all reactants are consumed [115].

$$S_{H_2} = -\frac{M_{w,H_2}}{2F} R_{an} \quad (7)$$

$$S_{O_2} = -\frac{M_{w,O_2}}{4F} R_{cat} \quad (8)$$

$$S_{H_2O} = \frac{M_{w,H_2O}}{2F} R_{cat} \quad (9)$$

where, parameters R denote the exchange current densities (A/m^3) at the cathode, and anode respectively and M is the molecular weight of species (kg/kmol), which are calculated using BV equations [116]

$$R_{an} = \left(\zeta_{an} j_{an}^{ref}\right)\left(\frac{[A]}{[A]_{ref}}\right)^{\gamma_{an}}\left(e^{\alpha_{an}F\eta_{an}/RT} - e^{-\alpha_{cat}F\eta_{an}/RT}\right) \quad (10)$$

$$R_{cat} = \left(\zeta_{cat} j_{cat}^{ref}\right)\left(\frac{[C]}{[C]_{ref}}\right)^{\gamma_{cat}}\left(-e^{+\alpha_{an}F\eta_{cat}/RT} + e^{-\alpha_{cat}F\eta_{cat}/RT}\right) \quad (11)$$

where, ζ is the specific active surface area (1/m), j^{ref} is the reference exchange current density per active surface area (A/m^2), [ ] & [ ]$_{ref}$ are local species concentration and its reference value (kmol/m^3), A & C refer to the anode side reactant, H_2 & cathode side reactant, O_2 respectively, α is the transfer coefficient, γ is the concentration dependence coefficient, η_a and η_c are the cathode & anode over potentials (V), respectively, R is the universal gas constant (J/mole.K) and F is the Faraday constant (C/kmol).

- Proton and electron transport equations

Electrochemistry is computed by calculating the reaction rates of anode and cathode reactions. The difference between the phase potentials of solid and membrane is the driving force for the electrochemical reactions. The electron transport in the conducting medium is solved by Equation 12 while Equation 13 solves the protonic transport in the membrane. Proton equations are:

$$\nabla.(\sigma_{sol}\nabla\phi_{sol}) + R_{sol} = 0 \quad (12)$$

$$\nabla.(\sigma_{mem}\nabla\phi_{mem}) + R_{mem} = 0 \quad (13)$$

where,

ϕ = electric potential (volts)

σ = electrical conductivity (1/ohm-m)

R = volumetric transfer current (A/m^3)

ϕ_{mem} is the membrane phase potential, ϕ_{sol} is solid phase electric potential and σ_{mem} denote protonic conductivity for the membrane and σ_{sol} denote electrical conductivity for solid phase. The source terms R_{mem} and R_{sol} indicate the volumetric exchange currents for the membrane and solid phases, respectively. These source terms are non-zero inside the catalyst layers and are applied in solid phase as, $R_{sol} = -R_{an}$ for anode and $R_{sol} = +R_{cat}$ for cathode. In membrane phase, $R_{mem} = -R_{cat}$ for cathode side and $R_{mem} = +R_{an}$ for anode side. These sources terms are computed from Butler-Volmer equations as presented in Equations (10) and (11).

The potential gained because of electron transfer from anode to cathode is calculated by deducting open circuit voltage (OCV) on cathode electrode. Cathode and anode overpotentials are calculated from Equations 14 and 15.

$$\eta_{an} = \phi_{sol} - \phi_{mem} \quad (14)$$

$$\eta_{cat} = \phi_{sol} - \phi_{mem} - V_{oc} \quad (15)$$

The membrane conductivity (σ_{mem}) is a function of its water content, λ and temperature, which is calculate as [117]

$$\sigma_{mem} = (0.514\lambda - 0.326)e^{1268\left(\frac{1}{303}-\frac{1}{T}\right)} \quad (16)$$

The membrane water content is associated with the electro-osmotic phenomena, which depends on the osmotic drag coefficient. The work of springer et al. [118] shows that an average of 2.5 water molecules are dragged by each proton from the anode to the cathode electrode through the electrolyte, which is expressed as

$$n_d = 2.5\frac{\lambda}{22} \quad (17)$$

When there is a large liquid water gradient between cathode and anode sides, the produced water on the cathode will back diffuse to anode through the membrane. The back diffusion flux can be expressed as:

$$J_w^{diff} = -\frac{\rho_m}{M_m} M_{h2O} D_l \nabla\lambda \quad (18)$$

where, M_m and ρ_m are the equivalent weight of the dry membrane and density respectively and membrane water diffusivity (D_l) can be expressed as a function of λ

$$D_l = f(\lambda) e^{2416\left(\frac{1}{303}-\frac{1}{T}\right)} \quad (19)$$

and the water content, λ is given by:

$$\lambda = 14 + 1.4(a-1) \quad (a > 1) \quad (20)$$

$$\lambda = 0.043 + 17.18a - 39.85a^2 + 36a^3 \ (a < 1) \quad (21)$$

Here, a is the water activity that can be determined by

$$a = \frac{P_{wv}}{P_{sat}} + 2s \quad (22)$$

where, P_{wv} is the water vapour pressure and is calculated based on the molar fraction of the vapour χ_{H2O} and the local pressure:

$$P_{wv} = \chi_{H2O} P \quad (23)$$

The water saturation pressure is calculated, as

$$log_{10}P_{sat} = -2.1794 + 0.02953(T - 273.17) - 9.1837 \times 10^{-5}(T - 273.17)^2 + 1.4454 \times 10^{-7}(T - 273.17)^3 \quad (24)$$

- Liquid water formation

As the operating temperature of the fuel cell is relatively low (< 90°C), the formed water stays in the liquid state, which helps in hydrating the membrane, thereby improving the proton conductivity. In present study, saturation model is used for calculating production and transport of liquid water. In this model, formation of liquid water and its transportation are governed by conservation equations (Equation 25) for the volume fraction of liquid water, s

$$\frac{\partial(\varepsilon\rho_l s)}{\partial t} + \nabla.\left(\rho_l \vec{V}_l s\right) = r_w \quad (25)$$

where, subscript 'l' refers to the liquid water and r_w is the condensation rate which is modelled as:

$$r_w = c_r \, max\left(\left[(1-s)\frac{P_{wv}-P_{sat}}{RT} M_{w,H_2O}\right], [-s\rho_l]\right) \quad (26)$$

Condensation rate, r_w is considered only in CL and GDL because the formed water will stagnate in flow channels if it is not appropriately evacuated. The condensation rate

constant (c_r) is fixed at 100 s^{-1}. The presence of water in liquid form will block gas diffusion layer's pores which in turn will reduce the interaction between reactants and catalyst surface. The rate at which the formed water vapour is condensed is called as condensation rate, r_w. As the pores are finer in the diffusion layer, movement of water through the porous layer will not happen by diffusion but by capillary action. Hence, inside the porous zones, the capillary diffusion term replaces the convective term in Equation 25 as follows

$$\frac{\partial(\varepsilon\rho_l s)}{\partial t} + \nabla.\left[\rho_l \frac{Ks^3}{\mu_l}\frac{dP_c}{ds}\nabla s\right] = r_w \quad (27)$$

Equation 27 models processes such as vaporization, condensation, surface tension and capillary diffusion. The flooding of the reaction surface and blockage of the porous media are modeled by multiplying the active surface area and the porosity by (*1-s*). The capillary pressure is computed using *s* (Leverett function), which is dependent on wetting phase as shown in Equation 28.

$$P_c = \frac{\sigma cos\theta_c}{\left(\frac{K}{\varepsilon}\right)^{0.5}}(1.417(1-s) - 2.12(1-s)^2 + 1.263(1-s)^3) \quad \theta_c < 90^o \quad (28)$$

$$P_c = \frac{\sigma cos\theta_c}{\left(\frac{K}{\varepsilon}\right)^{0.5}}(1.417s - 2.12(s)^2 + 1.263(s)^3) \quad \theta_c > 90^o \quad (29)$$

where, σ is the surface tension (Pa), ε is the porosity, K the absolute permeability and θ_c is the contact angle.

- Energy conservation

The steady state energy conservation equation adopted is:

$$\nabla.\left(\rho\varepsilon C_p T\vec{u}\right) = \nabla.\left(k_{eff}\nabla T\right) + s_h \quad (30)$$

where, C_p is the specific heat capacity (J/kg.K) and k_{eff} is the effective thermal conductivity (W/m.K) accounting for the contribution of the fluid phase and solid matrix of porous media expressed as:

$$k_{eff} = \varepsilon k_f + (1-\varepsilon)k_s \quad (31)$$

The k_s and k_f are the thermal conductivities of the solid and fluid phases of the porous media, respectively, and mixture kinetic theory is used to calculate the thermal conductivity of the gaseous mixture. Additional volumetric sources to the thermal energy

equation are used because of the irreversibilities of the processes which hinder the total conversion of chemical energy released in the electrochemical reactions to electrical work. The total source term in the thermal energy equation (that is, enthalpy) is:

$$s_h = h_{react} - R_{an,cat}\eta_{an,cat} + I^2 R_{ohm} + h_L \quad (32)$$

where, $R_{an,cat}\eta_{an,cat}$ is the product of the transfer current and the overpotential in the anode or the cathode (Triple Phase Boundary), h_{react} is the net enthalpy change due to the electrochemical reactions, h_L is the enthalpy change due to condensation/vaporization of water and R_{ohm} is the ohmic resistivity of the conducting media.

Assumptions

Following are the assumptions considered in this study:

1. The PEMFC is operating under steady state condition and its temperature is maintained at the operating temperature.
2. The pure form of hydrogen and air are used for the simulation and these gasses follow the ideal gas law.
3. Both the reactant gases flow in the laminar region in flow channels.
4. They are incompressible due to low pressure gradients and small velocities.
5. Catalyst layers, gas diffusion layers and membrane are homogeneous and isotropic materials.
6. The membrane is impermeable to gasses i.e., there is no leakage current.
7. The ohmic potential drop is very low in electrically conductive parts like bipolar plates, catalyst layers and gas diffusion layers.
8. There are negligible contact resistance and minimum swelling of the membrane.
9. The mass flow rate is constant at the inlet of the channel and channel outlet is at constant pressure.
10. In the gas flow channels, the liquid water droplets are assumed in fine mist form and hence liquid water velocity is equivalent to the gas velocity inside the gas channel.

3.2 Computational domain and boundary conditions

PEM fuel cell assembly consists of 7 different parts such as membrane and a set of catalyst layers, gas diffusion layers and current collectors on both cathode and anode sides. The 3-D geometry of PEM fuel cell consisting of all the fuel cell parts which is created in solid works® 2010 and a representative image of the assembly is shown in Figure 3.1. The created geometry is imported to Design Modeller 17.2 for the generation of computational domain. For achieving the objectives of the present study, rectangular fuel cells of active area 55.55 cm^2, 50 cm^2, 100 cm^2, 150 cm^2 and 200 cm^2 are generated. The fuel cell dimensions used in this work are listed in Tables 3.1 and 3.2.

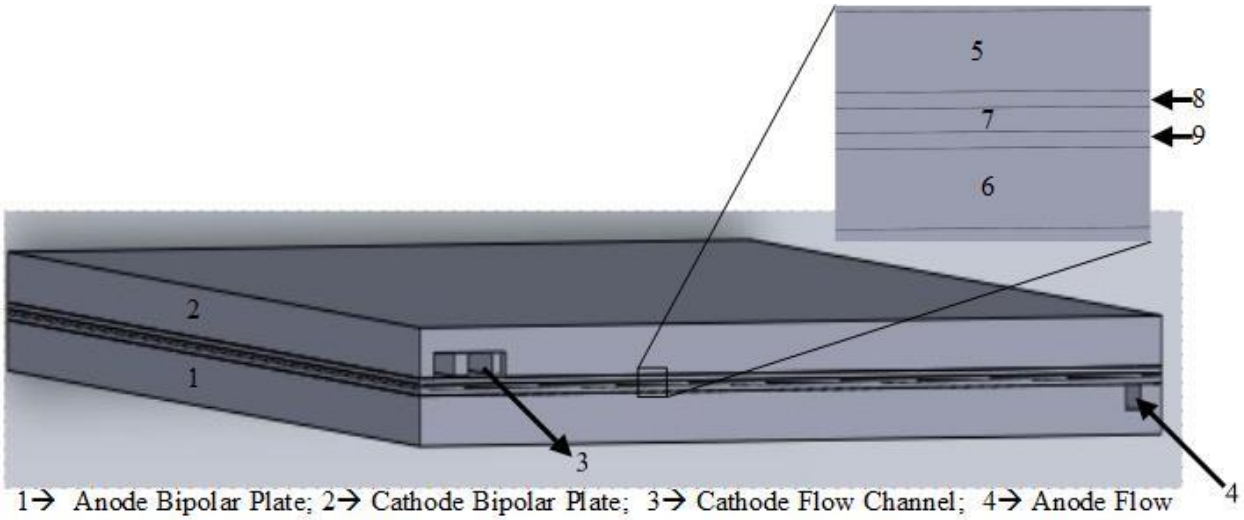

Figure 3.1 Computational model of fuel cell assembly.

Table 3.1 Dimensions of the fuel cells considered in this study.

Area, cm^2	**Rectangular fuel cell**	
	Length, cm	**Width, cm**
55.55	5.5	10.1
50	5.5	9.1
100	7	14.3
150	8.2	18.3
200	10	20

Table 3.2 Thickness of different components in fuel cell assembly.

Component	Thickness, cm
Membrane	0.0125
Anode Catalyst Layer	0.0005
Cathode Catalyst Layer	0.0005
Gas Diffusion Layer	0.025
Bi-polar Plate	0.2

Flow field layouts considered in the study

Throughout this study in all the simulations, ECSSFF layout is used on the cathode side, while a parallel flow field design is used on the anode side. To compare the performance of the cells with ECSSFF design on cathode side against the cells with other flow field designs such as triple serpentine flow field and single serpentine flow field designs are modelled and all the flow filed designs generated are shown in Figure 3.2. Typical channel dimensions of the different flow field designs used in the present study are presented in Table 3.3.

Table 3.3 Typical channel dimensions of flow field designs.

Type of flow field design	Dimensions of the flow channel in Rectangular Cell	
	Height, cm	Width, cm
SSFF	0.1	0.1
TSFF	0.1	0.1
ECSSFF	0.1	0.2

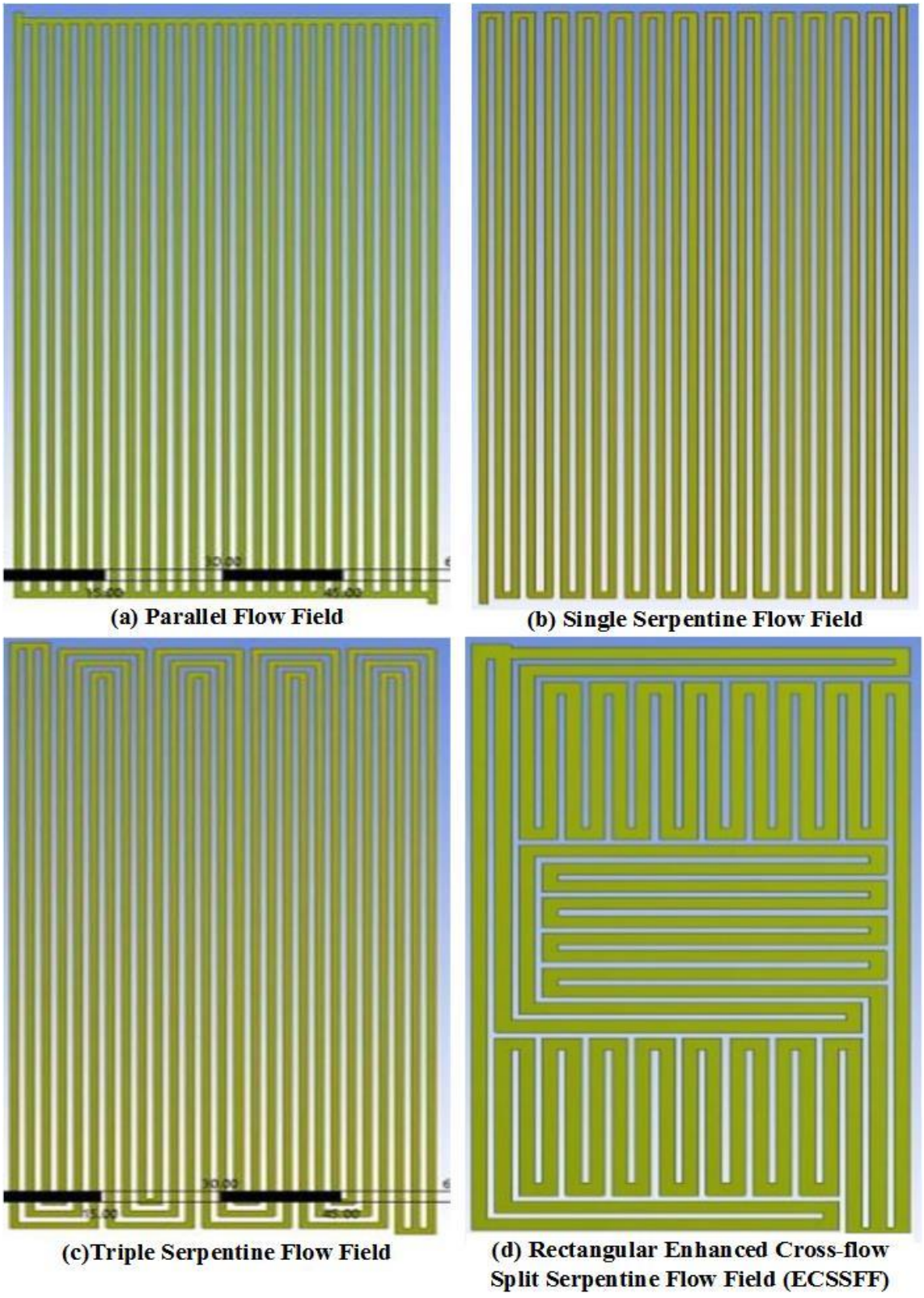

Figure 3.2 Flow Channel layouts used in present study.

Computational mesh generation

The geometry created is imported to ICEMCFD®17.2, for discretizing the flow domain into small computational cells. Hexahedral mesh is used for the mesh generation as they do not form highly skewed cells and helps in getting stable and accurate solution [119]. The entire geometry is divided into discrete elements, and volume of each element is controlled by the number of nodes in each part of the fuel cell. Edge sizing for all the edges is used in the mesh generation. This gives a good control on the mesh elements as it can be ensured that significant number of elements are present in all parts of fuel cell. Number of nodes in Z-direction (thickness direction), X - direction (length direction) and Y- direction (breadth direction) are varied for carrying out the grid independence studies. For instance, 105 divisions in X-direction, 193 divisions in Y-direction and - 22 divisions for bipolar plates, 10 divisions for each GDL, 8 divisions for cathode side catalyst layer, 6 divisions for the anode side catalyst layer and 5 divisions for membrane in Z-direction for a 50 cm^2 active area fuel cell with ECSSFF design resulted in mesh having 2.11 million number of cells. As oxygen reduction reaction is slower compared with hydrogen oxidation reaction, finer mesh is used in the cathode catalyst layer compared with anode catalyst layer to capture the profiles properly. Similar procedure is followed for meshing other geometries in the present study. Figure 3.3 shows the computational mesh for a typical 50 cm^2 PEM fuel cell with ECSSFF flow field. The grid independent study and the final meshed used for various geometries are discussed in the next section, 3.3.

Boundary conditions

Temperature, mole fraction of the species and mass flow rate are defined at inlets of the anode and cathode flow channels. The mole fractions of Y_{H2} & Y_{H2O} at the anode inlet and Y_{O2} & Y_{H2O} at the cathode inlet are determined by using operating percentage of relative humidity (RH) and operating p ressure. Pressure outlet condition with atmospheric pressure is applied at the outlet of the flow channels. Counter current flow is applied in the present study as it produces higher current density compared to other flow patterns [120]. No slip boundary conditions are applied on all the solid surfaces and external walls are defined as isothermal.

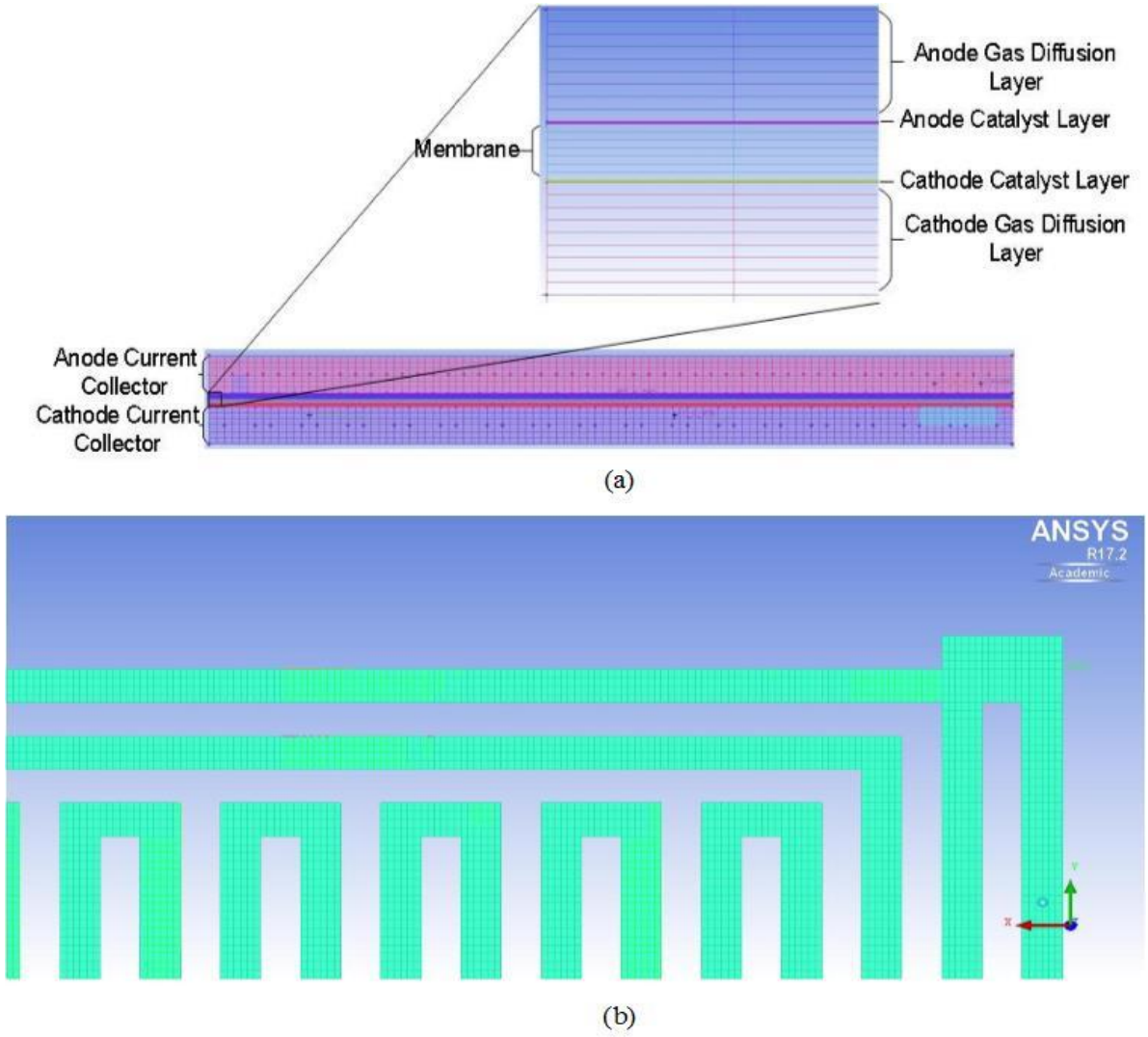

Figure 3.3 (a) Mesh generated for the computational domain of a typical 50 cm^2 area fuel cell (b) Mesh generated on the flow channel.

Zero flux boundary condition is applied for membrane phase potential, ϕ_{mem} on all the boundaries as ionic current does not go out of the cell from any external boundary. On the external sides of the current collectors, electrical potentials ϕ_{sol} are applied. The potential at anode side is set as 0 V while, the operating voltage is set as the cathode potential. The current generated from the redox reactions only flows through these two boundaries. On all the remaining boundaries, the electric potential ϕ_{sol} is set as zero. Material properties considered for the present simulations are taken from Iranzo et al. [121] and are listed in Table 3.4. The operating conditions used in the simulation work presented in Table 3.5.

Table 3.4 Materials properties used in present work (Iranzo et. al., 2010) [121].

Parameter		Units	Value
BP	Density	kg/m^3	1990
	Specific Heat Capacity	J/(kg K)	710
	Thermal Conductivity	W/(m K)	120
	Electric Conductivity	1/(Ω m)	92,600
GDL	Density	kg/m^3	321.5
	Specific Heat Capacity	J/(kg K)	871
	Porosity	-	0.82
	Permeability	m^2	10^{-12}
	Thermal Conductivity	W/(m K)	10
	Electric Conductivity	1/(Ω m)	280
	Viscous Resistance (Anode)	$1/m^2$	1.0×10^{12}
	Viscous Resistance (Cathode)	$1/m^2$	3.86×10^{12}
	Wall Contact Angle	deg	110
Membrane	Density	kg/m^3	1980
	Specific Heat Capacity	J/(kg K)	2000
	Thermal Conductivity	W/(m K)	0.16
	Electric Conductivity	1/(Ω m)	10^{-16}
	Equivalent Weight	kg/kmol	1100
CL	Density	kg/m^3	2719
	Specific Heat Capacity	J/(kg K)	871
	Thermal Conductivity	W/(m K)	10
	Electric Conductivity	1/(Ω m)	5.0×10^3
	Porosity	-	0.5
	Permeability	m^2	10^{-12}
	Surface-to-volume ratio	m^2/m^3	1.25×10^7
	Open Circuit Voltage	V	0.98
	Voltage at Anode terminal	V	0
	Voltage at Cathode terminal	V	0.95-0.3
	H_2 Diffusivity	m^2/s	8.0×10^{-5}
	O_2 Diffusivity	m^2/s	2.0×10^{-5}
	H_2O Diffusivity	m^2/s	5.0×10^{-5}
	Pore Blockage Saturation Exponent	-	2.0
	Concentration Exponent (Anode)	-	0.5
	Concentration Exponent (Cathode)	-	1.0
	Charge Transfer Coefficient (Anode)	-	1.0
	Charge Transfer Coefficient (Cathode)	-	1.0
	Reference Exchange Current Density (Anode)	$\mu A/cm^2_{Pt}$	448×10^5
	Reference Exchange Current Density (Cathode)	$\mu A/cm^2_{Pt}$	448

Table 3.5 Operating conditions in present study.

Parameter		**Units**	**Value**
Operating Temperature		^{o}C	50, 60, 70 and 80
Operating Pressure		kPa	100, 200, 300 and 400
Fuel Cell Current Density		A/cm^2	1
Anode Gas Flow rate		kg/s	1,1.5,2 and 2.5 times of stoichiometry
Cathode Gas Flow rate		kg/s	1,2,3 and 4 times of stoichiometry
RH of Inlet Gas	Anode	-	0%, 50%, 80% and 100%
	Cathode	-	0%, 50%, 80% and 100%

3.3 Simulation Strategy

The system of partial differential equations governing the entire PEM fuel cell physics is solved using built-in fuel cell module of ANSYS Fluent® 17.2 [122]. While carrying out the simulations, different options available in the module have been used to consider the heat effects and predict different aspects of the fuel cell. Joule heating effect is enabled to consider the generation of heat in the fuel cell due to the resistance to electron flow through the gas diffusion layers, catalyst layers, bipolar plates and protons flow through the membrane. When joule heating is activated, I^2R term is added in Equation 32. Reaction heating considers heat generated due to electrochemical reactions including the product of transfer current, heat of reaction and the over-potentials in the energy term of Equation 32. Electrochemistry sources option is used to consider electrochemistry effects. The transfer currents on the surface of the catalyst are calculated using BV equation. Membrane Water Transport option is used to compute water diffusion across the membrane. The multiphase option is considered for calculating the liquid transport in the gas diffusion layer in the present study. To calculate the gas species mass diffusivity, full multicomponent diffusion method is opted. Fuel cell working pressure is kept constant at 200000 Pa.

The present studies are carried out at constant boundary conditions by varying operating temperatures and relative humidity of inlet reactant gas. Flow rates are calculated by assuming a

current density of 1A/cm^2 with stoichiometric ratios of 3 and 1.5 on cathode and anode sides respectively. All the relevant equations are solved in F-Cycle using BCGSTAB (Bi-Conjugate Gradient Stabilize method). 100% pure hydrogen gas is considered on anode side in the present study. The various operating conditions used in this study are given in Table 3.5. The criteria for termination of the multi-grid cycles in solution control is used as 0.001 for species and saturation equations and 0.0001 for potential equations. The solution also depends on under-relaxation factors as it may lead to divergence if proper values are not used. The default under relaxations factors for water saturation, protonic potential and water content were changed to 0.95, pressure to 0.7 and momentum to 0.3. The criteria for convergence is taken from the literature [123–125] in which it is shown that, monitoring of the residual alone is not sufficient to check the convergence. So, convergence is checked in three ways in the present study and they are - residual monitoring of the species, evaluation of the calculated current from the amount of mass consumed and consistency of the calculated voltage with number of iterations. In the present study, convergence criteria for species residual is set as 10^{-6} [26]. The computational mesh used for the entire fuel cell domain is decided based on the grid independence study, which is discussed in the next section. The modeling methodology explained till now is represented in the form of flow chart as shown in Figure 3.4.

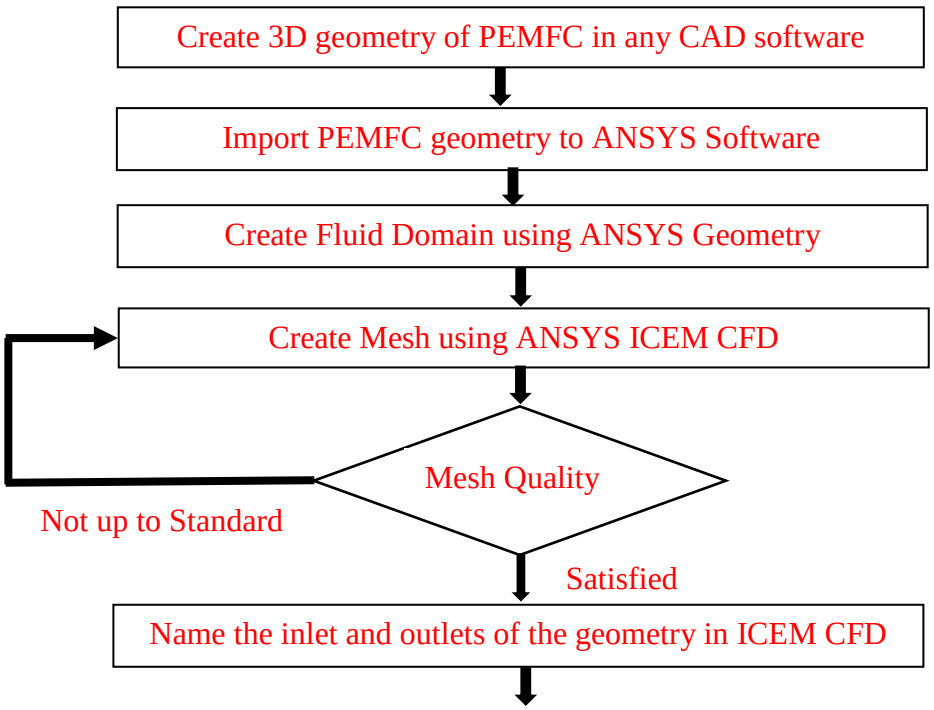

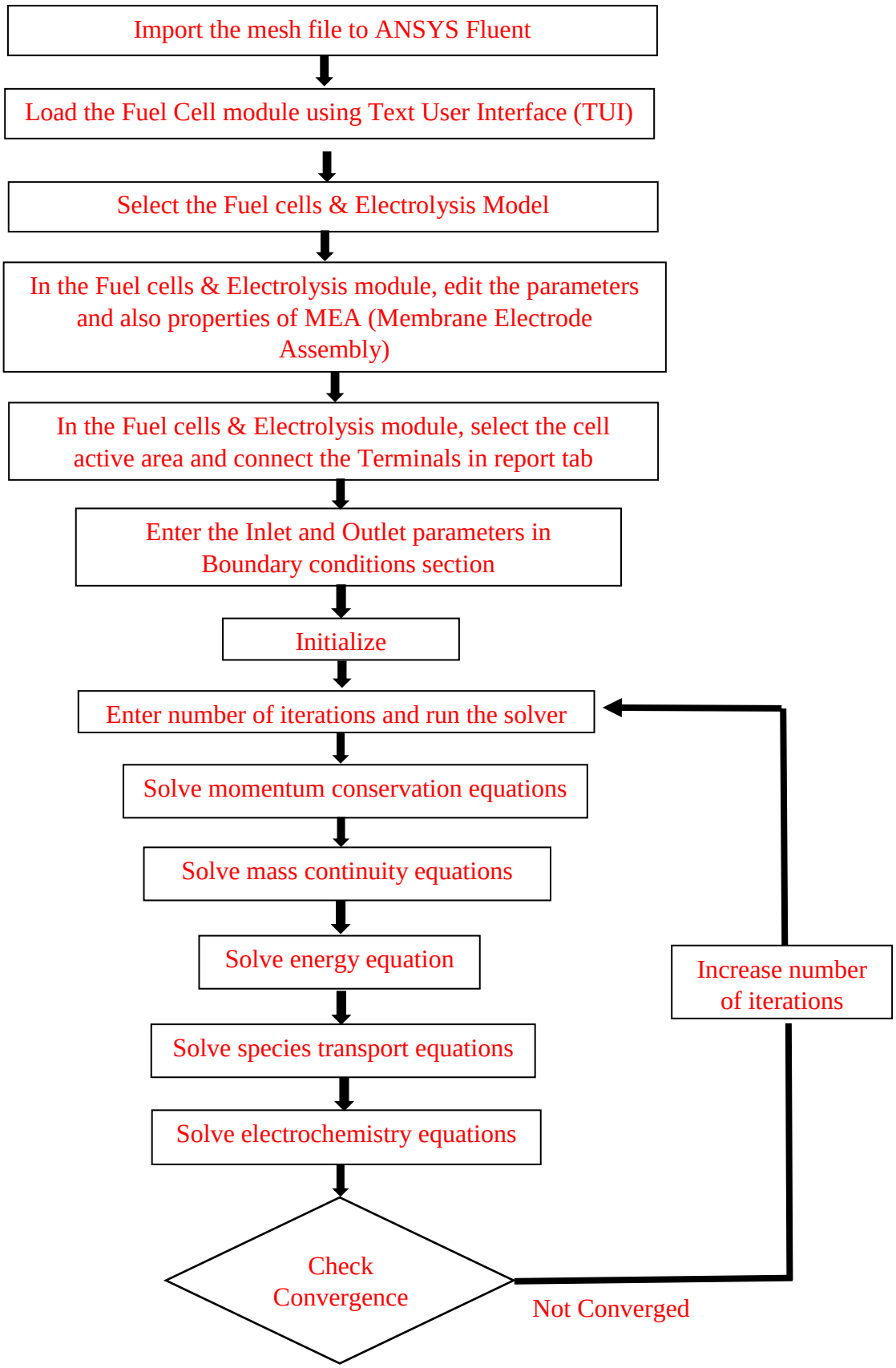
Import the mesh file to ANSYS Fluent
Load the Fuel Cell module using Text User Interface (TUI)
Select the Fuel cells & Electrolysis Model
In the Fuel cells & Electrolysis module, edit the parameters and also properties of MEA (Membrane Electrode Assembly)
In the Fuel cells & Electrolysis module, select the cell active area and connect the Terminals in report tab
Enter the Inlet and Outlet parameters in Boundary conditions section
Initialize
Enter number of iterations and run the solver
Solve momentum conservation equations
Solve mass continuity equations
Solve energy equation
Solve species transport equations
Solve electrochemistry equations
Check Convergence
Not Converged
Increase number of iterations

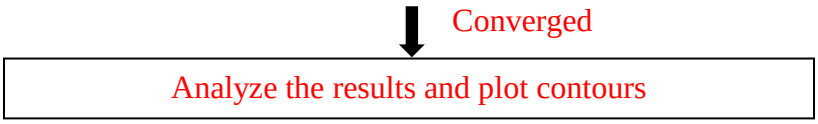

Figure 3.4 Flow chart of solution procedure.

3.4 Grid independent and Iteration independent studies

The multiphysics involved in PEM fuel cell require computational cells of high quality to reach a converged solution. To achieve this converged solution with minimal computational power and time, grid and iterative independence studies are needed to be carried out [126]. Grid independent studies are conducted to find the optimum grid size with the available computational resources while the iterative independent studies are conducted to find the minimum number of iterations to reach the final solution within the acceptable error limit. These studies are carried out at an operating temperature of 70 ^{o}C, reactant relative humidity of 100 % and operating pressure of 200 kPa.

Figure 3.5 (a) and (b) show the results of grid and iterative independence studies performed for 50 cm^2 active area at an operating voltage of 0.5 V. The total number of grid elements are varied by changing the distance between the adjacent nodes along the channel, through plane and in-plane in the fuel cell. For instance, a total of 6 different grid sizes with number of elements as 0.29 million, 1.022 million, 1.795 million, 2.113 million, 3.978 million and 7.82 million respectively are generated for 50 cm^2 active area. Figure 3.5 (a) shows the variation of current density estimated at 0.5 V with the number of grid elements. It can be observed that, the corresponding percentage improvement in current density is (i) 10.12% for the mesh size increase from 0.29 million to 1.022 million (ii) 6.74% for mesh increase from 1.022 million to 1.7935 million, (iii) 1.92 % for increment of elements from 1.7935 million to 2.113 million, (iv) 0.3015% and 0.3 % for the mesh size increase from 2.113 million to 3.978 million and further to 7.82 million respectively. Hence for present analysis, the mesh size of 2.113 million elements is chosen for 50 cm^2 area cell because the improvement in current density is less than 2% in higher meshes. In the same way, the suitable mesh which gives grid independent solution is identified for other active areas. The higher mesh sizes of 5.264 million, 7.727 million and 9.898 million cells have resulted in less than 2% difference in the current density at 0.5 V compared to the meshes of 3.8 million, 5.7 million and 7.5 million cells for 100cm^2, 150 cm^2 and 200 cm^2 active area fuel cells respectively. These

simulations were performed using HP – DL 380 G8P Server with 128 GB RAM and 16 core Xeon E5-2650 processor. Table 3.6 lists the final meshes obtained after grid independent study for various geometries considered in the present study. These meshes have been used for further studies carried out with these fuel cell assemblies.

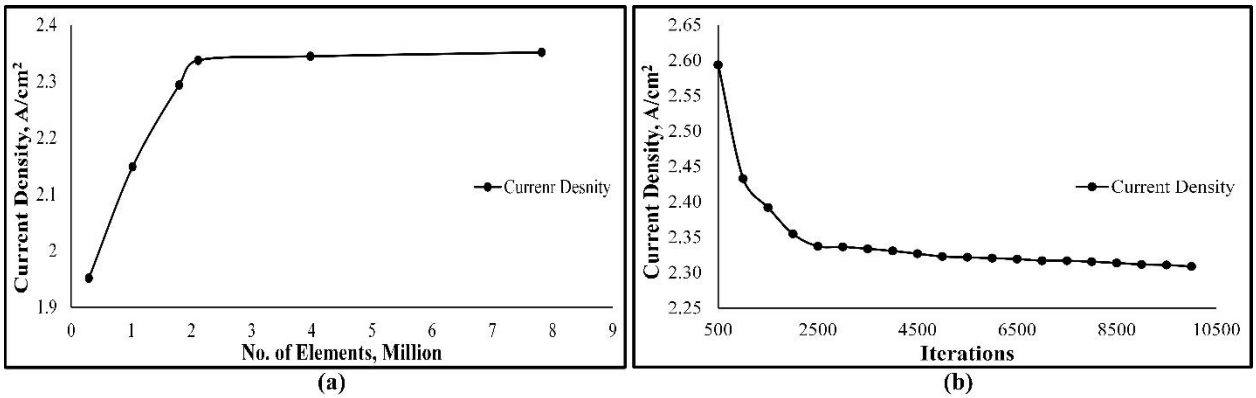

Figure 3.5 (a) Grid independent and (b) Iterative independent studies at V=0.5V for 50 cm^2 active area cell with ECSSFF design.

Table 3.6 Finalized computational meshes of different fuel cell assemblies after grid independent study.

Fuel cell assembly with cathode side flow field specification	**Computational mesh (in million elements) obtained after grid independent study**
55.55 cm^2 Fuel cell with TSFF	1.41
55.55 cm^2 Fuel cell with ECSSFF	1.39
55.55 cm^2 Fuel cell with single serpentine FF	1.37
50 cm^2 Fuel cell with ECSSFF	2.11
50 cm^2 Fuel cell with TSFF	2.14
100 cm^2 Fuel cell with ECSSFF	5.26
100 cm^2 Fuel cell with TSFF	5.29
150 cm^2 Fuel cell with ECSSFF	7.72
150 cm^2 Fuel cell with TSFF	7.75

200 cm^2 Fuel cell with ECSSFF	9.89
200 cm^2 Fuel cell with TSFF	9.91

The final output value in case of an iterative solution is sensitive to the number of iterations as it reaches close to the true value. The time required to obtain the solution will increase with the increment in number of cells and iterations [119], so for the present study, the number of iterations are fixed when the percentage improvement in current density is below 1% compared to the previous 500 iterations. Current density value is noted down for every 500 iterations. Figure 3.5(b) displays the graph between numbers of iterations vs current density at 0.5V for 50 cm^2 active area cell with ECSSFF design, it can be witnessed that the percentage improvement in current density is decreasing as the number of iterations are increasing. The percentage improvement is 1.55 % in case of 2000 iterations compared to 1500, 0.75 % for 2500 iterations compared to 2000 and is 0.04% for 3000 iterations compared to 2500. In the same way, the percentage improvement in current density with number of iterations at 0.5V was determined for other active areas. From this study, number of iterations is fixed at 2500 as the improvement in current density is found to be below 1% above 2500 iterations for all the cases considered.

3.5 Pressure drop and net power calculations

When the reactants flow through channels in a PEM fuel cell, there will be a loss of pressure due to friction and presence of water. For compensating this pressure drop, reactants are needed to be sent at an elevated pressure which requires energy. This excess energy required to maintain the pressure high enough for the reactants to flow through channel is called parasitic power loss. Parasitic power loss due to pressure drop is calculated by multiplying the pressure drop with reactant flow rate (Eq. 33) as suggested by Heidary et al. [50]. Net power output is the useful power output from the PEM fuel cell after subtracting the parasitic power loss, which incur during the operation of the fuel cell from its gross power output. In general, when air is used as cathode reactant, compressor is employed to pump air into the fuel cell. Han et al. [127] showed that the compressor power takes a large chunk of total system power consumption. The realistic power output from a PEM fuel cell operation can be calculated after subtracting the compressor power requirement from the produced cell power. The power required for the compressor to pump air at

higher pressures is calculated as suggested by Tirnovan and Giurgea [19] using equation (34). The overall efficiency of the compressor is assumed to be 0.8. To know the practical usable power produced from a PEM fuel cell, the power losses due to pressure drop across channel and power required by the compressor are to be subtracted from the Gross Power (equation (35)).

$$P = q \times \frac{\Delta p}{\rho} \tag{33}$$

$$W_{comp} = \frac{\dot{m} \times c_p \times T\left[\left(\frac{p^{out}}{p^{in}}\right)^{\frac{k-1}{k}} - 1\right]}{\eta} \tag{34}$$

where, q is flow rate (m^3/s), ρ is air density (kg/m^3), Δp is pressure drop across channel (Pa), $\dot{m}$ is air mass flow rate (kg/s), c_p is specific heat capacity (J/kg.K) and k is heat capacities ratio.

$$Net\ power = Gross\ power\ output - Power\ loss\ due\ to\ pressure\ drop - compresor\ power \tag{35}$$

3.6 Model Validation

The accuracy of a modelling approach can be verified by validating the proposed model with the available experimental data. The experimental results of Limjeerajarus et al. [123] and Iranzo et al. [121] have been utilized to validate the modelling methodology used in present study. In the first validation study, a 5 cm^2 active area fuel cell having parallel channel design has been simulated and compared with the experimental resutls of Limjeerajarus et al. The material properties used from Limjeerajarus et al. are listed in Table 3.7. In the second validation study, a fuel cell having active are of 50 cm^2 with 5-path serpentine channel design has been simulated and the results are compared with the experimental results presented in Iranzo et al. The material properties used for this study are taken from Iranzo et al. as shown in Table 3.4. The operating conditions of both the validation studies are listed in Table 3.8 as per the two experimental works. Figure 3.6 shows the numerical validation against the experimental studies of Limjeerajarus et al. and Iranzo et al. As can be observed from Figure 3.6, there is a good agreement between the experimental IV curve and IV curve obtained from CFD simulations. The percentage error between experimental and simulation results is found to be less than 3%. This validates the followed

modelling methodology and simulation strategy and shows that they can be used to simulate the performance of the PEM fuel cell with ECSSFF design and conduct further studies.

Table 3.7 Materials properties of Limjeerajarus et. al. [123].

Parameter		**Units**	**Value**
GDL	Density	kg/m^3	321.5
	Porosity	-	0.6
	Electric Conductivity	$1/(\Omega\ m)$	280
	Wall Contact Angle	deg	110
Membrane	Density	kg/m^3	1980
	Thermal Conductivity	W/(m K)	0.16
	Equivalent Weight	kg/kmol	1100
CL	Porosity	-	0.4
	Surface-to-volume ratio	m^2/m^3	1.227×10^7
	Open Circuit Voltage	V	1.05
	Anode Voltage	V	0
	Cathode Current density	A/cm^2	0.0025- 1.80
	Pore Blockage Saturation Exponent	-	2.0
	Concentration Exponent (Anode)	-	1.0
	Concentration Exponent (Cathode)	-	1.0
	Charge Transfer Coefficient (Anode & Cathode)	-	1.0
	Reference Exchange Current Density (Anode)	A/m^2-Pt	7.17
	Reference Exchange Current Density (Cathode)	A/m^2-Pt	7.17×10^{-5}

Table 3.8 Operating conditions for Model validation

Variable		**Units**	**Limjeerajarus et. al.** [123]	**Iranzo et. al.** [121]
Operating Temperature		^oC	60	60
Operating Pressure		kPa	100	400
Fuel Cell Current Density		A/cm^2	1	1
Anode Gas Flow rate		kg/s	1.1 times of stoichiometry	1.5 times of stoichiometry
Cathode Gas Flow rate		kg/s	2.2 times of stoichiometry	3 times of stoichiometry
RH of Inlet Gas	Anode	-	90%	60%
	Cathode	-	90%	60%

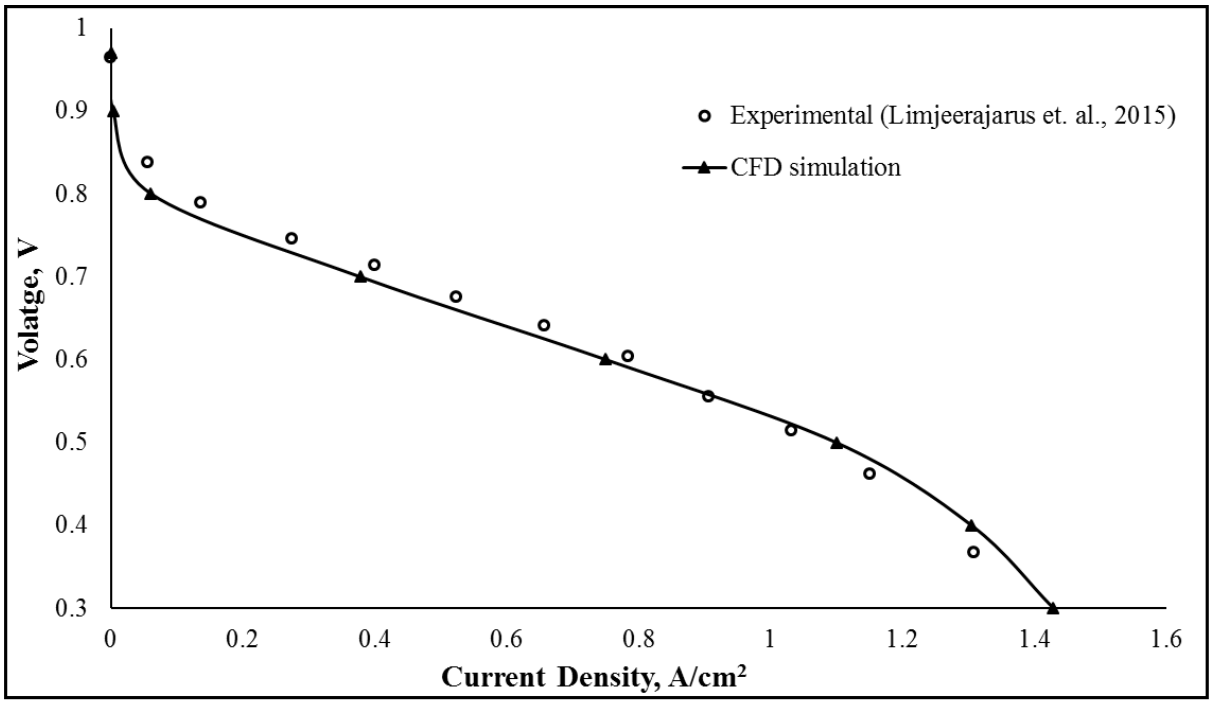

(a)

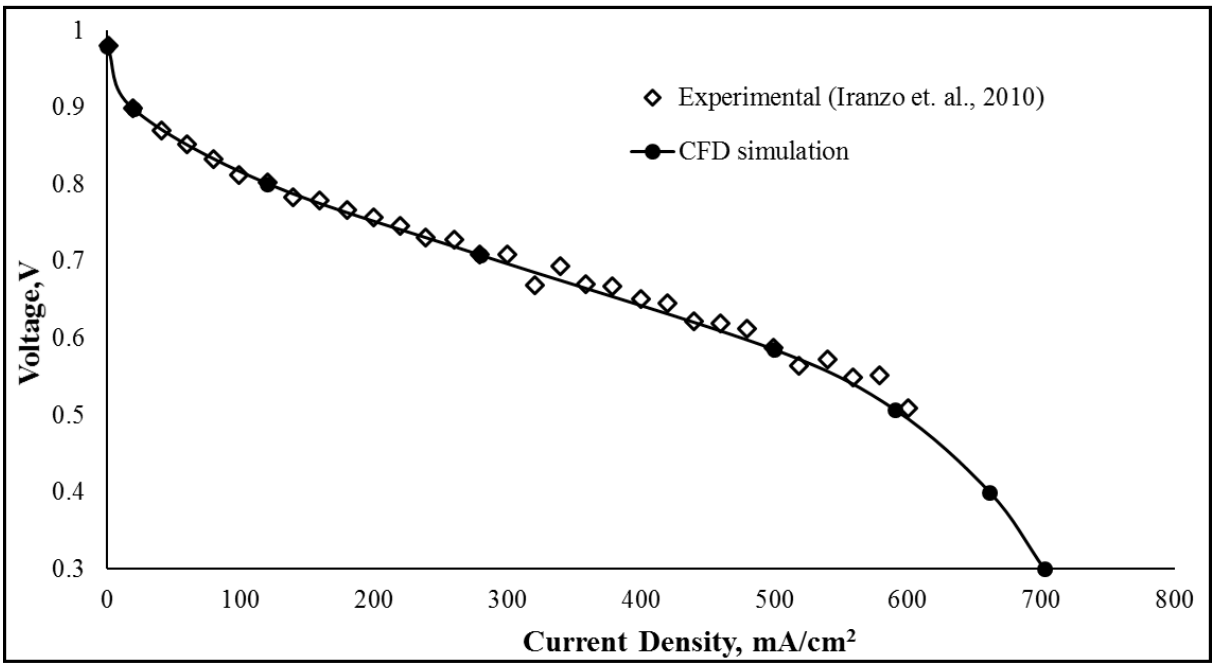

(b)

Figure 3.6 Model validation against the experimental works of (a) Limjeerajarus et. al. [123] with parallel flow field and (b) Iranzo et al. [121] with 5- path serpentine flow field.

Chapter 4

Superiority of ECSSFF Design over Triple Serpentine Flow Field

Superiority of ECSSFF design over Triple serpentine flow field design

The first objective of the present study is addressed in this chapter by conducting a detailed performance analysis of a rectangular cross-sectional PEM fuel cell with a 3-channel ECSSFF flow field on cathode side. The performance of the cell with ECSSFF design is also compared against the performance obtained from triple serpentine flow field design. The cell performance is simulated using a 3-D multiphase CFD model and the modelling methodology and simulation strategy followed are detailed in Chapter 3. The performance is evaluated in terms of their polarization curves at different cell operating temperatures and inlet reactants relative humidity. The simulation results are discussed in detail in the following sections.

4.1 Description of cases and geometries considered

In the present work, performance comparison of two cases is presented using CFD modelling of full-scale PEM fuel cell. 3-D model of PEM fuel cell is developed in Solid works® 2010 and ANSYS® 17.2. The two cases studied are – (i) Fuel cell having ECSSFF flow filed design on cathode side and parallel flow filed on anode side and (ii) Fuel cell with Triple serpentine channel design on cathode and parallel flow channel on anode side. The performance of both the fuel cells are compared by their polarization curve by varying operating temperature and relative humidity of reactant gasses.

This work has been inspired from the study by Suresh et al. [68] and extended it for the detailed analysis on the ECSSFF design using full-scale fuel cell modelling. Hence, PEM fuel cell with active area of 55.55 cm^2 with the same flow channel and rib dimensions of 1 mm × 1 mm (used in Suresh et al. [68]) is considered for this part of the work. The dimensions of the cell considered are given in Table 3.1 and Table 3.2. The reactants entry into channels is considered in counter current direction. Another cell of the same active area with TSFF channel design having same channel and rib dimensions is simulated for performance comparison. The layouts of the two flow field designs, TSFF and ECSSFF are shown in Figure 3.2 (c) and (d). Both the fuel cells have

parallel flow design (Figure 3.2 (a)) on anode side. The generated PEM fuel cell geometry is meshed using cartesian grid. Grid & iterative independence studies are carried out as explained in Chapter 3. Figure 4.1 shows the variation in the simulated power density for different grid sizes and number of iterations. The mesh size finalized has 1.39 million elements and the number of iterations are fixed at 2500 after these grid and iterative independence studies.

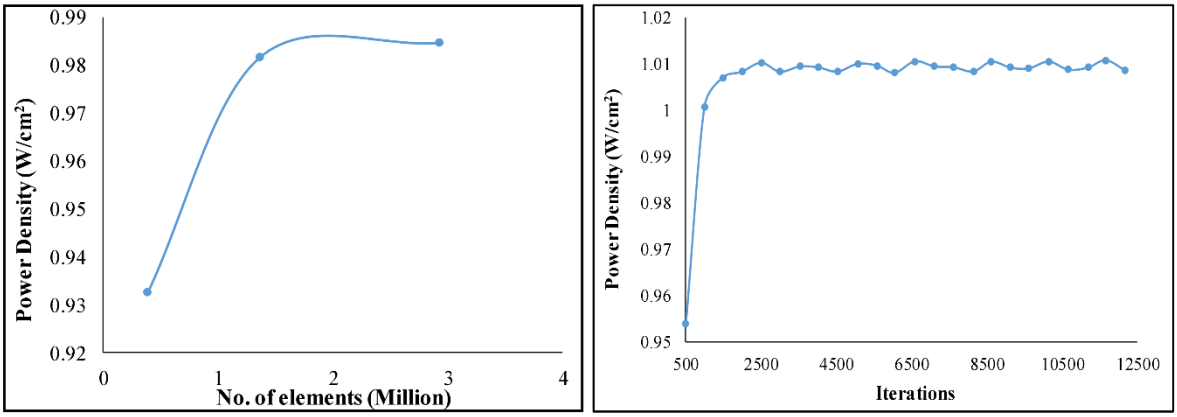

Figure 4.1 Grid and Iterative independence studies with ECSSFF design on cathode side at V=0.5 V.

4.2 Operating conditions

The present studies are carried out at constant boundary conditions by varying operating temperatures and relative humidity of inlet reactant gas. 100% pure hydrogen gas is considered on anode side in the present study. Material properties considered for the present simulations are taken from Iranzo et al. [121] and are listed in the Table 3.1 of previous chapter. The best combination of reactant flow rates in terms of anode stoichiometry (S_a) and cathode stoichiometry (S_c) is found by following the below procedure.

The performance of a fuel cell is largely dependent on the reactant availability at catalyst sites. To get an optimum PEMFC performance, it is desirable to have optimum reactant flow rates. Too little flow reduces the performance due to high concentration polarization resulting from lower available reactant concentration. On the other hand, too much flow also leads to lower performance due to increase in the ohmic loses resulting from higher water evacuation. In the present work, the

reactants stoichiometry is systematically analysed by fixing the anode stoichiometry (S_a) at 1 and varying the cathode stoichiometry (S_c) from1 to 4, with an increment of 1. The same procedure is followed for other values of S_a of 1.5, 2 and 2.5.

Table 4.1: Operating Conditions used in the present study

Variable	**Units**	**Value**
Fuel cell temperature	^oC	50, 60, 70 and 80
Operating pressure	kPa	200
Fuel cell current density	A/cm^2	1
Anode gas flow rate	kg/s	1.38×10^{-5}
Cathode gas flow rate	kg/s	5.96×10^{-05}
RH of inlet gas on anode and cathode sides	-	100%, 80%, 50% and 20%

Figure 4.2 shows the polarization and power curves of the PEM fuel cell with ECSSFF design on cathode side at different anode and cathode stoichiometries, along with the maximum current and power densities (Figure 4.2(e) & (f)) generated at different S_a and S_c. These are obtained at the cell operating temperature of 70 ^oC, 2 atm operating pressure and fully humidified reactants. It can be observed from Figures 4.2 (a) to (d) in general that the cell performance increases for any value of S_a with the increase in S_c because of supply of higher oxygen flow. As the ORR is the limiting reaction in a PEMFC, with higher O_2 concentration, more conversion takes place, which results in improved power output. Higher air flow rates also improve the water evacuation in the cell. The performance improvement is noticed till S_c increases to 3, beyond that the performance started decreasing. This trend is observed because, very high values of S_c (>3) reduces the residence time of the reactant in the cell and causes drying of the membrane, which ultimately deteriorates the cell performance [128]. Higher flow rates also increase the parasitic losses, which reduce the net power output [101].

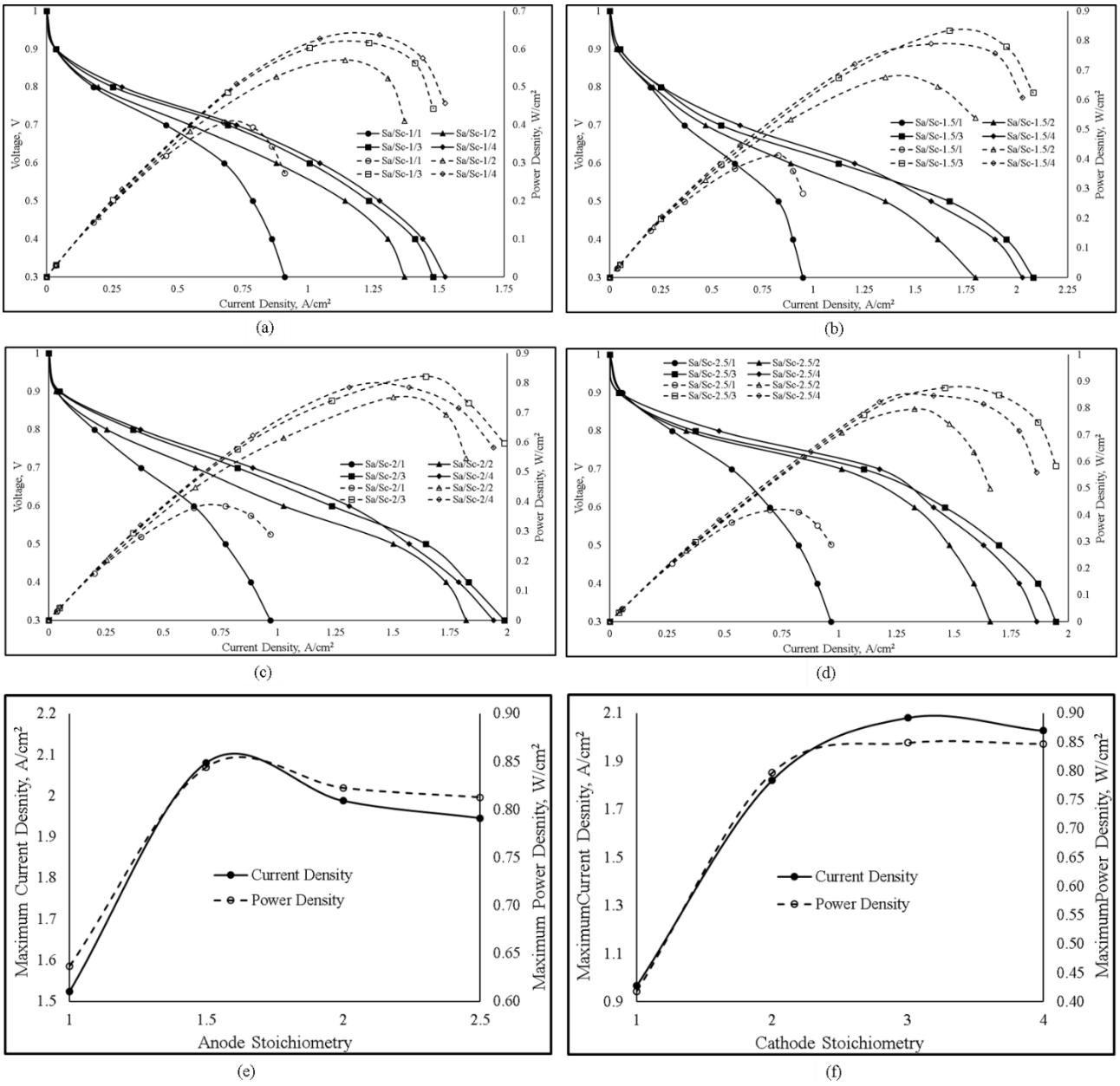

Figure 4.2 Polarization and power curves at different cathode stoichimetries (S_c) and anode stoichiometry (S_a) of (a) 1, (b) 1.5, (c) 2, (d) 2.5 and plots of (e) maximum current density and peak power density at 0.3 V obtained at various (e) S_a and (f) S_c.

Similarly, same was observed for hydrogen flow rate also, where the cell power output increased from S_a from 1 to 1.5 and then onwards, the performance decreased. The optimum set of stoichimetries for hydrogen and air can be clearly observed from the plots of maximum current

density at 0.3 V and peak power density generated at different anode and cathode stoichimetries as shown in Figures 4.2 (e) & (f). It can be noticed from this study that the maximum power density and maximum current density at 0.3 V are obtained at the optimum set of S_a = 1.5 and S_c = 3. Hence, the stoichiometry of 1.5 times for anode and 3 times for cathode is selected for further analysis. These results are in consistent with the studies of Badduri et. al [129] and Zhenzhong et. al [130]. Hence, flow rates of inlet gases are used as 3 times of stoichiometry which is equal to 5.96×10^{-5} kg/s in case of air and 1.5 times which is equal to 1.38×10^{-5} kg/s for hydrogen gas in further studies. The various operating conditions used in this study are given in Table 4.1.

4.3 Performance comparison between the PEM fuel cells with ECSSFF design and TSFF design

The performance analysis of PEM fuel cell using ECSSFF design on cathode side, in terms of the polarization curves, contour plots of the oxygen and water mass fractions in the catalyst layer and channels, contours plots of membrane water content and current flux density, pressure drop and net power output, is obtained for different operating temperature and relative humidity ranges used for the reactants in practical situations. The performance is also compared against that of the cell using Triple serpentine flow design on cathode side.

4.3.1 Polarization curves

For comparing the performance of flow field designs, the polarization curve (IV) and IP curve of the two fuel cells are compared. Both the fuel cells are operated under similar operating conditions and all the material properties are same for both the cells except the cathode side flow field designs. Figures 4.3(a) and (b) show the IV and IP curves of both the fuel cells with ECSSFF and TSFF on cathode sides operated at a relative humidity of 20 % for both the reactants with varying operating cell temperatures. It can be observed that at lower current densities, the fuel cells with ECSSFF and TSFF show similar performance and at higher current densities, ECSSFF shows better performance at lower relative humidity of 20% of the reactants. At lower current densities, formation of the water is less and hence both the flow fields show the same performance, whereas at higher current loads, formation of water is high and ECSSFF gives better performance because of its better water management capability. Decrease in the cell performance with increasing the

temperature can also be noted at this lower humidification of the reactant gas streams from Figure 4.3 (a) and (b). As the cell temperature increases, humidification of the gases on anode and cathode and the water formed may not be sufficient to keep the membrane sufficiently hydrated, resulting in higher ohmic losses and hence displays reduction in the performance.

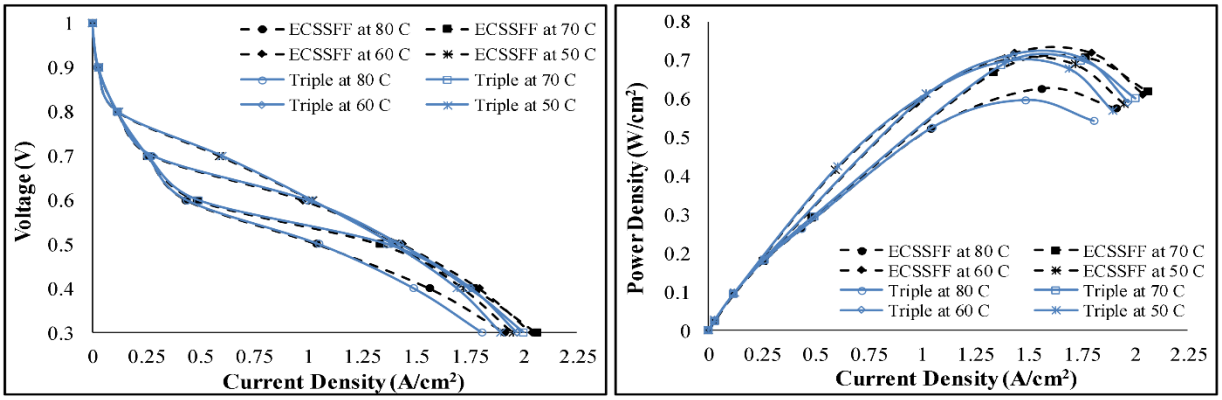

(a) (b)

Figure 4.3 Comparison of (a) IV and (b) IP curves between fuel cells with ECSSFF and TSFF at RH = 20 % on both sides and different cell temperatures.

Figures 4.4 (a) and (b) illustrate the polarization curve and IP curves of PEMFC with ECSSFF and TSFF at constant RH of 50 % on both anode and cathode sides and varied cell temperatures. Fuel cell with ECSSFF performed better than that with triple serpentine at higher current densities at RH of 50%. But when operated at lower current densities both flow channels performed alike. At this humidification level on both sides, the increase in cell temperature improves the performance and an extended current density values at lower voltages can be seen. This is because of the better water management capability of the ECSSFF design over TSFF.

Figures 4.5(a) and (b) show the IV and IP curves of the fuel cells with the two different cathode side flow field designs operated at constant RH of 80 % on cathode and anode sides and varying cell temperatures. Similarly, the performance comparison curves corresponding to cathode and anode side relative humidity of 100% are shown in Figures 4.6(a) and (b).

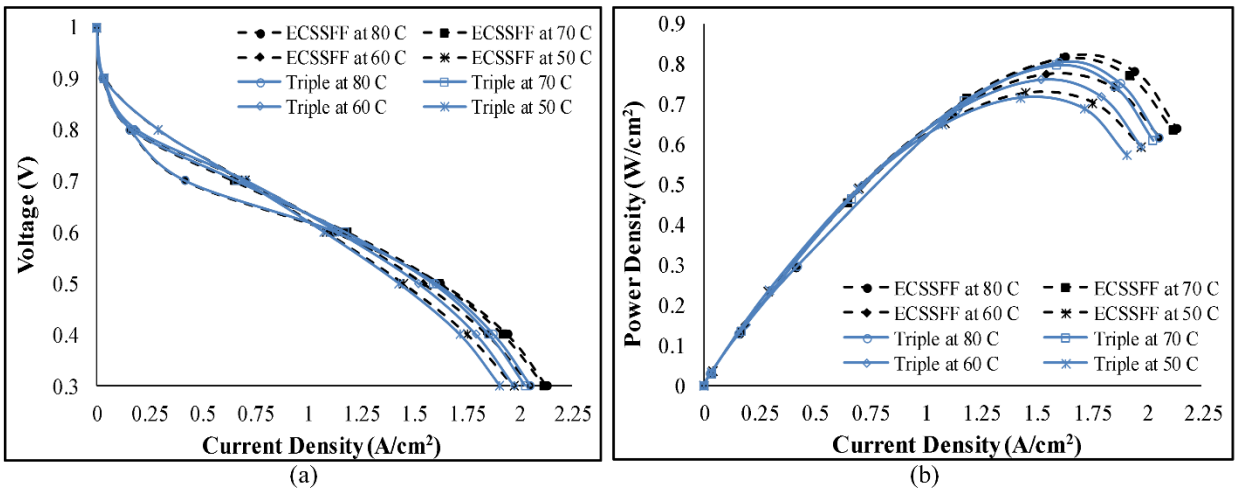

Figure 4.4 Comparison of (a) IV and (b) IP Curves between fuel cells with ECSSFF and TSFF at RH = 50 % on both sides and different cell temperatures.

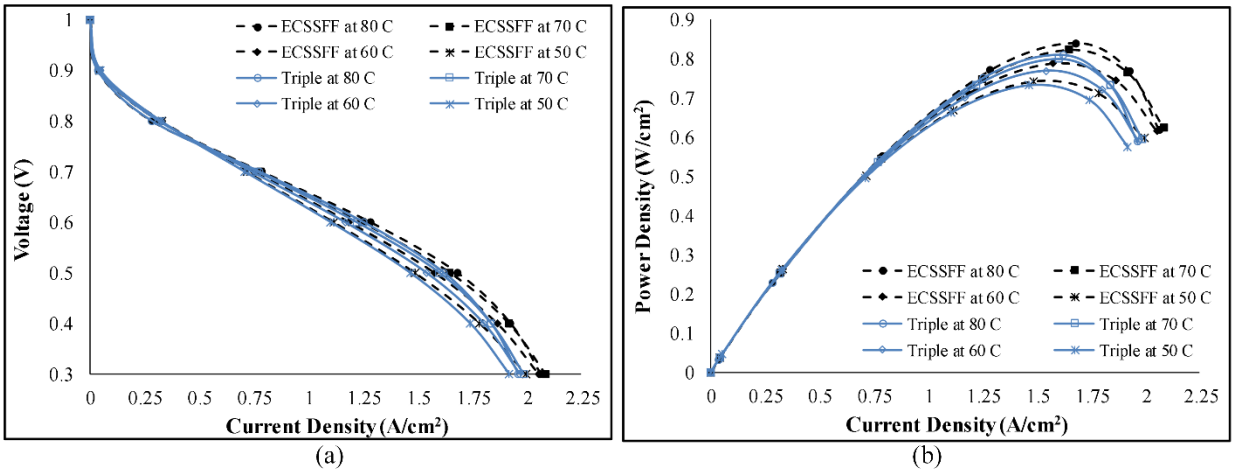

Figure 4.5 Comparison of (a) IV and (b) IP Curves between fuel cells with ECSSFF and TSFF at RH = 80% on both sides and different cell temperatures.

In all these cases, it can be clearly observed that ECSSFF exhibits better performance than TSFF, when higher currents are drawn from the cell at lower voltages. It can also be observed that the rise in cell temperature beyond 70°C slightly has a detrimental effect on the performance of cell at higher operating relative humidities of the reactant gases and higher current densities. This could be because of more generation of water at high temperatures and higher % RH of the gases on both sides.

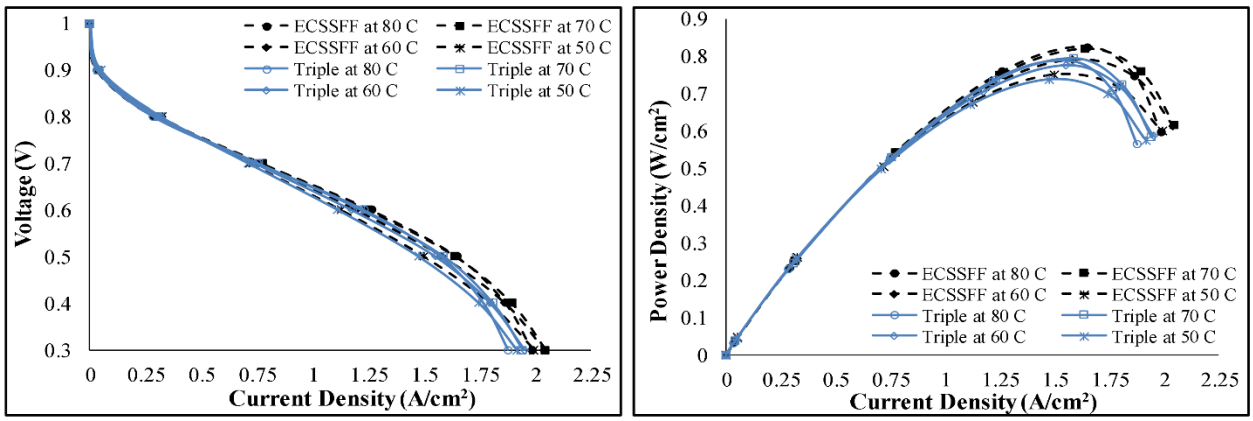

(a) (b)

Figure 4.6 Comparison of (a) IV and (b) IP Curves between fuel cells with ECSSFF and TSFF at RH = 100% on both sides and different cell temperatures.

It can be observed from Figures 3 through 6 that the difference between the values of highest current density in ECSSFF and triple serpentine is increasing as the relative humidity of reactant gasses is increased. In general, all these trends of effect of % RH and temperature on the cell performance are qualitatively in consistent with the studies reported by Ozen et al. [95], Carcadea et al. [17] and Zhang et al. [131].

Figures 4.7(a) and (b) show the IV & IP plots of the PEM Fuel Cell with both flow field designs used on cathode side operated at a constant temperature of 70 ^{o}C and different % RH of the reactant gas streams. It can be clearly seen from these figures that the ECSSFF exhibits superior performance especially at lower voltages in extending the power of drawing more current load. Hence, these figures demonstrate that ECSSFF is very useful flow field design to be used on cathode side, if one wants to draw higher current densities at all humidification conditions. This is mainly because of better water removal capability and good hydration of the membrane leading to better water management within the cell and better reactant distribution resulting from enhanced cross-flow of the reactant to the reactant-lean areas in case of the fuel cell with ECSSFF layout on cathode side as compared to that with TSFF design. Similar behaviour is observed for all other cell temperatures (50^{o}C, 60^{o}C & 80^{o}C) considered in this study.

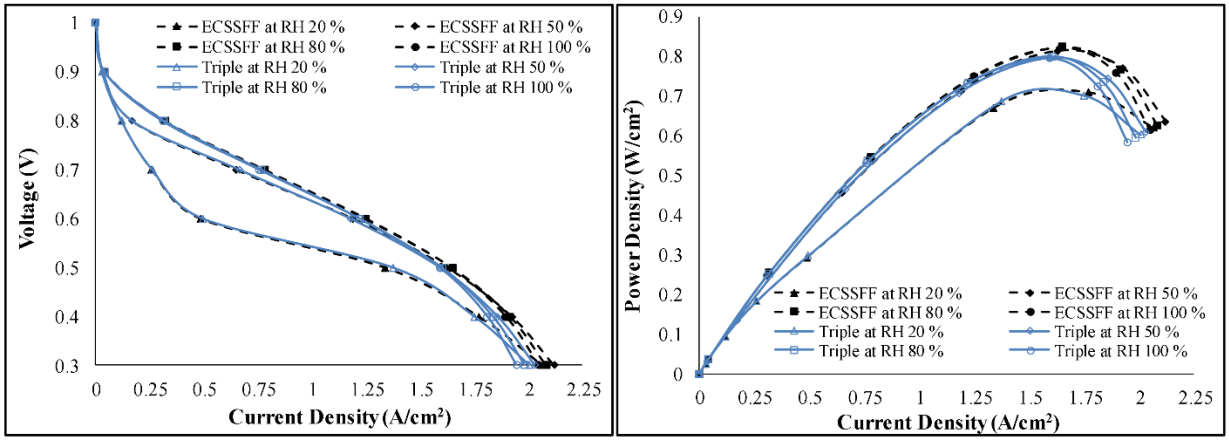

(a) (b)

Figure 4.7 Comparison of (a) IV and (b) IP Curves between fuel cells with ECSSFF and TSFF at cell temperature of 70°C and different % RH of the gas streams.

4.3.2 Contour plots

The superiority of ECSSFF design over TSFF design in extending range of current densities can be clearly elucidated by observing the contour plots of water mass fraction, oxygen mass fraction in catalyst layer and flow channels; water content in the membrane and membrane protonic conductivity; and current density distribution in the cathode catalyst layer. These are shown in Figures 4.8 to 4.11 for the operating condition of 80% relative humidity and 70 °C temperature at 0.5 V. Mid-planes in the thickness direction are created for cathode side flow field, cathode catalyst layer and membrane for observing the contours of the above parameters.

Figures 4.8(a) and (b) display the contours of water mass fraction at the mid-plane of cathode catalyst layer and cathode flow channel in the fuel cells with ECSSFF and triple serpentine flow field respectively. It can be observed from the water mass fraction contours in the cathode catalyst layer and flow channel of cell with TSFF that, there are some areas which are colored green indicating higher water mass fractions in the catalyst layer and also about 40% of the flow channels region is having higher water content. On the other hand, the water mass fraction profiles in case of ECSSFF shows lesser water content throughout the cell area and only less than 10% of the flow channels is having higher water content compared to other areas. This shows the

superiority of ECSSFF over TSFF in water evacuation capability because of its enhanced cross-flow of the reactant to the flooding prone zones in the cell.

Figures 4.9(a) and (b) show the contours of oxygen mass fraction at the mid-plane of cathode catalyst layer and cathode flow channel in the fuel cells with ECSSFF and triple serpentine flow field respectively. From these contour plots, it can be observed that there are more areas in the catalyst layer and flow channels with high mass fraction of oxygen in case of ECSSFF compared to TSFF. This shows that oxygen is more evenly distributed and oxygen lean areas are replenished with fresh oxygen from the enhanced cross of the reactant because of the arrangement of the channels in the ECSSFF layout. This leads to an improved performance of the cell particularly at higher current loads.

Figures 4.10(a) and (b) represent the contours of membrane water content and membrane proton conductivity (S/m) at the mid-plane of the membrane. As the membrane proton conductivity of perfluorinated ion-exchange membrane such as Nafion is a strong function of its water content, higher the water content in the membrane reduces the dehydration of the membrane and increases its protonic conductivity. As can be observed from Figure 4.10(a), the water content in the membrane is high in case of ECSSFF compared to TSFF and hence higher and better distribution of proton conductivity is observed in case of cell with ECSSFF compared to that of Triple serpentine channel, as shown in Figure 4.10(b).

The contours of the current density at mid-plane of the cathode catalyst layer are shown in Figure 4.11. It can be noticed that the current flux density is higher at the U-bends in case of ECSSFF than the other portions because of cross-flow from the adjacent feeder channels into the U-bends. Overall, there are more such areas with higher current density flux in cell with ECSSFF compared to that of triple serpentine channel. This results in improvement in overall power output of ECSSFF.

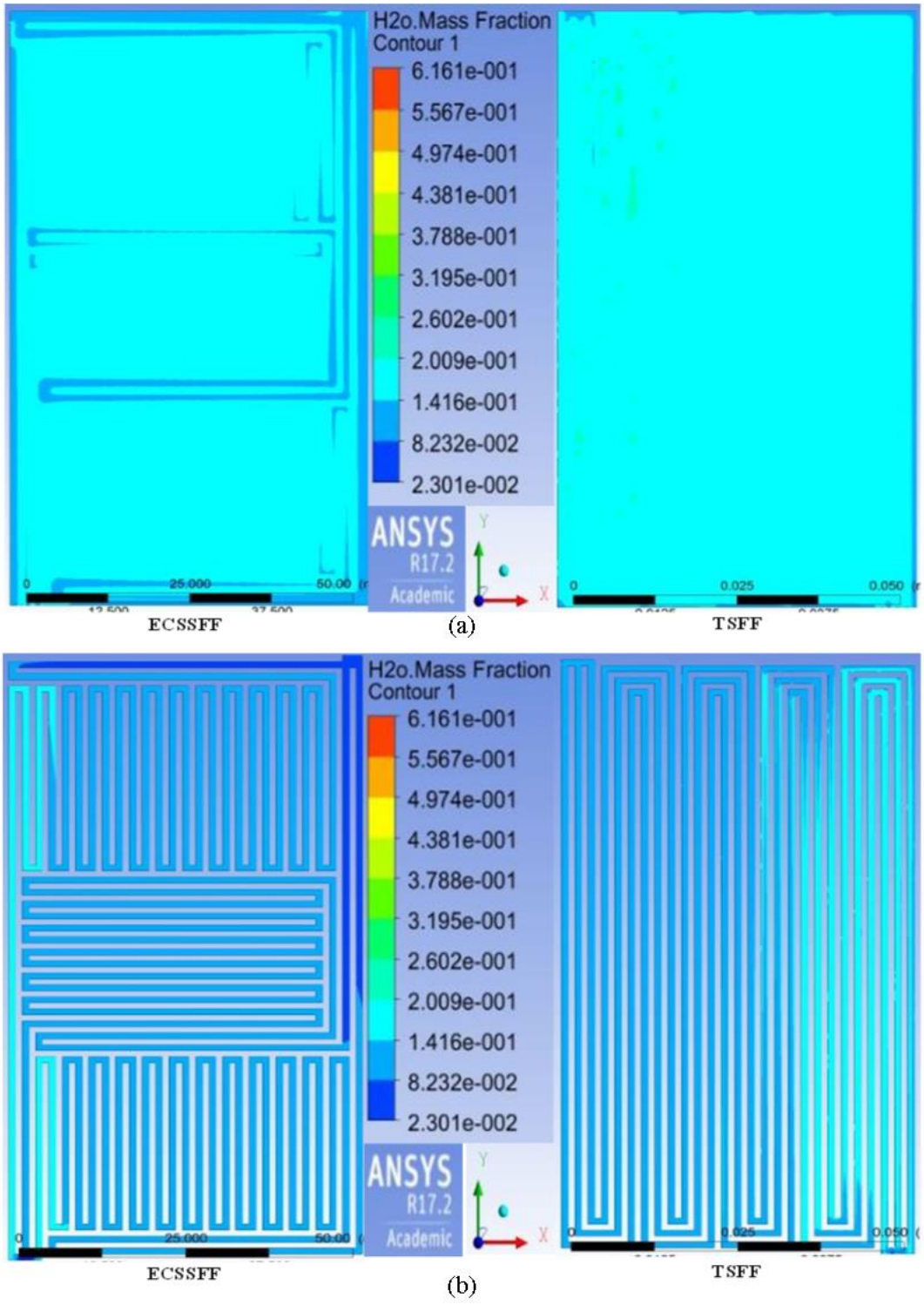

Figure 4.8 Contours of water mass fraction at the mid-plane of (a) Cathode catalyst layer and (b) Cathode flow channels in the cell.

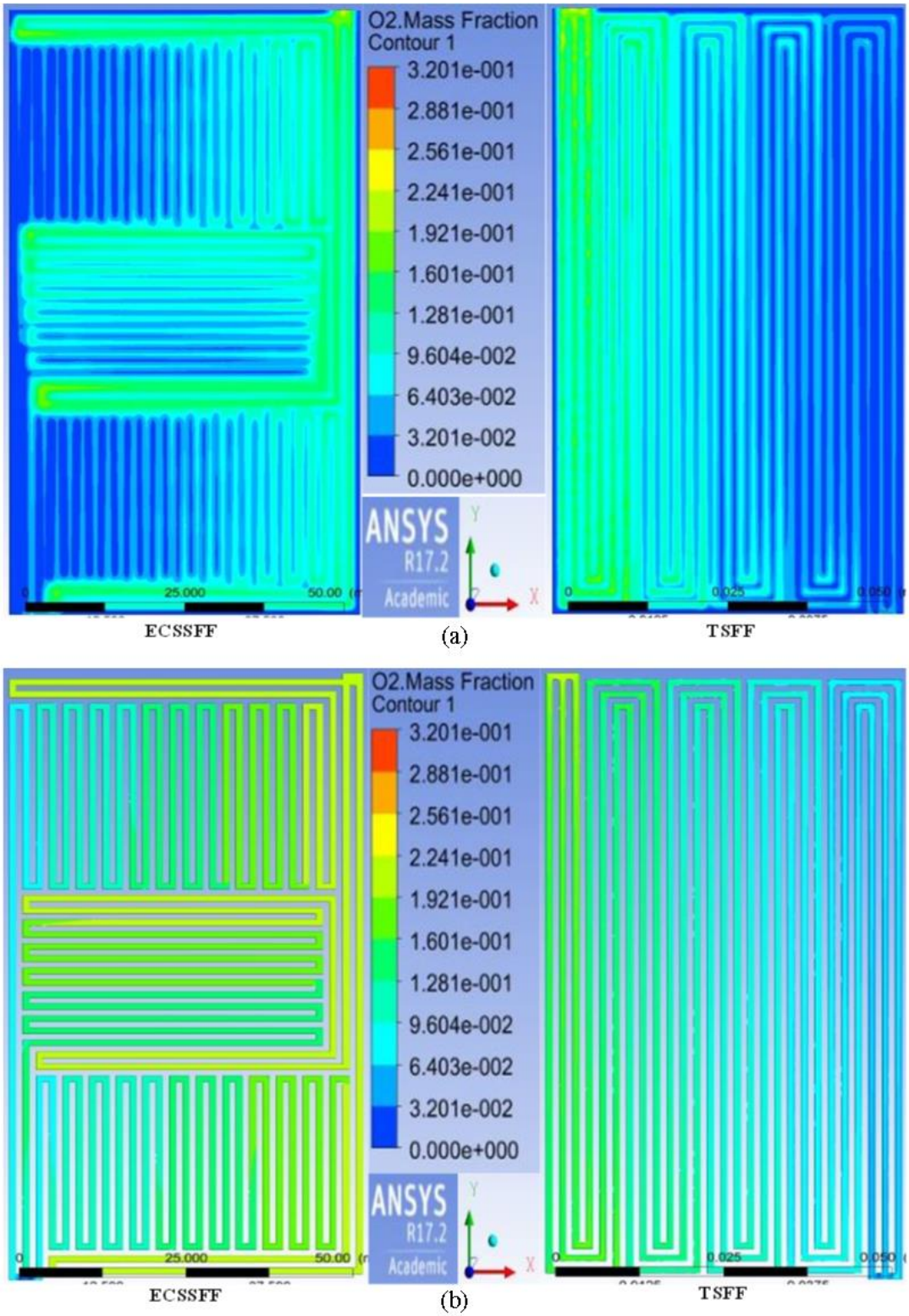

Figure 4.9 Contours of oxygen mass fraction at the mid-plane of (a) Cathode catalyst layer and (b) Cathode flow channels in the cell.

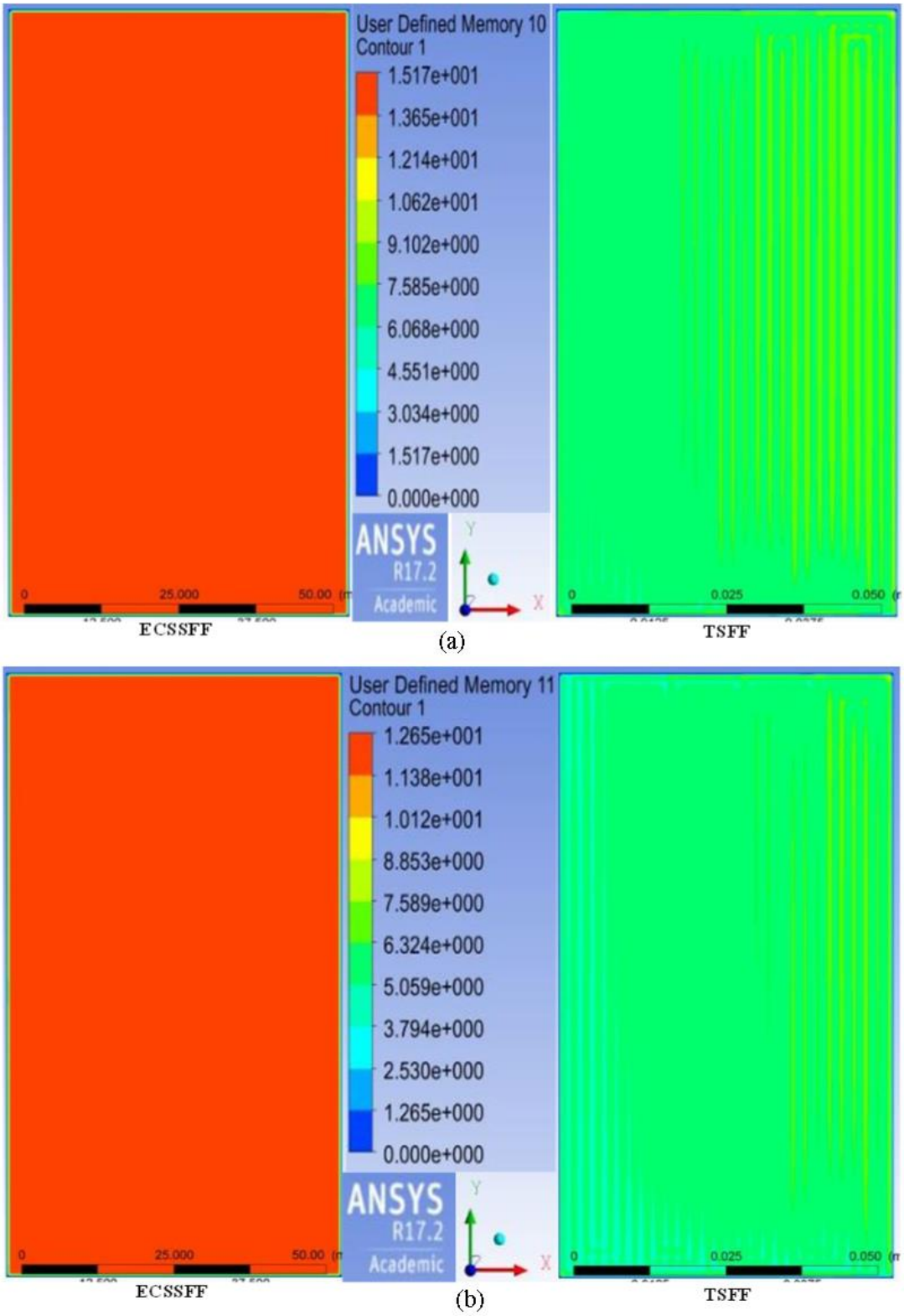

Figure 4.10 Contours of (a) Membrane water content and (b) membrane proton conductivity (S/m) at the mid-plane of the membrane in the cell.

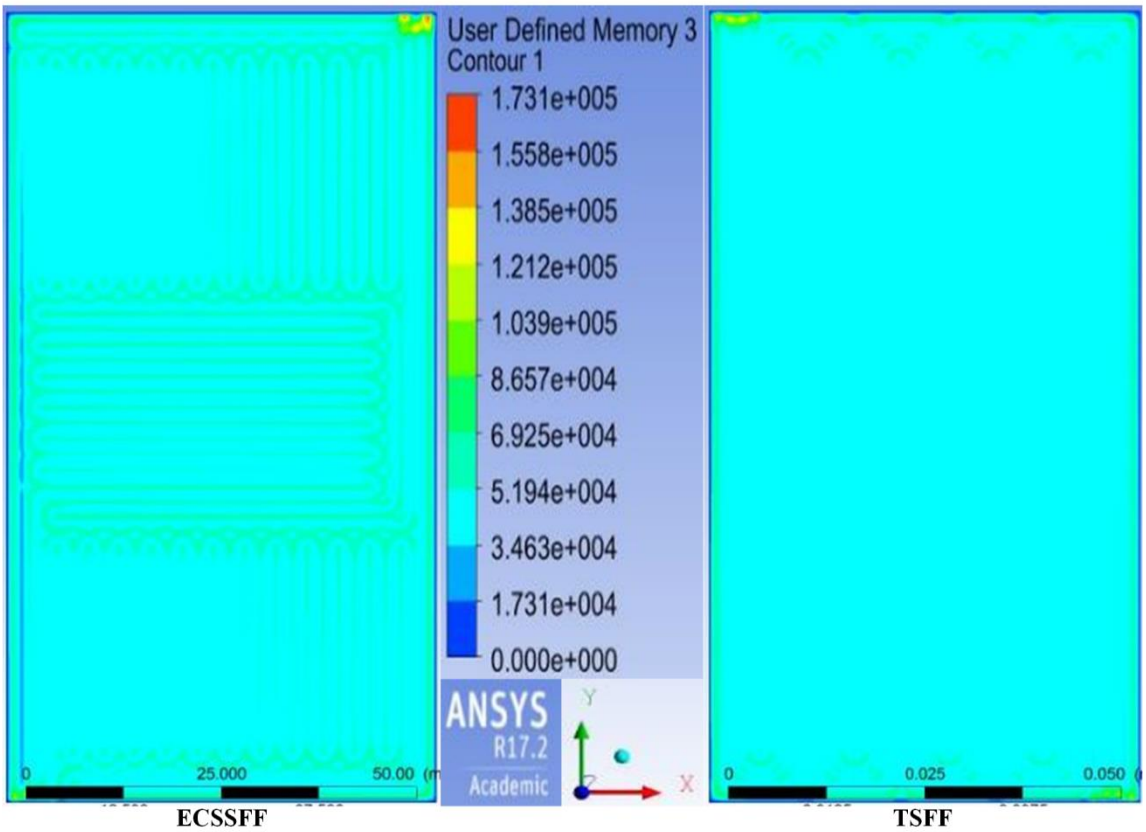

Figure 4.11 Current flux density contours at cathode catalyst layer in the cell with (a) ECSSFF and (b) TSFF on cathode side.

4.3.3 Comparison of pressure drop and net power output

The pressure drop for the flow of air in the two cathode side flow fields is computed and a comparison of the pressure drops in the flow fields at different relative humidities and cell temperatures is shown in Figure 4.12(a). It can be observed from Figure 4.12(a) that, pressure drop is increasing with increasing % RH and operating cell temperature. The increase in temperature improves the reaction kinetics, thereby forming more water and increase in %RH also increases the water content in the cell. This leads to higher pressure drops across the flow field. These trends are in agreement with the study of effect of relative humidity by Zhang et al. [131]. Under all the conditions of relative humidities and cell temperatures, it can be clearly observed that the pressure drop incurred in ECSSFF design is less (~ 20-23%) compared to that in TSFF. This is another important advantage of ECSSFF design as it reduces the parasitic losses, thereby improving the net

power output from the PEM Fuel cell. The calculation of parasitic (excess) power required for compensating the pressure drop is calculated as discussed in section 3.5 of chapter 3. The net power output from the cell is then calculated by subtracting the parasitic power from the gross power output. Figure 4.12(b) shows the effect of flow field design on the gross and net power outputs. The calculated pressure drop and the parasitic power for both the flow field designs at 100% RH of the gases, 80^{o}C cell temperature and 0.5 V operating voltage are also shown in Figure 4.12(b). This clearly shows that higher power output is obtained with ECSSFF compared to TSFF. Total pumping power required for the supply of air with these pressure drops is also calculated and found to be 4.36 W for ECSSFF and 4.5 W for TSFF at voltage of 0.5 V. Though this difference seems to be small, it can be noted that it will be much significant when the cell area increases (55.55 cm^2 cell area is only considered in this study) and for more number of cells as in case of a stack. Finally, the percentage improvement in power output by ECSSFF over TSFF at all operating conditions at 0.5V is calculated and shown in the Table 4.2. As it can be seen, ECSSFF showed improved performance over TSFF under all the operating conditions except at low % RH and high cell temperature. The improvement in the overall power output is still higher at lower voltages with ECSSFF compared to TSFF. Hence, this study demonstrates the superiority of ECSSFF performance over TSFF for the range of operating conditions considered in the PEM fuel cell operation.

Table 4.2 Percentage improvement in the cell power density with ECSSFF over TSFF for different operating temperatures and % RH at 0.5V.

Temperature, ^{o}C	**Percentage improvement with ECSSFF over TSFF**			
	RH =100%	**RH = 80%**	**RH = 50%**	**RH = 20%**
80	7.51	6.18	4.08	-1.96
70	6.27	5.63	4.21	1.41
60	5.81	4.87	4.11	1.48
50	5.55	3.47	3.92	3.09

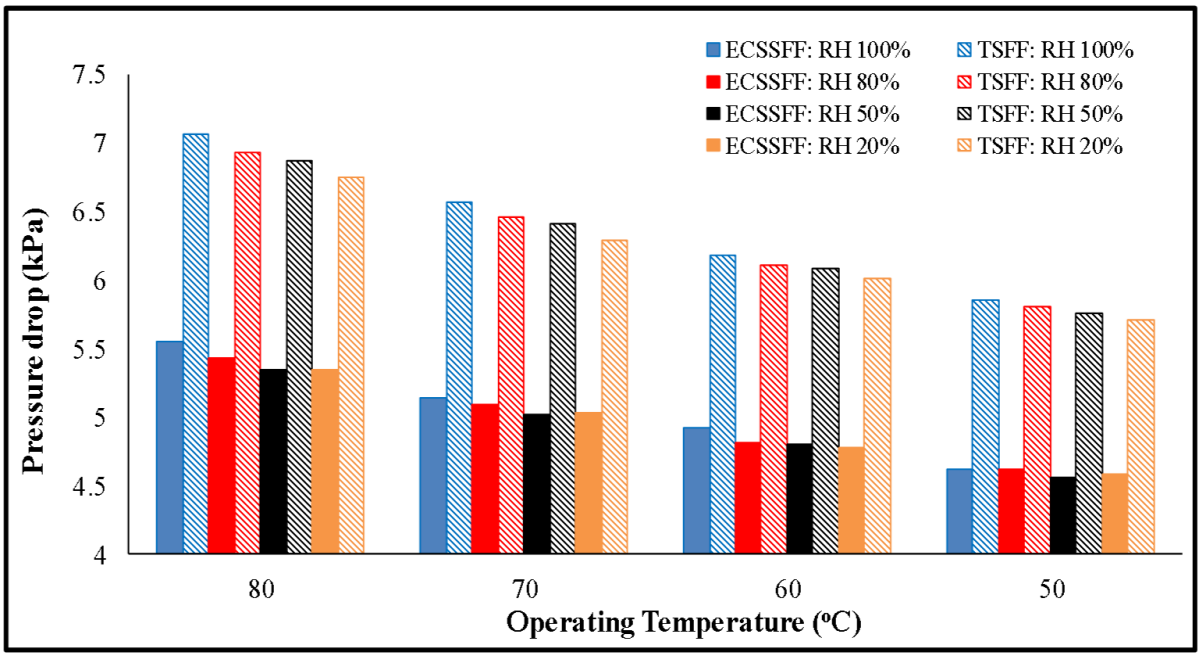

(a)

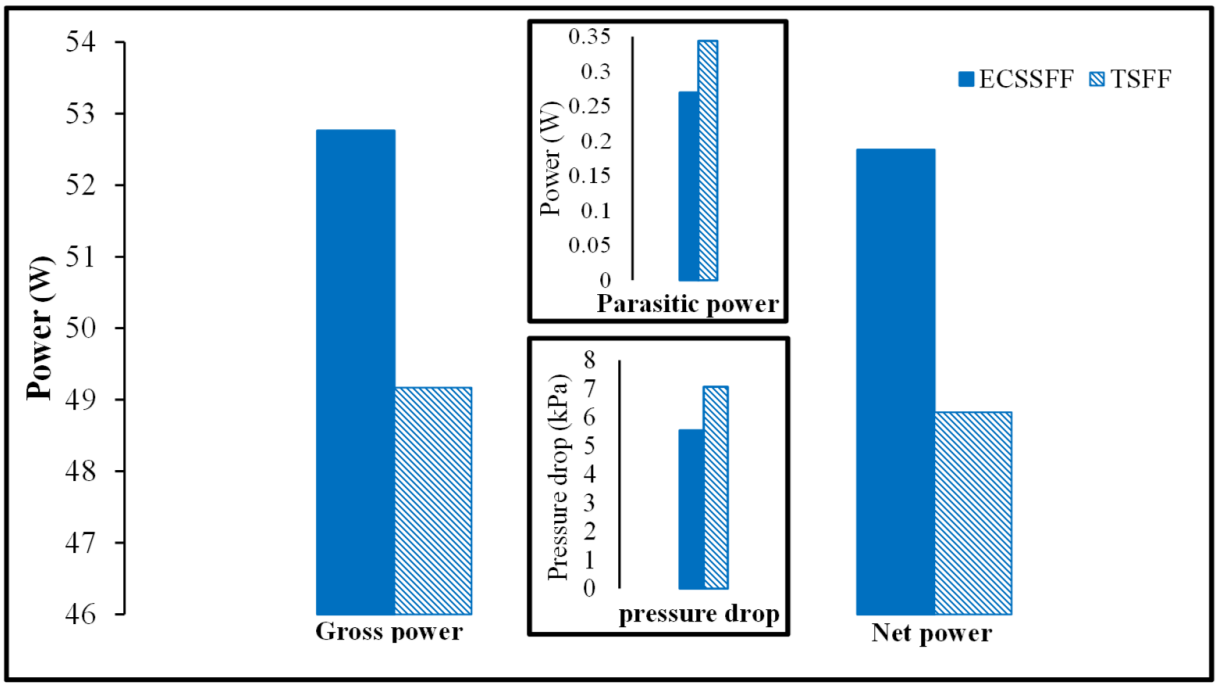

(b)

Figure 4.12 (a) Pressure drop comparison between ECSSFF and TSFF for different Operating temperatures and % RH at 0.5V and (b) Gross power, pressure drop, parasitic power consumption and net power comparison between ECSSFF and TSFF at RH 100% and 80 ^{0}C at 0.5V.

4.4 Summary

A complete 3-dimensional, two-phase CFD model of rectangular cross-sectional PEM fuel cell was used for comparing the performance of fuel cells using enhanced cross flow split serpentine flow field and triple serpentine flow field designs on cathode side. Detailed comparative analysis of the distribution of oxygen and water concentrations (in terms of mass fractions), membrane water content and protonic conductivity and current density were shown for both the flow field designs. The performance evaluation of ECSSFF and TSFF designs were carried out by varying the operating cell temperature and relative humidity of the inlet reactant gases. The key findings from present work can be summarized as,

- ECSSFF exhibited superior performance over TSFF under all operating conditions because of its inherent layout advantages of enhanced cross-flow in the flooding prone areas of U-bends in serpentine channels and oxygen replenishment in the oxygen lean areas of the cell.
- Membrane proton conductivity is better in ECSSFF compared to TSFF because of better water management.
- Parasitic losses are less in ECSSFF than TSFF due to less pressure drop and hence the net power output is high in the cell using ECSSFF on cathode side.

This study demonstrated the superiority of ECSSFF performance over TSFF for the rectangular cross-sectional PEM fuel cell and hence suggests ECSSFF design as a more desirable cathode channel layout over TSFF. The influence of channel and rib dimensions, especially channel width to rib width ratio, on the performance of the fuel cell is not studied in this chapter. This has been carried out in the next chapter. In addition, the performance comparison of the cells having ECSSFF design and single serpentine flow filed design under the identical operating conditions is also presented in the next chapter.

Chapter 5

Superiority of ECSSFF Design over Single Serpentine Flow Field Design

Superiority of ECSSFF design over Single Serpentine Flow Field design

The ECSSFF design is shown to be favorable over TSFF design in terms of offering high currents and low pressure drop, using detailed computational study conducted on the 55.55 cm^2 rectangular PEM fuel cell in the previous chapter. The power output of a PEM Fuel cell depends on the channel and rib dimensions, specifically ratio of channel width to rib width in the flow field and the operating conditions along with reactants and material properties. The present chapter focuses on the study of effect of ratio of channel width to rib width of ECSSFF design on the cell performance. In addition, the performance of the cell with ECSSFF design is also compared against the performance obtained with single serpentine flow field (SSFF) design. The SSFF design is chosen for comparison as it is one of the most widely used flow channel designs in commercial fuel cells. A parametric study is also carried out to find the best operating conditions for these channel designs. The performance of the cells with both the channel designs are compared using polarization curves for all the operating conditions to show the superiority of the ECSSFF channel design. Henceforth, the second and third objectives of the present study as listed in Chapter 2 (section 2.6) are addressed in this chapter.

5.1 Description of cases and geometries considered

Two full scale fuel cell geometries are considered one with ECSSFF design as cathode flow channel and another with SSFF design keeping anode side channel as SSFF for both the cells. All the geometries are created using SolidWorks® 2010 and then imported to ANSYS® 17.2. The active area of both the fuel cells is 55.55 cm^2. The dimensions of the cell considered are given in Table 3.1 and Table 3.2. The reactants entry into channels is considered in counter current direction. The ECSSFF channel design and SSFF designs are shown in Figure 3.2. Both the fuel cells have SSFF design (Figure 3.2 (b)) on anode side. The PEM fuel cell geometry is meshed using Cartesian grid in ANSYS ICEM CFD®17.2 and the grid for running the simulations is selected after grid independence study as explained in Chapter 3.

5.2 Operating conditions

Mass flow rates of the reactant gases are specified at the inlets by calculating them corresponding to a current density of 1 A/cm^2 with stoichiometric ratios of 3 and 1.5 times on cathode and anode sides respectively. The reactant flow rates are kept constant at 1.38×10^{05} kg/s for 100% pure hydrogen gas and 5.96×10^{-05} kg/s for air throughout the present work. The relative humidity of the reactants is fixed at 100%. Firstly, the channel to rib width ratios for both ECSSFF and SSFF channel layout are varied stepwise to find the best ratios of channel width to rib width. Then the channel layouts of ECSSFF and SSFF are designed with these best ratios and a parametric study of the fuel cells is carried out at different operating temperatures (60, 70 and 80^oC) & pressures (100, 200 and 300 kPa). The performances obtained by fuel cell with ECSSFF and SSFF are compared using polarization curves. The properties of the materials used in the present study are specified in Table 5.1 and the Table 5.2 lists the parameters which are used for the current study. The simulation strategy followed for obtaining the converged solution is as described in Chapter 3.

Table 5.1 Properties of the materials.

Property	Membrane	CL & GDL	Collector	Terminals
Density (kg-m^{-3})	1980 [132]	2719 [132]	2719 [132]	2719 [122]
Specific Heat (J-(kg-K)$^{-1}$)	2000 [132]	871 [132]	871 [132]	871 [122]
Thermal Conductivity(W-(m-K)$^{-1}$)	2 [132]	10 [132]	100 [132]	202.4 [122]
Electrical Conductivity (ohm-m)$^{-1}$	10^{-16} [132]	5000 [132]	1×10^{6} [132]	3.541×10^{7} [122]

Table 5.2 Parameters used in the current simulation study

Parameters		Value
Reference current density (A/m^2)	Anode	10,000 [132]
	Cathode	20 [132]
Reference concentration ($kmol/m^3$)	Anode	1 [132]
	Cathode	1 [132]
Concentration exponent	Anode	0.5 [132]
	Cathode	1 [132]
Exchange coefficient	Anode	2 [132]
	Cathode	2 [132]
Reference diffusivity	-	3×10^{-5} [132]
Viscous resistance of porous zone ($1/m^2$)		10^{12} [132]
Porosity	CL & GDL	0.5 [133]
Permeability (m^2)	CL & GDL	10^{-12} [70]

5.3 Effect of Channel width to Rib Width ratio of flow field designs on the cell performance

Cathode side pressure drop is generally higher than anode side pressure drop and is more sensitive to channel width to rib width ratio [26]. Hence in the present work, the effect of cathode channel dimensions is studied at operating temperature of 70 ^{o}C, pressure of 200 kPa with 100 % humidified reactants. Simulations are carried out systematically, by varying the channel width (CW) from 0.5 mm to 3 mm, while keeping the rib width (RW) constant at 1 mm for both SSFF design and ECSSFF design. The IV and IP curves of the fuel cell with SSFF design and ECSSFF design for different ratios of CW to RW are presented in Figure 5.1 with zoomed portion of the polarization curves to show the variation in ohmic loss region. It can be noticed that the performance of the fuel cell with SSFF is increasing with increase in CW to RW ratio from 0.5 mm to 1 mm and then it is decreasing for CW to RW ratios from 1 mm to 2 mm.

In the case of fuel cell with ECSSFF design, the improvement in performance is observed till CW to RW ratio of 2 mm and then it started decreasing with increase in CW to RW. The narrow

channel width increases the gas velocity which causes drying of the membrane near the channel inlet. This can be evidenced from the contour plots of membrane water content drawn at the mid-plane of the membrane for both the flow field designs as shown in Figure 5.2. The average membrane water content is lower for narrow channels and is improved for wider channels. This effects the proton transport and hence the ohmic losses are high for narrow channels. But with further increase in channel width, the reactant gas velocity decreases. At lower voltages, more water will be generated and should be evacuated to avoid flooding of the cell. The lower gas velocities have lower water evacuating capacity and hence causes flooding & results in higher concentration polarization. High CW will also result in low contact area between rib and GDL, which will affect the electron transport reducing the performance.

From Figure 5.1 (a), it can be perceived that for SSFF design, the maximum ohmic losses is observed for CW of 0.5 mm whereas the highest concentration losses is observed for CW of 2 mm. CW to RW ratio of 1 (CW=RW=1 mm) exhibited the best performance among all other channel widths considered for SSFF design. In case of ECSSFF design (Figure 5.1(b)), the CW to RW ratio of 2 (CW=2, RW=1) displayed the best performance compared to other channel ratios. This is because of the inherent characteristics of ECSSFF design such as induced cross-flow and better water evacuation capability [68], which help in reducing the water logging in the channels at higher CW to RW ratios up to 2 mm. The dimensions of the flow channel for the fuel cell should be selected in such a way that, the channels are neither too small which may cause hotspots and local drying of the membrane, nor too large which will significantly reduce the convective flow between channels [17]. CW by RW of 1mm by 1mm and 2 mm by 1mm displayed the best performance for SSFF design and ECSSFF design, respectively. The SSFF and ECSSFF channel designs with these CW by RW are used for further study. These results are in agreement with the observations made by [26] for SSFF design.

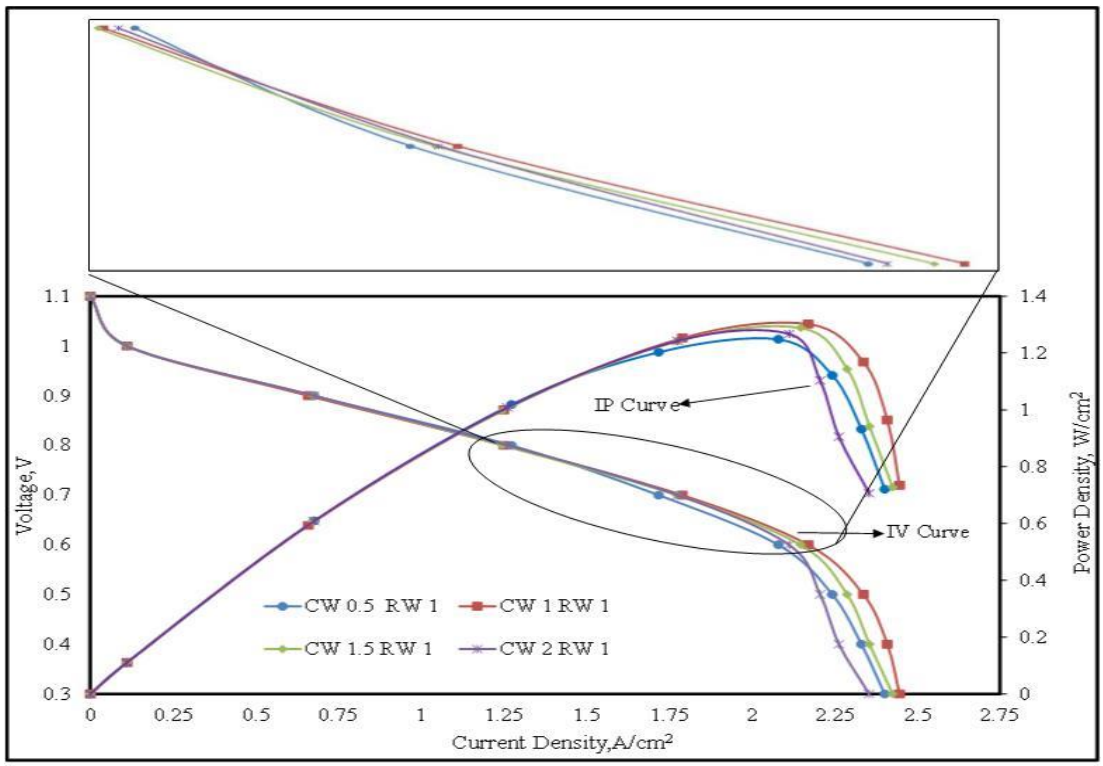

(a)

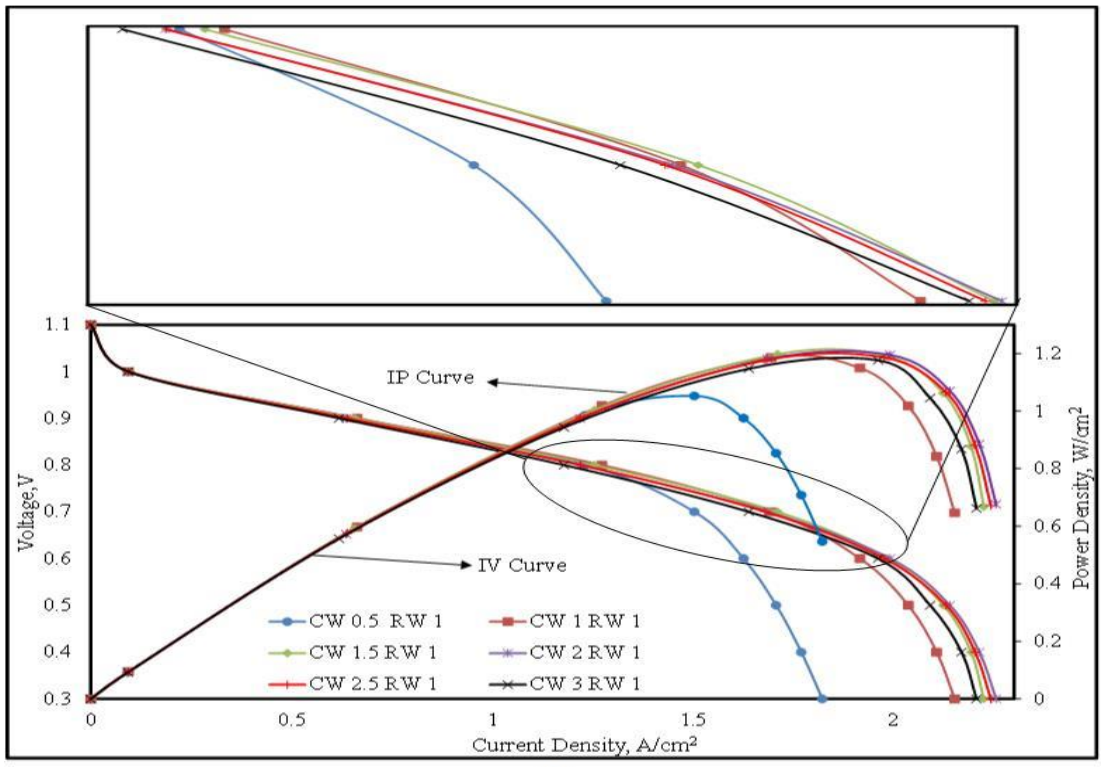

(b)

Figure 5.1 IV and IP curves of the fuel cell with (a) SSFF and (b) ECSSFF on cathode side.

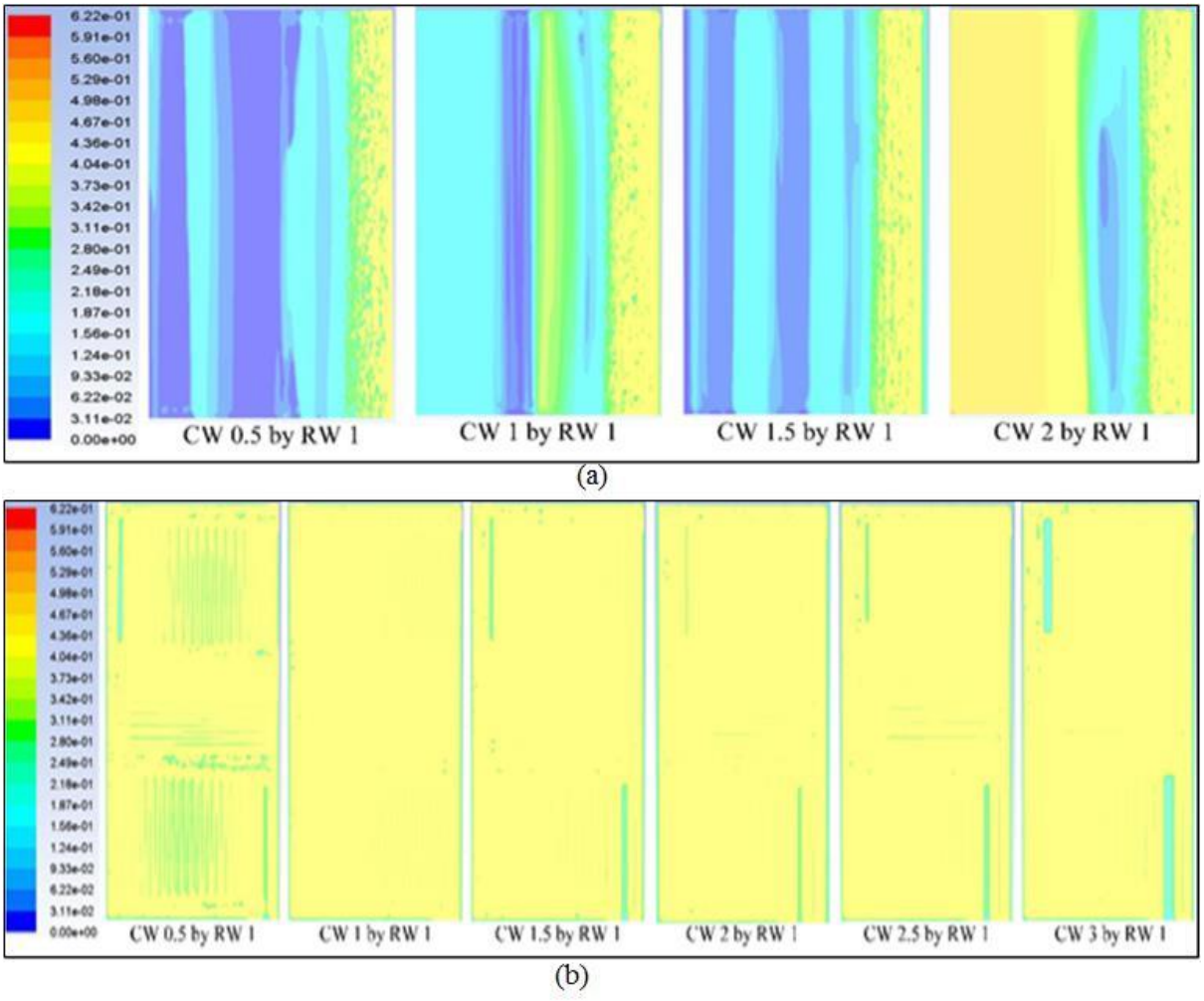

Figure 5.2 Contours of membrane water content for different CW at the mid-plane of membrane in the cell at 0.7V for (a) SSFF and (b) ECSSFF.

Figure 5.3 shows the variation of pressure drop with channel width on a semi-log scale for SSFF and ECSSFF designs at cell voltage of 0.4 V. In SSFF design, a single channel is running through the entire active area, hence the channel is long and all the reactant gases are forced through this long channel. Because of the lengthier channel and number of bends, the pressure drop due to friction is high. In case of the ECSSFF design, the flow gets split into three channels and they run through the entire active area as per the layout given in Figure 3.2 (d). The length of each channel and the reactant flow rate through each channel is less compared to the single channel in SSFF design and hence the pressure drop is one order of magnitude less for ECSSFF design. At lower channel widths of 0.5 mm, both the channels displayed highest pressure drop (245.23 kPa for SSFF

and 18.91 kPa for ECSSFF) as shown in Figure 5.3. About 70% decrease in pressure drop is observed for the increase in CW from 0.5 mm to 1 mm and 50% decrease in pressure drop for increase in CW from 1mm to 1.5 mm. With further increase in CW, the reduction in pressure drop decreases. High pressure drop causes more parasitic power losses and hence reduces the net cell power output. Too low pressure drop is also not advantageous as this will lead to very low cross flow, which causes flooding of the cell. At the CW to RW ratio of 1 for SSFF and 2 for ECSSFF, the pressure drops offered by these flow field designs are 56.7 kPa and1.5 kPa, respectively.

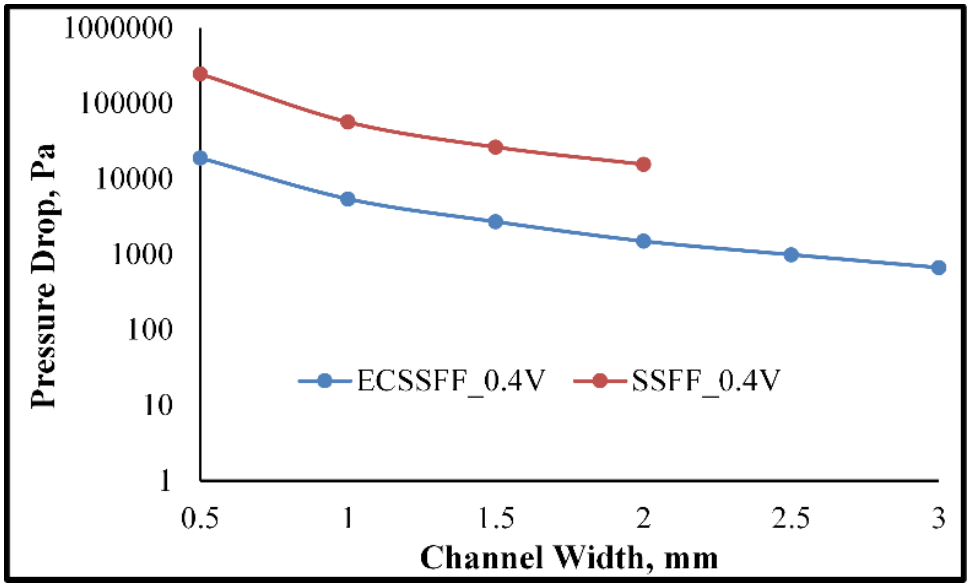

Figure 5.3 Pressure drop at different channel widths at operating voltage of 0.4V for SSFF and ECSSFF.

5.4 Performance comparison between fuel cells with ECSSFF design and SSFF design

The fuel cell IV and IP curves are obtained with the above finalized channel dimensions (CW to RW ratio of 1 for SSFF and 2 for ECSSFF) at 70 ^{o}C temperature, 200 kPa pressure and 100 % humidified reactants of both the flow field designs for performance comparison, which is shown in in Figure 5.4. It can be observed that the performance with ECSSFF design is almost similar to that with SSFF design, except only at low voltages, where the SSFF design could extend little more in offering the current densities. This difference is mainly because of the fact that entire reactant gas is entering through the single channel running throughout the domain causing less

mass transport losses at low voltages compared to ECSSFF, where the flow is divided into three channels. But this slight increase (average improvement is less than 2%) in the IV performance is at the expense of increased pressure drop with the SSFF. Hence, the pressure drop offered by the flow design, which is an important parameter in performance comparison is computed and compared in Figure 5.5.

The high pressure drop reduces the mass transport losses at the cost of increased parasitic losses. Parasitic loss is the excess power required to maintain the operating conditions. The actual useable power output from the fuel cell will be reduced with the increase in the parasitic losses. Figure 5.5(a) shows the pressure drop incurred in both SSFF and ECSSFF designs at different cell voltages and Figure 5.5(b) shows the corresponding parasitic losses. The method for finding the parasitic power loss due to pressure drop is same as discussed in section 3.2. It can be observed from Figure 5.5 that, the pressure drop in case of SSFF design is 30 times higher than that of ECSSFF design and results in greater parasitic losses (~20 times higher).

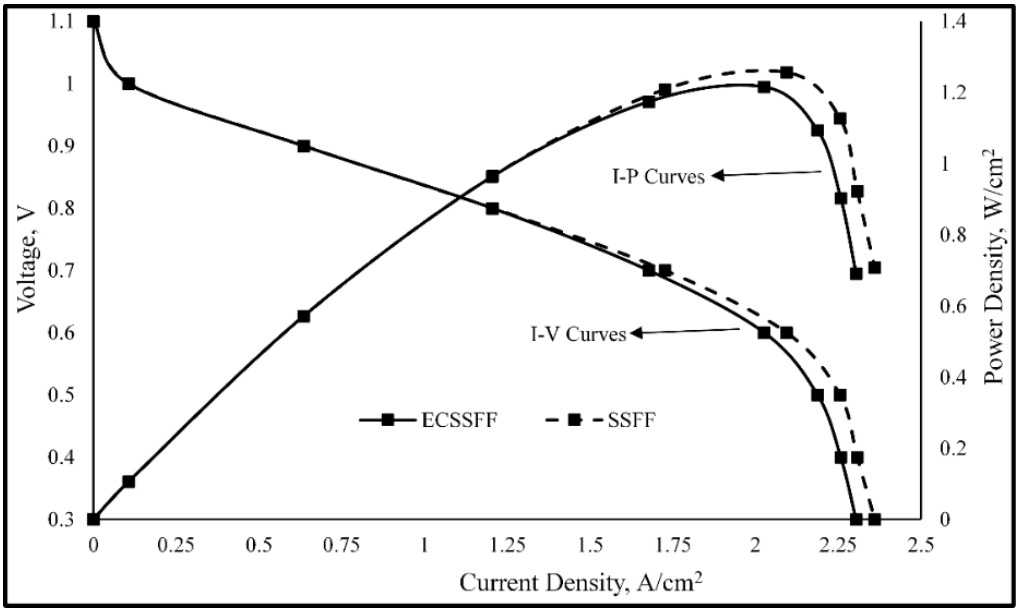

Figure 5.4 IV and IP curves of fuel cell with ECSSFF and SSFF at 70 ºC operating temperature, 200 kPa pressure and 100% relative humidity.

ECSSFF, with almost one third of flow rate in each channel, is showing almost equal performance (as shown in Figure 5.4) compared to the SSFF with full flow rate of reactants in the single channel by offering very less pressure drop and parasitic power (as shown in Figure 5.5). To further demonstrate the competitiveness of ECSSFF with respect to SSFF, two cases are investigated – (i) with same flow rate through each channel of ECSSFF as that of SSFF and (ii) maintaining equal pressure drop through ECSSFF and SSFF.

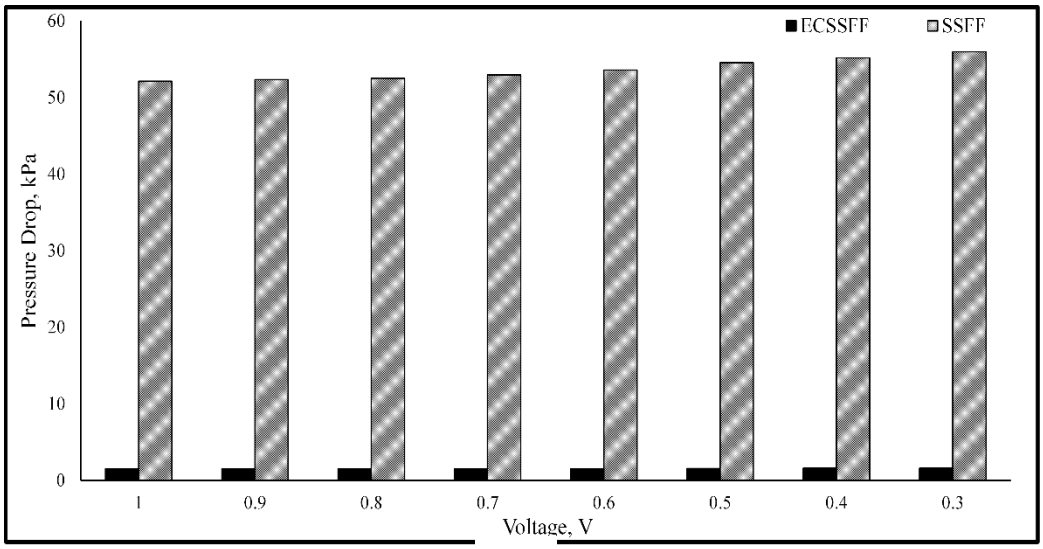

(a)

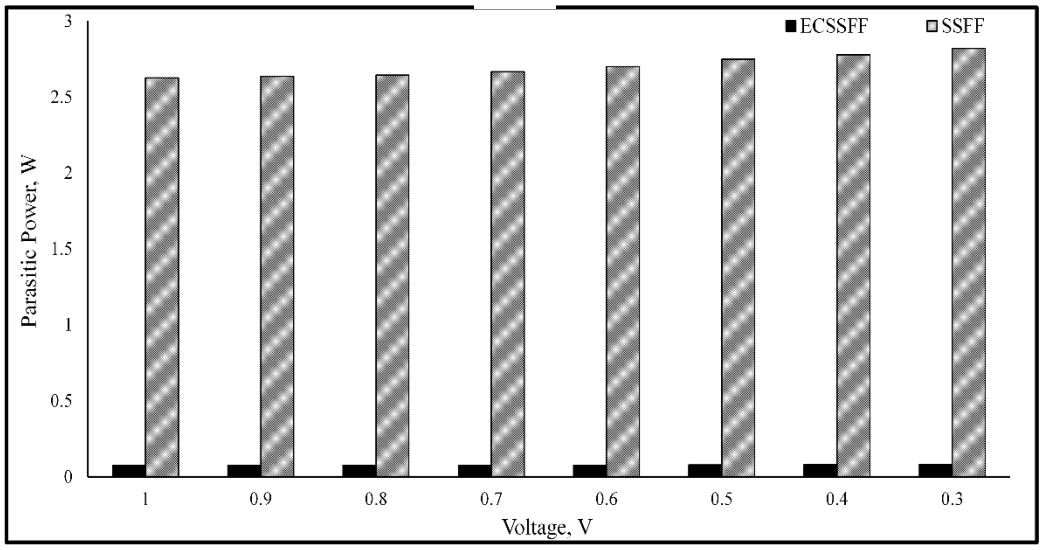

(b)

Figure 5.5 (a) Pressure drop and (b) Parasitic power loss of SSFF and ECSSFF at 70 ^{o}C operating temperature, 200 kPa pressure and 100% relative humidity.

5.4.1 Under same flow rate

In the first case, simulations are carried out by maintaining one third of the flow rate in SSFF, which is same as the flow rate through each channel of ECSSFF. Figure 5.6(a) shows the polarization and IP curves of the fuel cell and the pressure drop incurred is presented in Figure 5.6(b) for this case with the two flow fields. The limiting current density as well as peak power shown by ECSSFF are higher by around 145% and 70% compared to that shown by SSFF.

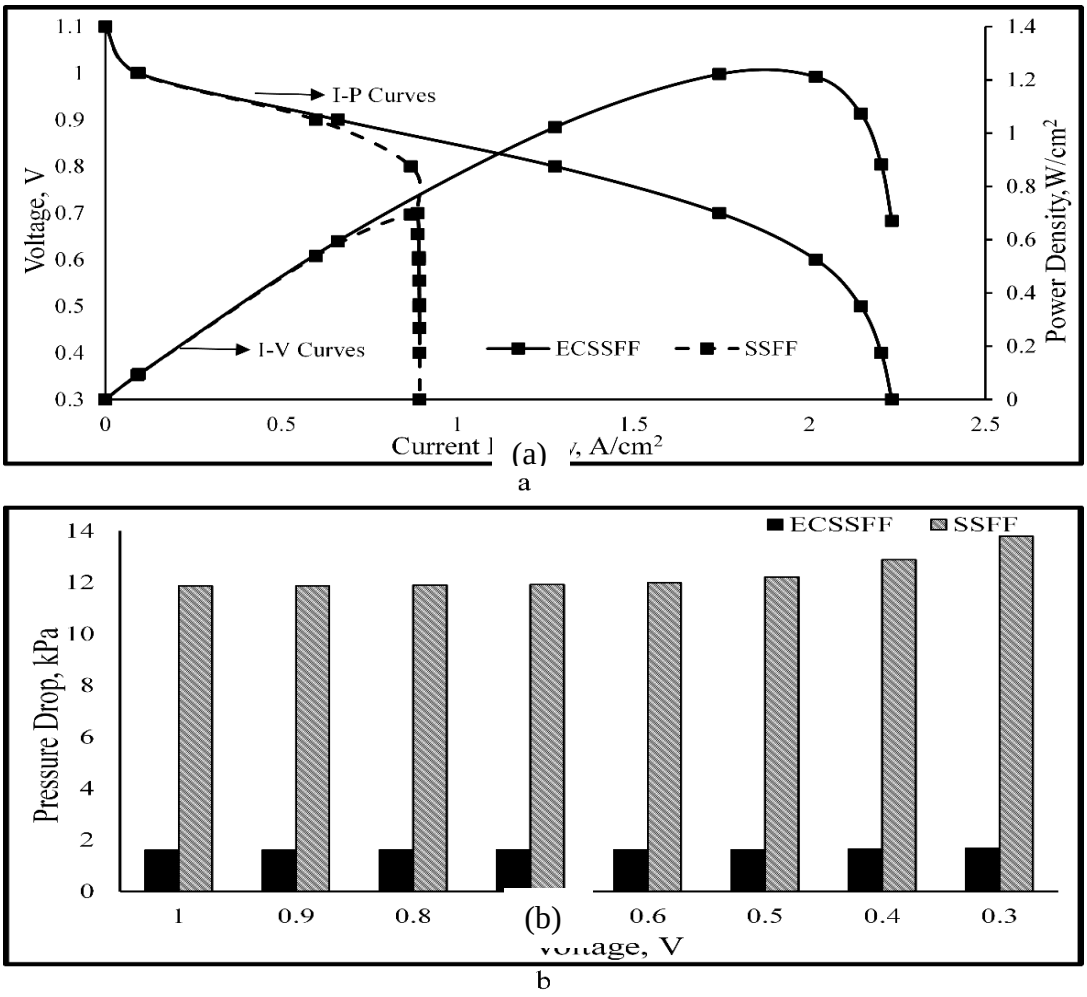

Figure 5.6 Comparison of (a) IV and IP curves and (b) pressure drop variation of fuel cells having equal air flow rate through SSFF and each channel of ECSSFF at 70 ^{o}C operating temperature, 200 kPa pressure and 100% relative humidity.

On the other hand, the pressure drop offered by ECSSFF is almost 10 times lower compared to that of SSFF, even though the flow rate in ECSSFF is 3 times that of SSFF. ECSSFF outperforms SSFF both in terms of extending to higher current densities and offering low pressure due to its inherent advantages of improved reactant cross-flow in the flow channel and higher tolerance to flooding.

5.4.2 Under same pressure drop

For the second case, simulations are carried out to observe the improvement in power output when the pressure drop in the fuel cell with ECSSFF is matched with the pressure drop of SSFF (Figure 5.7b). This is achieved by increasing the air flow rate by 10 times in case of ECSSFF when compared to that of SSFF. Figure 5.7 shows the polarization and IP curves of the cell with ECSSFF and SSFF flow fields and the pressure drops incurred for this case at operating temperature of 70 ^{o}C, pressure of 200 kPa with 100 % humidified reactants. It is evident from Figure 5.7(a) that the fuel cell with ECSSFF design does not experience mass transport losses even at low operating voltage of 0.3 V, and the maximum current density has been pushed by almost 100% more compared to that of SSFF. This is because of high flow rate of air, which improves the distribution of oxygen in the catalyst layer besides increasing the water evacuation capacity of the channel, thereby reducing the chances of flooding in the flow channel. ECSSFF could attain this higher current density by offering almost the same pressure drop as that of SSFF.

In general, the pressure drop that can be handled by a PEMFC is dependent on the capacity of the membrane/MEA to withstand the pressure difference before puncturing. So the fuel cells can only be operated within that pressure drop range to have better performance and also higher life span. The proposed ECSSFF channel is showing minimal pressure drop even when operated at high flow rates and better performance for the same pressure drop. From this comparison, it can be established that, ECSSFF channel layout is a better choice over SSFF layout.

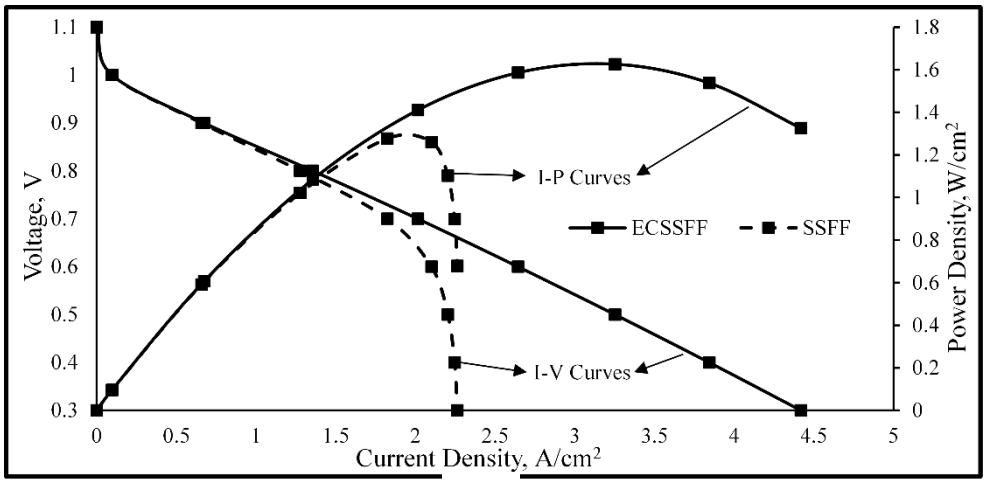

(a)

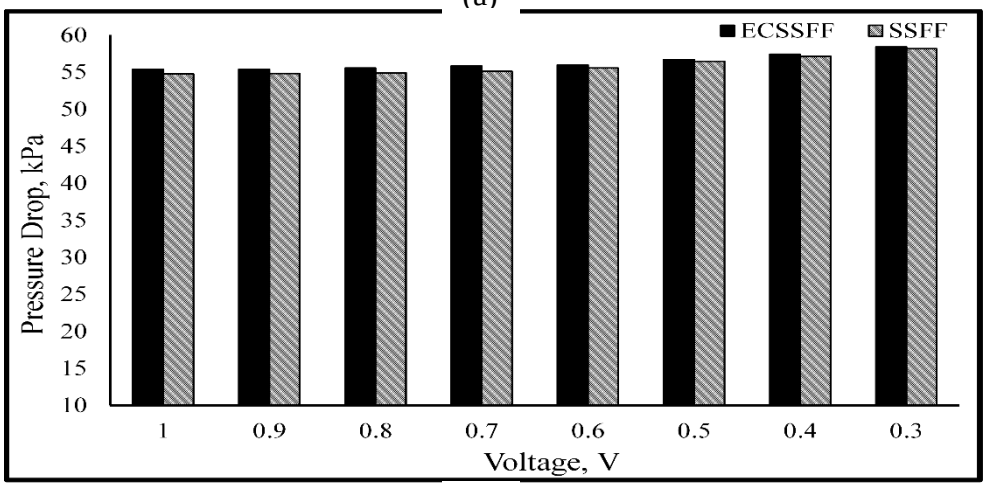

(b)

Figure 5.7 Comparison of (a) IV and IP curves and (b) pressure drop for fuel cells having air flow 10 times more with ECSSFF compared to that with SSFF at 70 ^{o}C operating temperature, 200 kPa pressure and 100% relative humidity.

5.5 Effect of parameters on the performance

Effect of Temperature:

To examine the effect of temperature on the fuel cell power output with the two flow field designs, both the cells are operated at a fixed pressure of 200 kPa and relative humidity of 100%. Temperature of the cell is varied from 60 ^{o}C to 80 ^{o}C with an increment of 10 ^{o}C. Figure 5.8(a) shows the polarization and IP curves of SSFF and ECSSFF at various cell operating temperatures.

It can be noticed that the maximum power density of both the fuel cells improves as the operating temperature is increased.

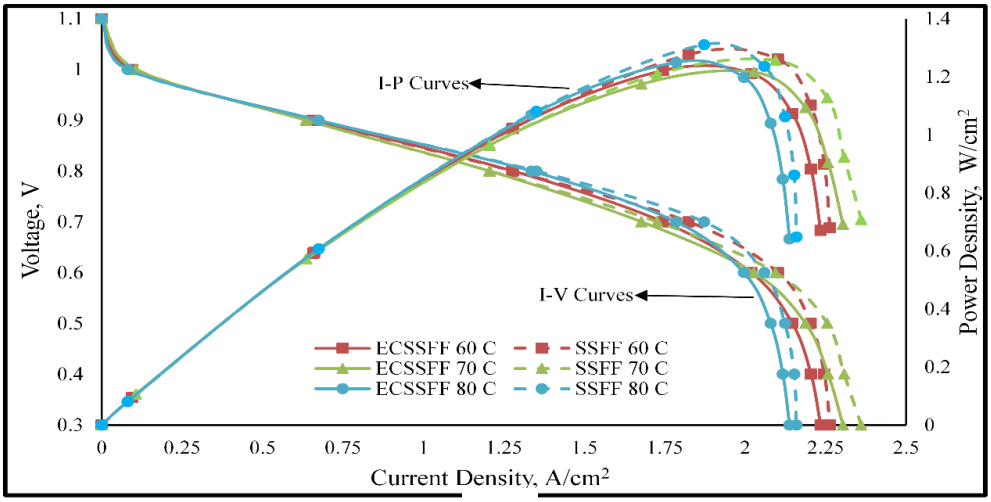

(a)

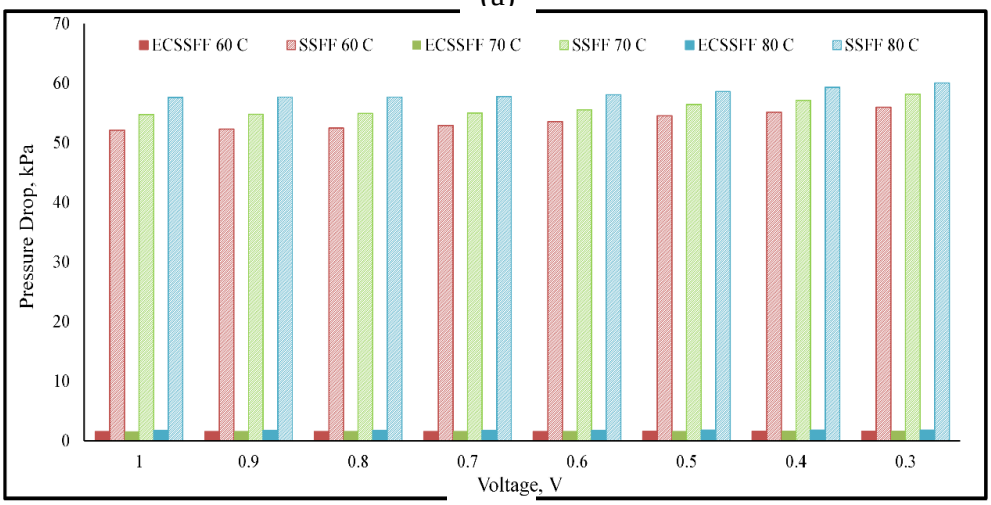

(b)

Figure 5.8 (a) IV and IP curves and (b) pressure drop of fuel cell with ECSSFF and SSFF for different operating temperatures at 200 kPa pressure and 100% relative humidity.

This trend is observed because, the reaction kinetics improves as the operating temperature increases[134]. This improvement in reaction kinetics is advantageous only up to the operating voltage of 0.7 V because, the water produced from the reaction is less. When the fuel cells are operated below 0.6 V, more water is produced. As the fuel cells are being operated at fully humidified condition, the excess water will result in flooding of the channel which will hinder

diffusion of reactant gases to the reaction sites, increasing the mass transport losses[83]. So a drop in the fuel cell performance with both the flow fields below 0.7 V is observed at low current densities with the increase in operating temperature. As discussed earlier, the performance of ECSSFF and SSFF is very close for all the temperatures. However, the pressure drop offered by ECSSFF is much lower compared to that of SSFF at all the temperatures as shown in Figure 5.8(b). So, the net power output from the cell with ECSSFF is higher than that with SSFF.

Effect of Pressure:

To explore the effect of the operating pressure on the performance, fuel cells with both the flow fields are operated at fixed RH of 100% and a temperature of 70 ^{o}C. The operating pressure is varied from 100 kPa to 300 kPa. Figure 5.9(a) shows the IV and IP curves of SSFF and ECSSFF at different operating pressures. It can be observed that the power output of both the fuel cells are improving as the operating pressure is increased which is consistent with the findings of Kahveci and Taymaz 2018[89].

This is due to the augmentation of mass transfer of gas reactants to catalyst layers. The higher operating pressure increases the reactant diffusivity, which decrease the mass transport resistance [105]. The reactant partial pressure and concentration upturns with increase in the operating pressure. The pressure drop incurred in a fuel cell increases as the operating pressure is increased which can be observed from pressure drop variation plot for the SSFF and ECSSFF in Figure 5.9(b). The performance displayed by the ECSSFF is on-par with that of SSFF with very low pressure drop even at high operating pressures. As can be seen from Figure 5.9, with increase in operating pressure from 100 kPa to 200 kPa, the performance improvement in terms of offering high currents is prominent compared to that from 200 kPa to 300 kPa. In addition, the increase in pressure drop with change in operating pressure from 100 kPa to 200 kPa is less compared to that with 200 kPa to 300 kPa. Hence, in view of operating with low compressor pumping power, it is preferable to operate the cell at the operating pressure of 200 kPa than 300 kPa.

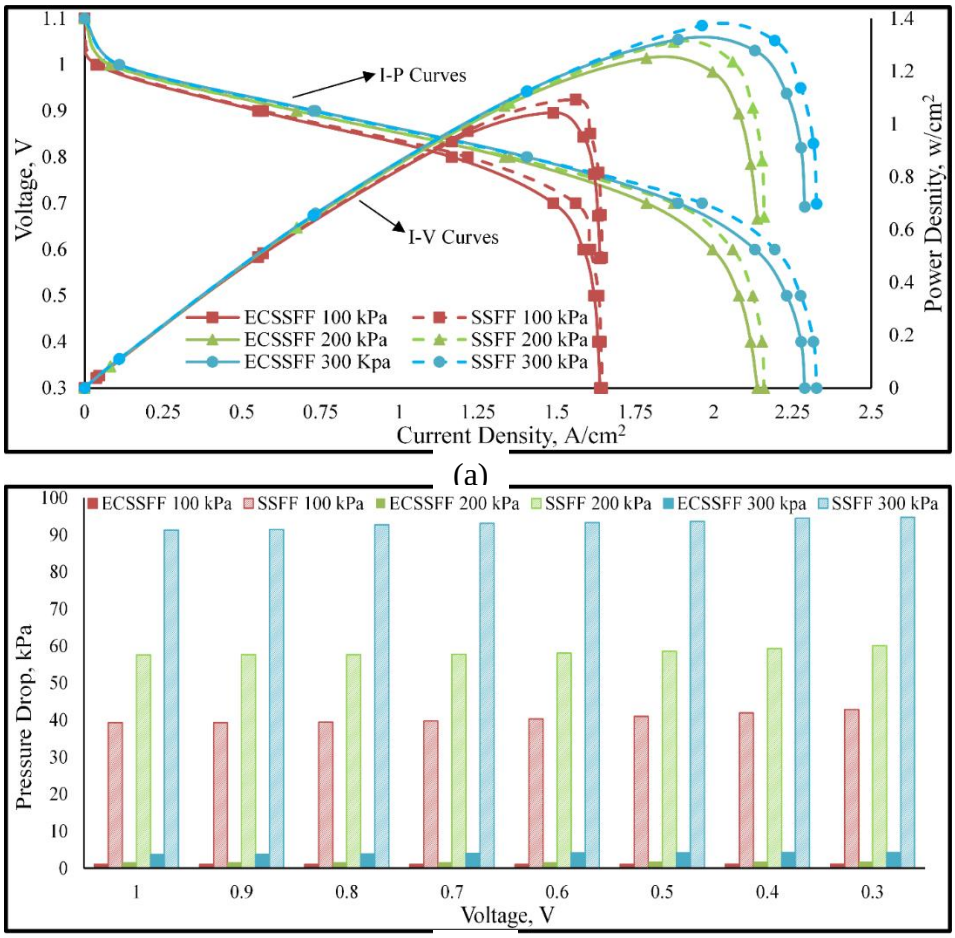

Figure 5.9 (a) IV and IP curves and (b) pressure drop of fuel cell with ECSSFF and SSFF for different operating Pressures at 100% Relative Humidity and 70 ^{o}C Temperature.

5.6 Summary

This study demonstrated the effectiveness of enhanced cross flow split serpentine flow field over the single serpentine flow field using three-dimensional, multiphase, full scale CFD simulations. In this work, the ratios of channel width to rib width for ECSSFF and SSFF designs which show the best performance are found and the performance of both the flow field designs are compared at different operating pressures and temperatures. From the present study, the following conclusions are drawn

- CW by RW of 1 mm by 1 mm for SSFF design, while 2 mm by 1 mm for ECSSFF design are found to display the best cell performance.

- The performance displayed by ECSSFF design through IV and IP characteristics is on-par with that of SSFF design with almost 30 times lesser pressure drop. If the same pressure drop is maintained across both the flow fields, the fuel cell with ECSSFF does not show concentration polarization and the maximum current density offered is 100% more than that of SSFF.

- Cell temperature of 70 ^{o}C and 200 kPa pressure are found to be the best operating conditions for both the flow field designs with 100% humidified reactants. Results showed that ECSSFF performing is almost similar to SSFF at all the operating temperature and pressure conditions used in present study.

- ECSSFF design has shown superior performance compared to SSFF by offering lower pressure drop even at high flow rates of the reactants. As less pressure drop increases the life span of the delicate polymer membrane and MEA in a PEM fuel cell, ECSSFF channel design is a better choice over SSFF for building fuel cell stacks.

The area of the fuel cell considered in this study is also 55.55 cm^2 similar to the cell area considered in the previous chapter. In general, PEM fuel cells can be made in any size and shape depending on the application. The reactant distribution becomes more non-uniform as the active area of the cell is increased. Hence, the efficacy of ECSSFF design needs to be evaluated for higher active area cells, in order to project it as more reliable and robust flow field design for the application in PEM fuel cells. So in the next chapter the performance of the fuel cell with ECSSFF design on cathode side is evaluated for different active areas viz. 50, 100, 150 and 200 cm^2 at fixed operating temperature of 70 ^{o}C and relative humidity of 100%.

Chapter 6

Efficacy of ECSSFF Design for Higher Active Areas

Efficacy of ECSSFF design for higher active areas

The pre-eminence of the ECSSFF design over single serpentine and parallel serpentine was demonstrated and discussed using a 55.55 cm^2 rectangular cross-sectional fuel cell in the previous two chapters. As the PEM fuel cells can be made in any size and shape depending on the application, the ECSSFF layout should be effective even for higher active area cells, in order to stand as the favorable option for flow fields. As the increase in the power output and pressure drop are not linear with increase in the area, it requires a separate study and is thus interesting to see how effective is the ECSSFF lay out for higher active areas when compared to standard parallel serpentine designs. This information will be useful when designing a scaled up fuel cell stack for commercial purposes. The fourth objective of the study (as listed in Chapter 2) i.e. to investigate the efficacy of the 3-channel ECSSFF design for higher active area rectangular shaped PEM fuel cells is addressed in this chapter. Performance of these higher area cells have been further compared with performance of the cells obtained with triple serpentine flow field (TSFF) design. The power output from the cells and the pressure drop incurred in the cells have been evaluated and a detailed performance comparison analysis with increase in the active area is presented in this chapter.

6.1 Description of cases and geometries considered

The present study has been carried out systematically by simulating the performance of fuel cells having active areas of 50 cm^2, 100 cm^2, 150 cm^2 and 200 cm^2 with three channel ECSSFF design on cathode side and parallel flow field on anode side. Performance of these larger area cells have been further compared with performance of the cells with triple serpentine flow field (TSFF) design on cathode side and parallel flow field on anode side. Hence, for each active area, two PEMFC configurations - one with ECSSFF channel layout and second with TSFF channel layout on cathode sides are generated using SolidWorks® 2010 and then exported to ANSYS® 17.2.

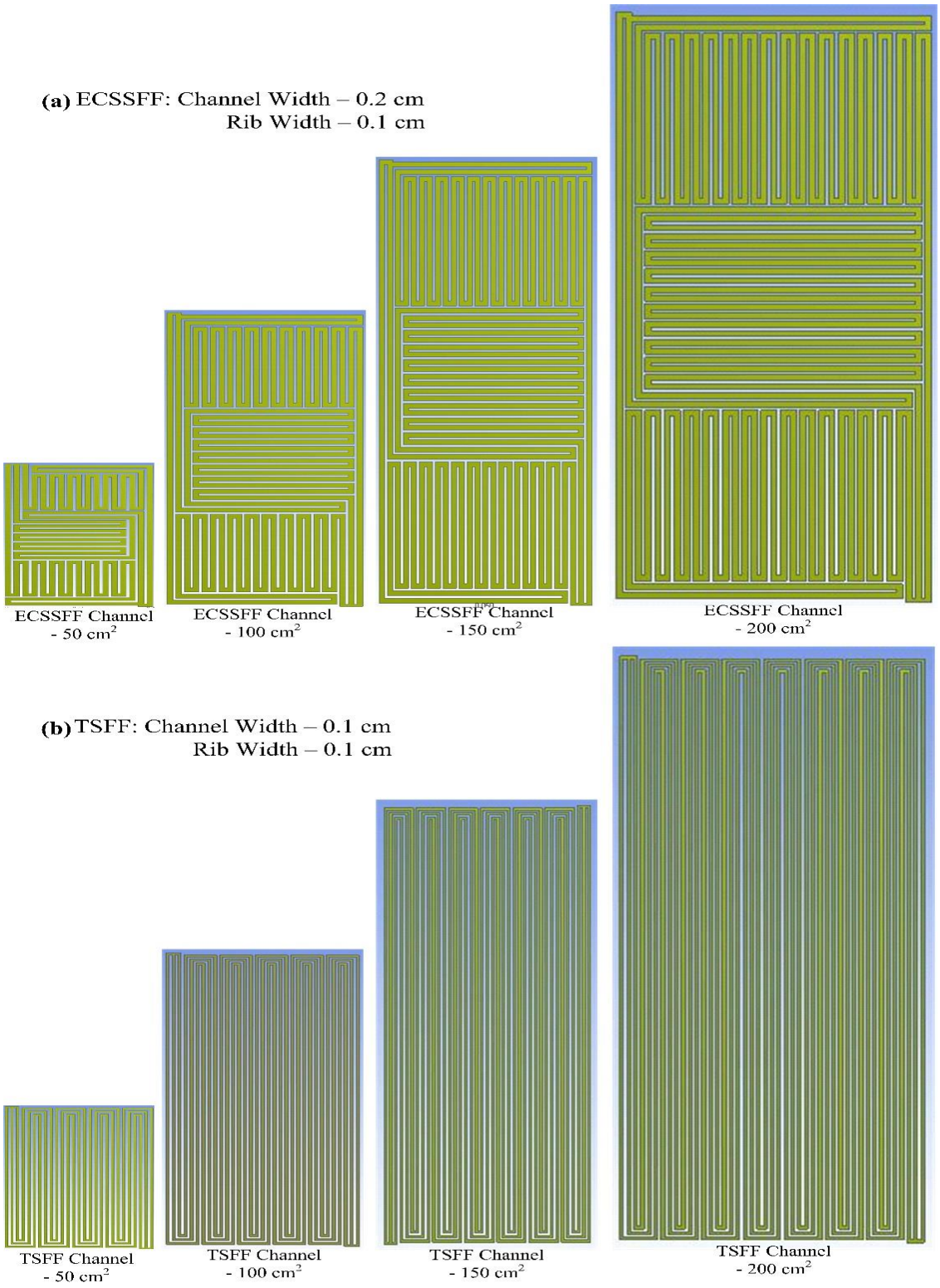

Figure 6.1 Patterns of (a) ECSSFF and (b) TSFF channel designs for 50 cm^2, 100 cm^2, 150 cm^2 and 200 cm^2.

Figure 6.1 shows the patterns of the ECSSFF channel and TSFF channel used in this study for different active areas. Dimensions of all the fuel cells and their individual components are detailed in Tables 3.1 to 3.3 of Chapter 3. The channel to rib width dimensions of 2 mm by 1 mm, which are found to be the best channel to rib width ratio for ECSSFF in the previous chapter have been used for the ECSSFF design for all the active areas. All these geometries are meshed in the same way as described in section 3.2 of Chapter 3. The grid and iterative independence studies are conducted as described in section 3.4 of Chapter 3. The finalized grids for all the cases used in the present simulations after the grid independence study are also listed in Table 3.6. The solution methods and simulation strategy used in the present simulations are also discussed in Chapter 3.

6.2 Operating conditions

The present studies are carried out at constant boundary conditions as specified in the section 3.2 of Chapter 3. As in previous chapters, flow rates are calculated by assuming a current density of 1 A/cm^2 with optimum stoichiometric ratios as obtained in the previous Chapter of 3 and 1.5 times on cathode and anode sides respectively. The relative humidity of both the reactants is fixed at 100%. Optimum operating temperature and pressures of 70 ^{o}C, and 200 kPa as obtained in the previous chapters are used in this analysis.

6.3 Performance comparison between fuel cells with ECSSFF design and TSFF design

Performance comparison of PEMFC with ECSSFF and TSFF channel layouts at different active areas is carried out by comparing the polarization (IV) curves and IP curves. The performance evaluation and comparative studies are conducted for the two flow field designs for different cell active areas – 50 cm^2, 100 cm^2, 150 cm^2 and 200 cm^2 at fixed operating conditions.

6.3.1 Polarization curves

Polarization (IV) and IP curves for different cell active areas with ECSSFF layout and TSFF layout at RH 100 % for both reactants, 200 kPa of operating pressure and operating temperature of

70 ^{o}C are shown in Figure 6.2. At higher operating voltages (≥0.7 V), as can be observed from the Figure 6.2, the difference in the cell power output obtained from both the flow field designs is not significant and hence the lines coincide. This is mainly because of lower currents drawn at higher voltages resulting in lower rate of electrochemical reaction, which requires limited amount of reactants (hydrogen and oxygen) at the catalyst sites to generate power. So the effect of reactant distribution and water evacuation capability have less prominence on the performance of PEMFC at high voltages. At lower voltages, rate of electrochemical reaction will be high and results in higher consumption of reactants. So the reactant distribution and water evacuation capacity have predominant impact on the PEMFC performance. Both reactant distribution and water evacuation strongly depend on the flow channels design. The difference in performance is clearly evident from Figure 6.2 for the two flow field designs - ECSSFF and TSFF below 0.7 V operating voltage.

When Figure 6.2 is inspected closely in low voltage region (<0.7 V), the following observations can be made: (i) the ECSSFF design exhibited a higher power output compared to TSFF design for all the active areas; (ii) the cell performance with TSFF decreases with increase in the cell area; (iii) the ECSSFF design shows better performance for 100 cm^2 cell area compared to other areas and (iv) the decrease in cell performance with increase in active area in case of ECSSFF is less compared to TSFF. Shorter path lengths in small area fuel cell will improve reactant distribution, water content and have uniform current density distribution [24]. As the cells having active areas of 50 cm^2 and 100 cm^2 have shorter channel lengths, the power output from these cells is higher compared to 150 cm^2 and 200 cm^2. In case of 100 cm^2 cell, the mass flow rate is higher than that of 50 cm^2 and the channels length is not large enough to cause uneven reactant distribution. Hence the performance is improved, when active area is increased from 50 cm^2 to 100 cm^2 in case of ECSSFF. For larger cell areas such as 150 cm^2 and 200 cm^2, the channel lengths are large which cause uneven reactant distribution and water stagnation in the lower sections of the flow channels, finally resulting in reduced power output. In both flow channel designs the maximum power density is observed for an active area of 100 cm^2. These results are consistent with the findings of Li et al. [112] where, the power output of single serpentine channel design increases from active area of 50 cm^2 to 100 cm^2 and decreased for 200 cm^2 with TSFF.

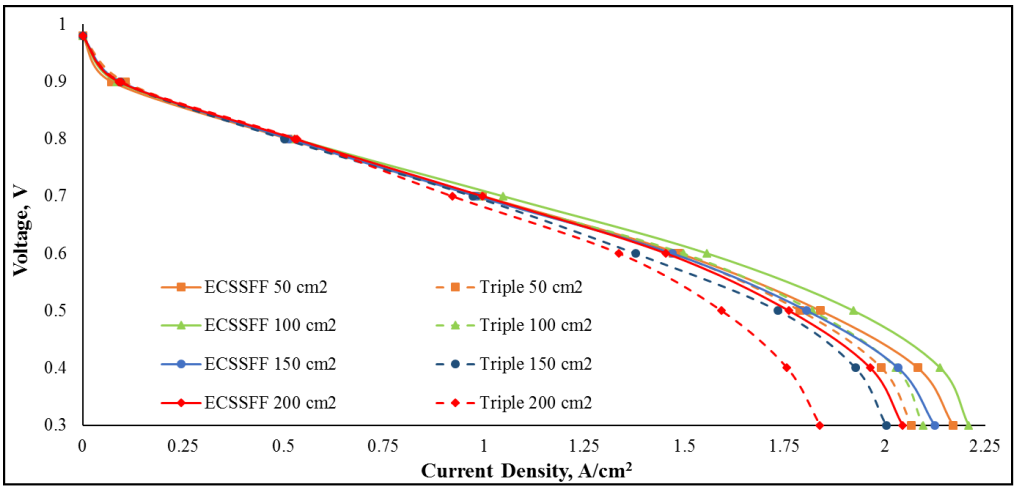

(a)

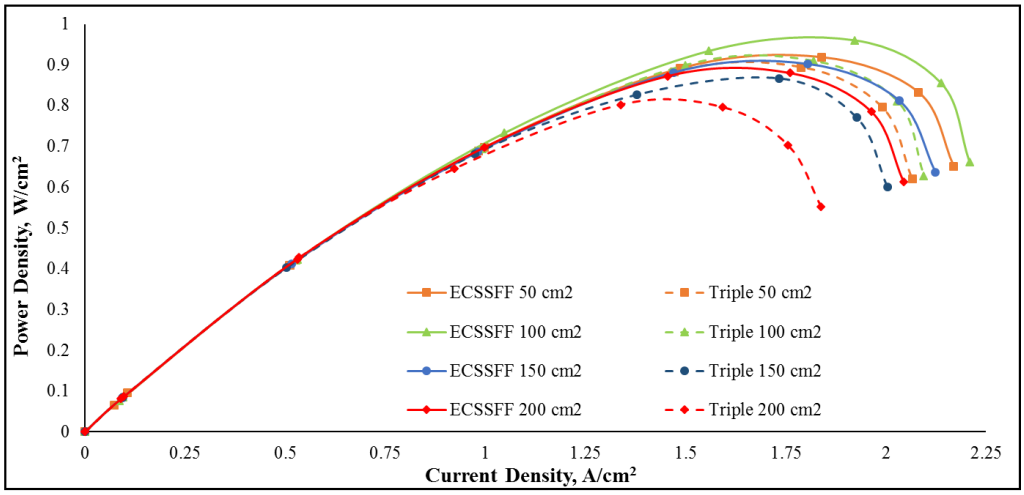

(b)

Figure 6.2 (a) IV curves and (b) IP curves for different active area cells with TSFF and ECSSFF at 100 % RH and 70°C operating temperature.

The pre-eminence of ECSSFF channel design over TSFF channel design can be further illustrated by line graphs of oxygen mass fraction and water mass fraction in Y- direction (breadth direction) at operating voltage of 0.4V. In ECSSFF design, different channels cover different sections of the active area, where as in case of TSFF design, three parallel serpentine channels cover the entire active area (Figure 6.1). Hence three lines, each one in the middle of top section, middle section and bottom section in the CL and GDL are drawn as shown in Figure 6.3. The mass fraction values are taken at all three lines and average values are calculated, and the average mass fractions are plotted in Figures 6.4-6.8.

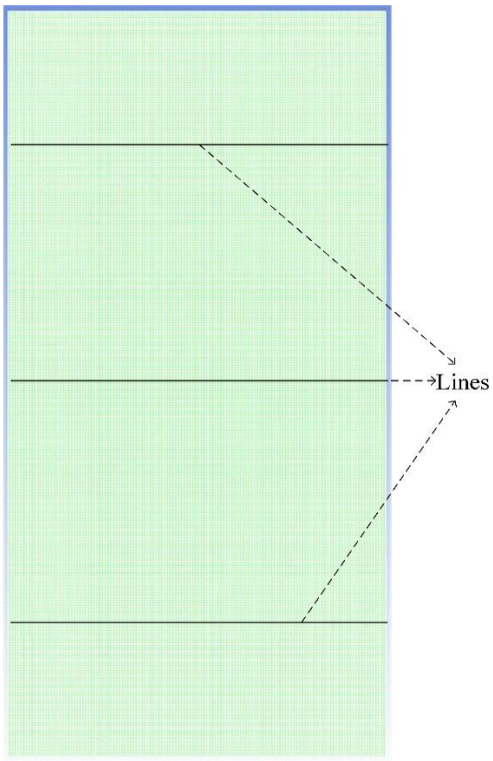

Figure 6.3 Lines drawn in the Cathode CL and GDL for the analysis.

Figure 6.4 presents the line graphs of oxygen mass fractions in cathode GDL along the Y-direction. It can be observed that the average oxygen mass fraction of ECSSFF design is higher compared to TSFF design for all active areas. In the initial portions along the breadth of the cells containing fresh feed channels, the oxygen mass fractions in cathode GDL are high and almost similar in both the designs. Later the average oxygen mass fraction is seen to be gradually increasing in case of ECSSFF design because of induced cross-flow from oxygen rich regions to the oxygen depleted regions due to the smart layout (arrangement) of the serpentines channels. In case of TSFF design, the oxygen concentration decreases to a very low value along the width of the flow field and this decrement is severe at higher cell active areas. On the other hand, significant oxygen mass fractions can be seen at the tail end of the flow field even for higher active area cells in case of ECSSFF design due to the maintenance of induced cross-flow. Because of the availability of higher oxygen concentrations under the rib, dead zones in the cell area are very few in case of ECSSFF.

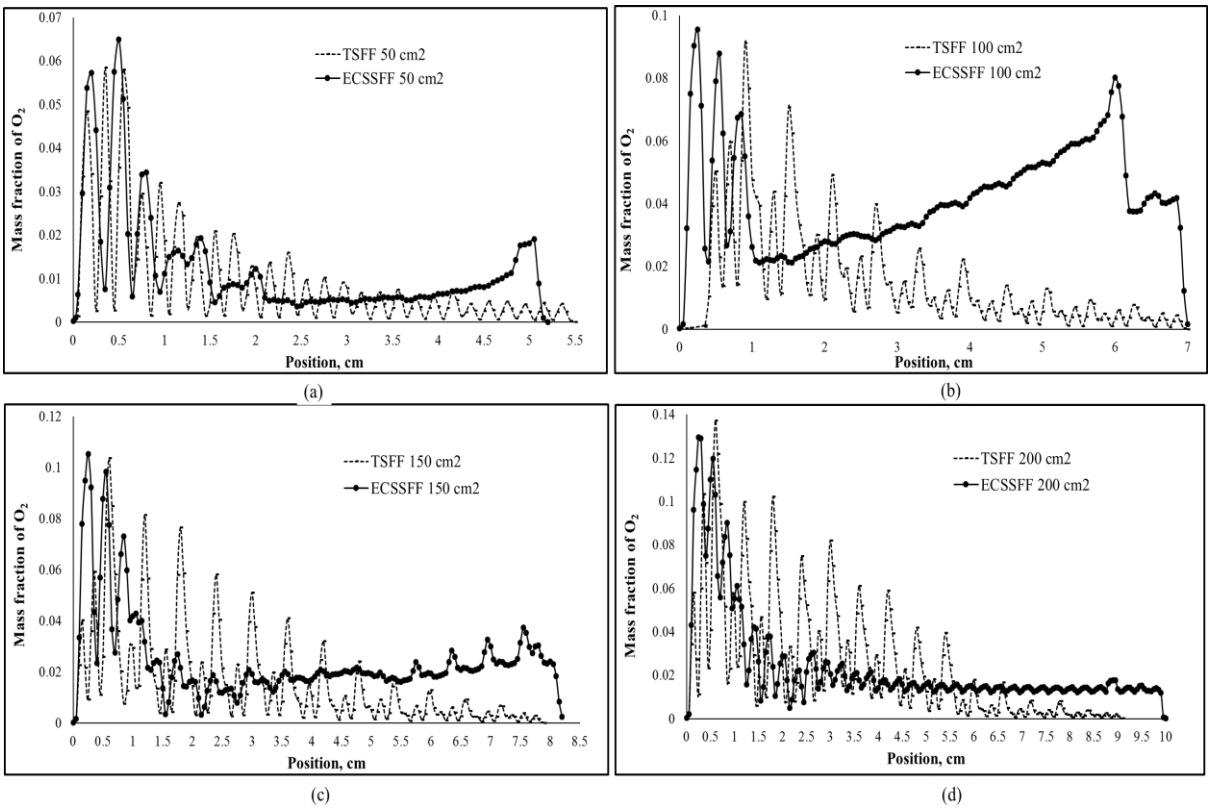

Figure 6.4 Line graphs of average mass fraction of oxygen in the cathode gas diffusion layer for different active areas at 100 % RH, 70^{o}C operating temperature and voltage of 0.4 V.

Similar trends can also be observed in Figure 6.5, which represents the line graphs of oxygen mass fractions in the cathode CL. Because of the sharing of reactant between different concentration regions due to cross flow, the average oxygen mass fraction is found to be less in the middle part of the CL along Y-direction with ECSSFF design compared to that with TSFF. However, throughout the catalyst surface, some minimum concentration of oxygen is maintained in case of ECSSFF unlike TSFF, which has a very low oxygen mass fraction along the end portion of the flow field. This makes the volume averaged oxygen mass fraction in the CL to be higher in case of ECSSFF (see Figure 6.8). Higher availability of reactants on the catalyst surface, improves the utilization of the available catalyst and the oxygen reduction reaction in case of cells with ECSSFF design, thereby produces higher currents. This effect is observed to be more pronounced with increase in cell area. Hence, fuel cell with ECSSFF design outperforms the cell with TSFF design for all active areas, specifically at higher active areas, when operated under similar conditions.

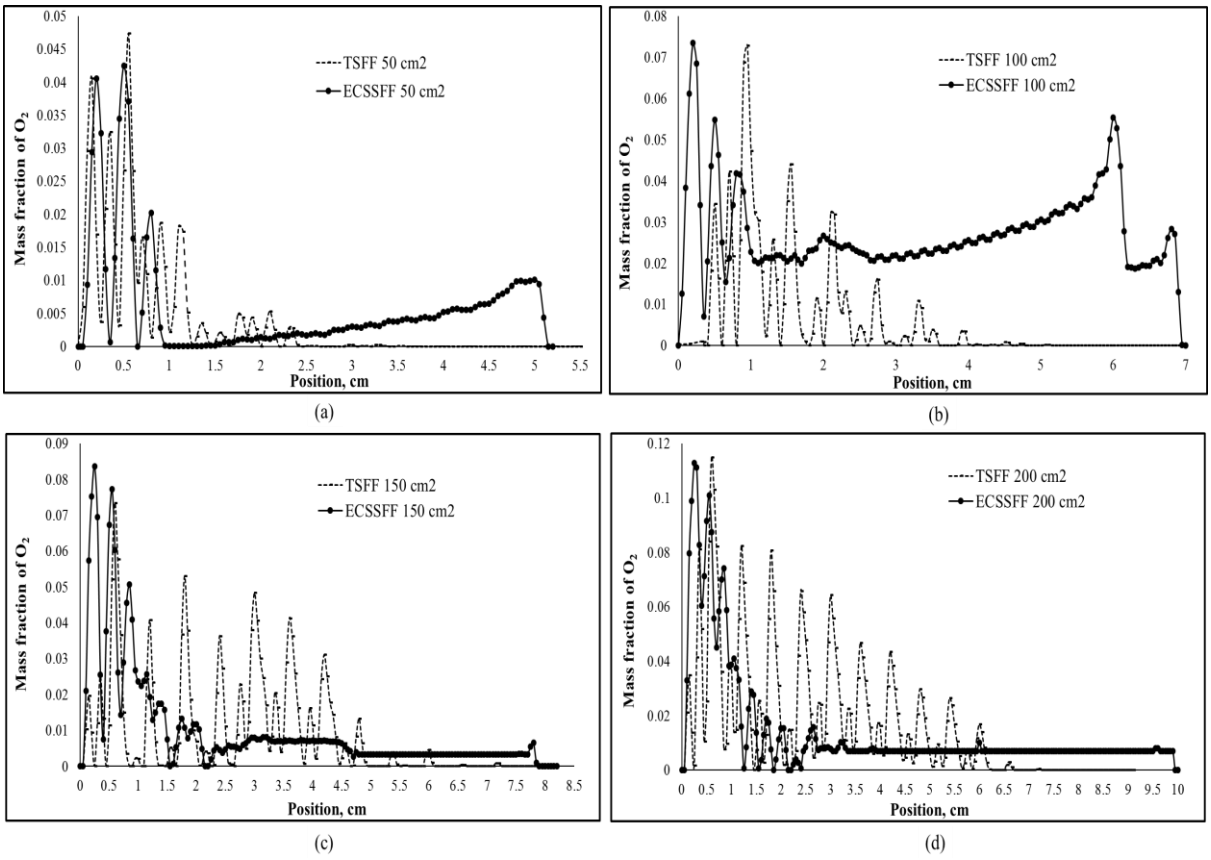

Figure 6.5 Line graphs of average mass fraction of oxygen in the cathode catalyst layer for different active areas at 100 % RH, 70^{o}C operating temperature and voltage of 0.4 V.

Figures 6.6 and 6.7 display the line graphs of water mass fractions in the cathode GDL and cathode CL respectively, along the Y- direction at 0.4 V. It can be noticed that the average water mass fraction is less for ECSSFF design compared to TSFF design because of the induced cross-flow, which evacuates the produced water effectively. This effective water evacuation capability of ECSSFF design reduces the chances of water stagnation in the GDL compared to TSFF design. Less water stagnation in the GDL and CL not only reduces the chances of flooding of the fuel cell but also reduces the total cell pressure drop with ECSSFF design (as can be seen from Figure 6.10(a)). This ultimately results in producing high currents from the cell with ECSSFF design compared to that with TSFF.

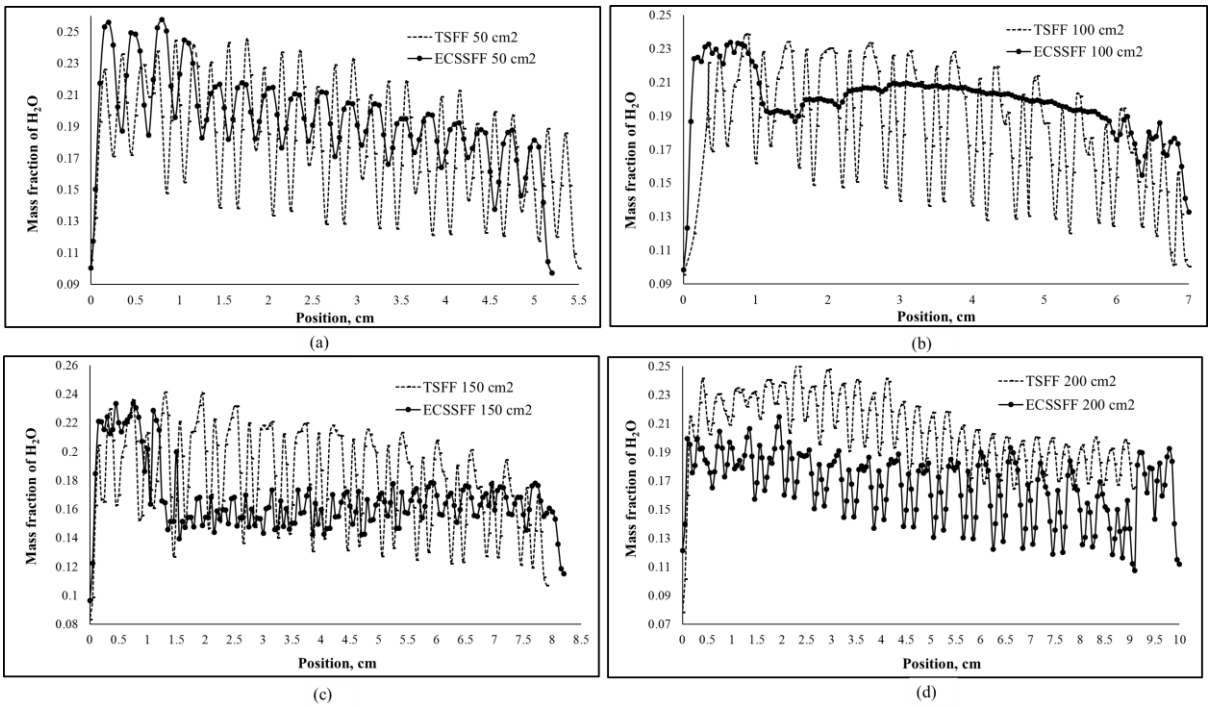

Figure 6.6 Line graphs of average mass fraction of water in cathode gas diffusion layer for different active areas at 100 % RH, 70^{o}C operating temperature and voltage of 0.4 V.

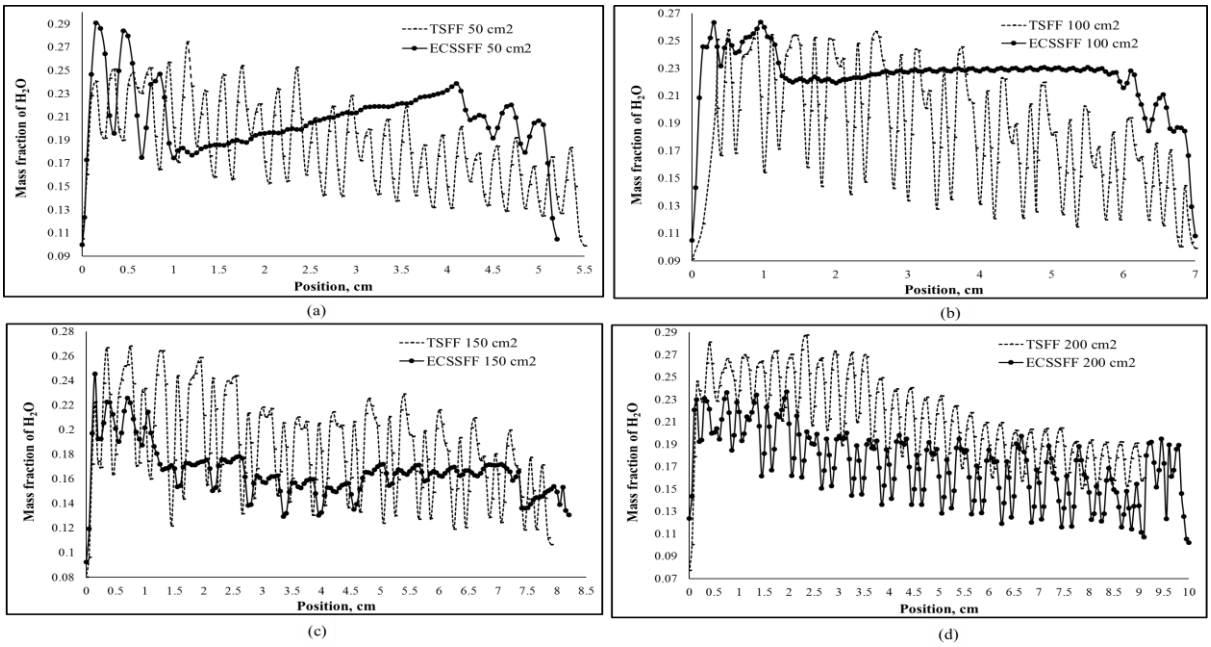

Figure 6.7 Line graphs of average mass fraction of water in cathode catalyst layer for different active areas at 100 % RH, 70^{o}C operating temperature and voltage of 0.4 V.

In addition to the line graphs, volume averaged values of the oxygen mass fraction and water mass fraction in the entire cathode catalyst layer and in the GDL have been calculated and they are compared for the two flow field designs in Figure 6.8. It can be clearly noticed that, the ECSSFF design has the better oxygen transport capability and water removal capacity than TSFF design as ECSSFF shows maximum oxygen mass fraction and minimum water mass fraction in the catalyst layer and GDL. For lower active areas such as 50 cm^2, both the flow field designs are comparable in terms of average mass fractions of oxygen in CL and GDL. But as the cell active area increases, the TSFF takes the back seat while the ECSSFF keeps up to be the promising layout by maintaining higher oxygen mass fractions in GDL and CL. In addition, ECSSFF design has also maintained lower average water mass fraction values at higher active areas.

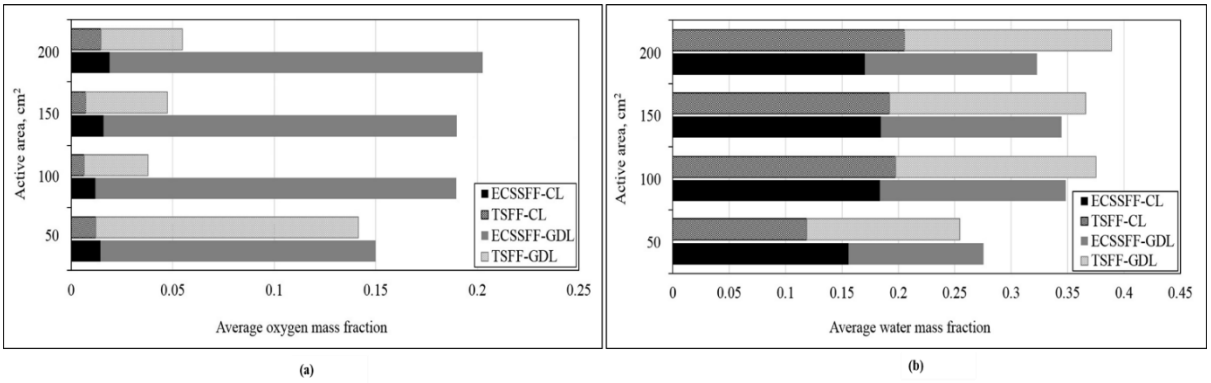

Figure 6.8 Comparison of volume average (a) oxygen mass fraction and (b) water mass fraction with the two flow field designs in the cathode catalyst layer and GDL for different cell areas at 100 % RH, 70^oC operating temperature and 0.4V.

As shown in Figure 6.9, the superiority of ECSSFF channel design over TSFF channel design at higher cell areas can be further illustrated by the contours of current flux density, plotted at the mid-planes created in the thickness direction of cathode CL at a voltage of 0.4 V. Current flux density can be noticed to be reducing with the increase in the cell area due to improper reactant distribution at higher active areas in case of cells with TSFF design. On the other hand, this decrease in current flux density with increasing cell area is less for the cells with ECSSFF design. Better water evacuation and reactant availability due to induced cross flow in ECSSFF make most of the fuel cell area to be active for the electrochemical reaction. In case of TSFF design, due to water stagnation in the channels, GDL and CL, the amount of reactants reaching the catalyst sites is

greatly affected. As the cell area increases, more channels are prone to flooding which reduces the power output. So a higher drop in power output is observed in the cells with TSFF design compared to cells with ECSSFF design at higher active areas.

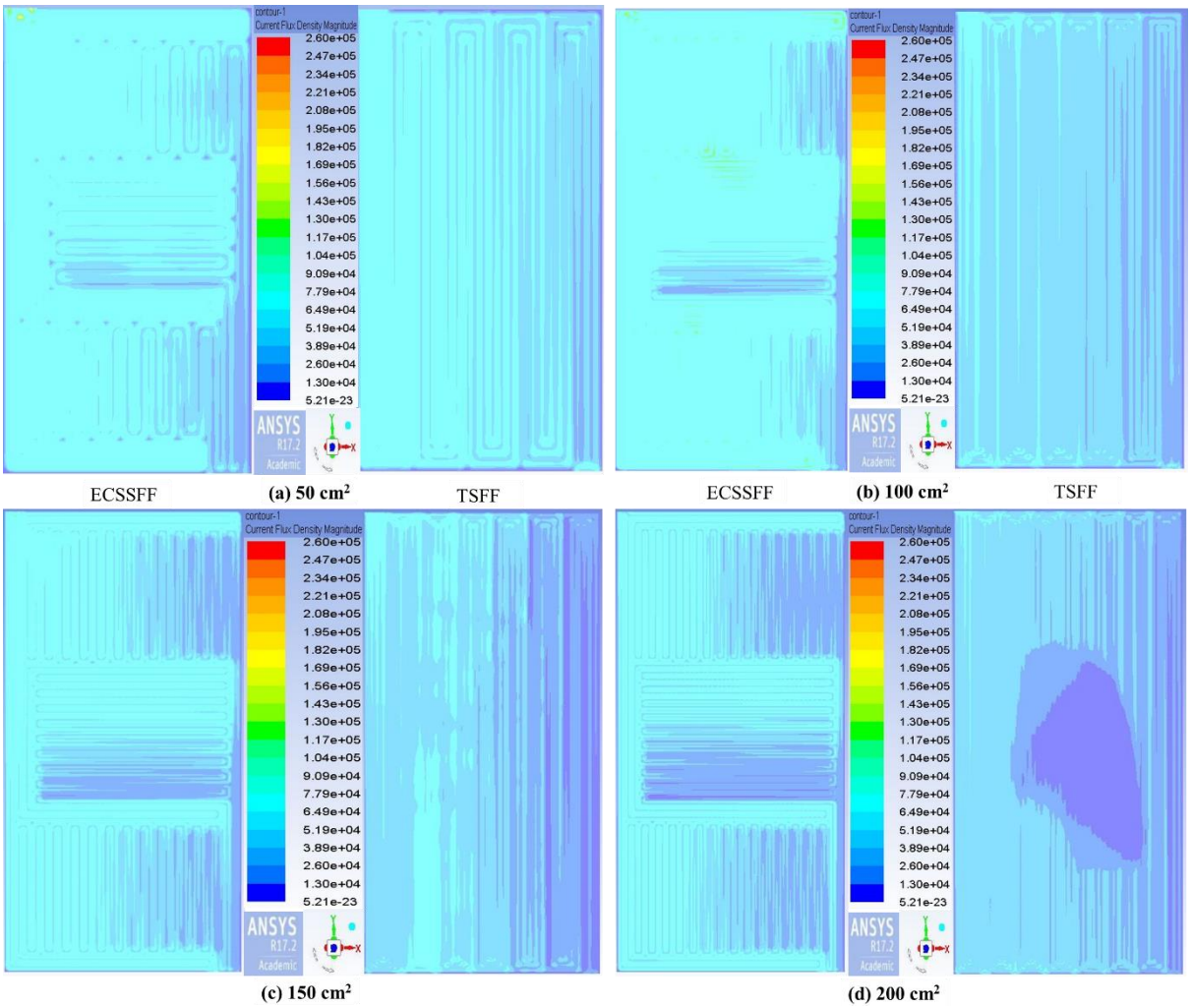

Figure 6.9 Contours of current flux density (A/m^2) at the mid-planes of cathode catalyst layer for different cell areas at 100 % RH, 70^{o}C operating temperature and 0.4V.

6.3.2 Pressure drop and power output comparison

When the reactants flow through channels in fuel cell, there will be a loss of pressure due to friction and presence of water. For compensating this pressure drop, reactants are needed to be sent at an elevated pressure by using a compressor, which requires energy. This excess energy or

power required by the compressor to maintain the pressure high enough for the reactants to flow through channels is called parasitic power loss. With increase in the pressure drop in the fuel cell, the power required by the compressor for the reactants increases. This increase in power requirement of the compressor is measured in terms of parasitic power loss. Parasitic power loss is given by the product of pressure drop and reactant flow rate [50]. Figure 6.10 shows the variation in pressure drop across the channel and the corresponding parasitic power loss with TSFF and ECSSFF designs for different cell areas at 0.4 V.

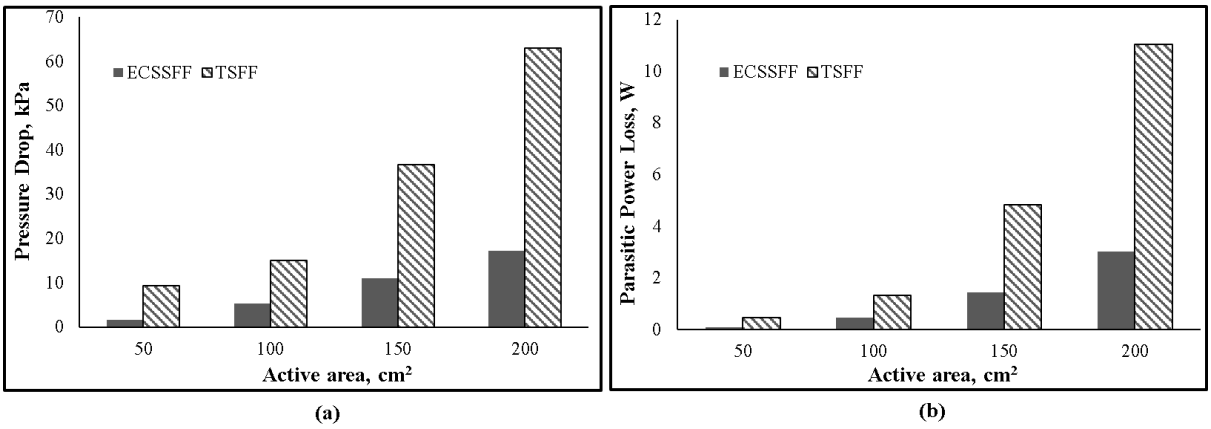

Figure 6.10 Comparison of (a) Pressure drop and (b) Parasitic power loss in cells with ECSSFF and TSFF designs for different active areas at 70 ^{o}C, 200 kPa and 0.4V.

With increase in the active area of the PEMFC and flow field, the length of the channels also increases, which result in increase of the pressure drop. Even though the active areas are similar for both the flow fields, ECSSFF channel design offers 70 % less pressure drop compared to TSFF channel design. Having less pressure drop across the channel is advantageous as it results in better distribution of the reactants, which leads to better temperature control and low mass transport loss [20] in addition to increasing the life span of the membrane. As the pressure drop increases with the cell active area, the parasitic power loss also increases, which can be seen from the Figure 6.10 (b). It can also be noted that the parasitic power loss for ECSSFF channel design is less compared to that with TSFF channel design.

Net power output is the useful power output from the PEMFC after subtracting the parasitic power loss, which incur during the operation of the PEMFC from its gross power output. To evaluate the flow field performance for the practical utilization in cells or stacks, it would be more reasonable to estimate this net power output. Because of higher pressure drop and parasitic power loss in case of PEMFC with TSFF channel, the net power output decreases further compared to that with ECSSFF channel design as shown in Figure 6.11(a) and this difference in the net power output increases with increase in cell active area. The percentage increase in the net power output with ECSSFF design over TSFF design increases from 4.5% to 13.5% with increase in cell area from 50 cm^2 to 200 cm^2.

The percentage drop in net power density in fuel cells with both the designs with increase in the active areas is plotted in Figure 6.11(b). As seen from the IV and IP curves (Figure 6.3), the power density has increased a bit with increase in cell area from 50 cm^2 to 100 cm^2 and then it decreases with increase in cell active area as shown in Figure 6.11(b). The percentage drop in net power density with increasing cell active area (from 100 cm^2 to 150 cm^2 and 150 cm^2 to 200 cm^2) in case of ECSSFF design is almost 55% less compared to that with TSFF design. The percentage reduction in power density with increase in active area from 50 cm^2 to 200 cm^2 is only 6% for the fuel cell with ECSSFF, while it is 15% in case of fuel cells with TSFF. Findings of Karthikeyan et al. [2014] showed that, the power density is reduced by almost 40% when the active area of the PEMFC with is increased from 25 cm^2 to 70 cm^2 [135]. It can be inferred from the comparison of the results of current study with outcomes of Karthikeyan et al. [2014] that ECSSFF is a favorable flow field layout for higher active areas.

The study shows that the overall power output of the cell with ECSSFF design is higher for all cell active areas compared to that of the cell with TSFF design and ECSSFF design does not lose its characteristics and quadruple advantages (as presented in Suresh et al. [68]) at higher active areas. The present work demonstrates the superiority of the ECSSFF channel design over TSFF channel design at high cell active areas. Hence, the ECSSFF is a potential flow field design to be considered for higher area fuel cells and stack of such cells for large scale power production.

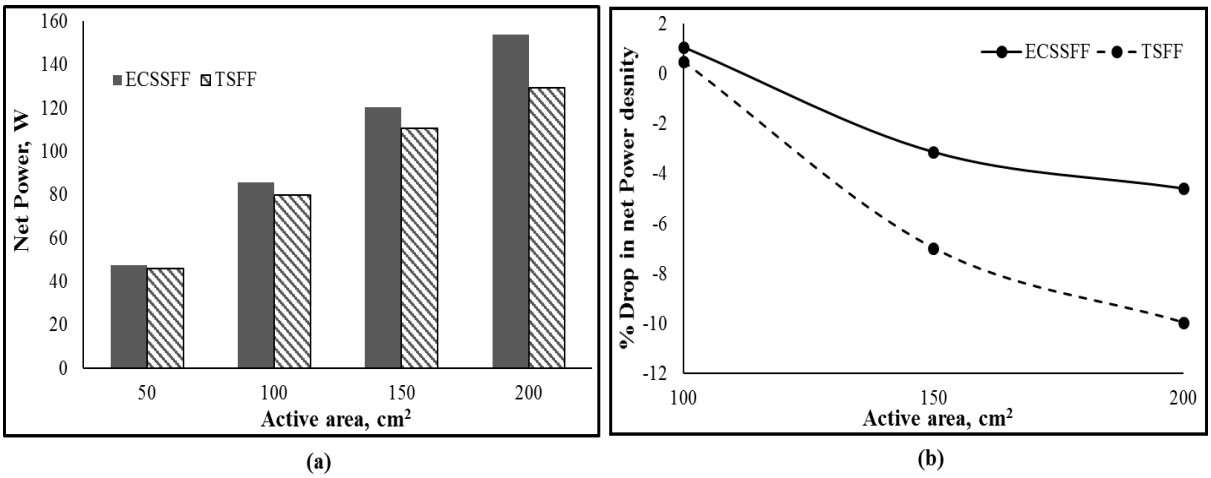

Figure 6.11 (a) Variation of net power with active area and (b) Percentage drop in net power density with increase in cell active area at 100 % RH, 70^{o}C and voltage of 0.4 V.

6.4 Summary

This work demonstrates the efficacy of the ECSSFF channel design over TSFF channel design rectangular cross-sectional cells having higher active areas. A comprehensive 3-D CFD modelling of PEM fuel cell was utilized to demonstrate on the capability of ECSSFF design as the better choice to be used on cathode side for higher active area cells over parallel serpentine flow field design. This was established systematically by comparing the performance obtained with ECSSFF design and TSFF design from PEMFC with four different active areas of 50 cm^2, 100 cm^2, 150 cm^2 and 200 cm^2. The average mass fraction of oxygen in the cathode gas diffusion layer and catalyst layer at higher active areas were found to be higher for the cells with ECSSFF compared to those with TSFF, whereas the water mass fractions in those layers were lower in case of ECSSFF because of the induced cross-flow and better water evacuation capability.

For all active areas considered in the study, the performance exhibited by the cells with ECSSFF in terms of offering higher current density, lower pressure drop (70% less) as well as higher net power is superior to that exhibited by the cells with TSFF. The drop in the net power output with increase in the cell active area in case of ECSSFF is 55% less compared to that with TSFF. These findings suggest that, use of ECSSFF design brings in lot of improvement in the total

power output from the PEMFC stacks containing series of higher active area cells for large scale power production.

Till now the study on ECSSFF channel design is confined to rectangular cross-sectional PEM fuel cells. But, for commercial purposes, PEM fuel cells can also be made in a square shape also. Hence, it would be interesting to extend the concept of induced cross-flow to get suitable ECSSFF layout for square cross-sectional cells. It is also required to find out how the ECSSFF layout, which displayed superior performance over parallel serpentine design in case of rectangular shaped cells, will perform for square shaped cells. This is explored in the next chapter.

Chapter 7

Studies on ECSSFF Design for Square Cross-Sectional PEM Fuel Cells

Studies on ECSSFF design for Square cross-sectional PEM fuel cells

Chapters 4 to 6 have shown that ECSSFF design is an effective and promising flow field design to be considered compared to single and parallel serpentine flow fields for rectangular cross-sectional cells, even for higher active areas. It will be interesting to see whether ECSSFF layout is also effective for square cross-sectional PEM fuel cell, as square shaped fuel cells are also being widely used. The distribution of reactant on the catalyst layer and the evacuation of water in a square type fuel cell will be different from rectangular fuel cell because of the difference in number of channel bends. In addition, the power output from the cells will not vary linearly with cell active area. Hence, a separate analysis is required to study the efficacy of the well appreciated ECSSFF layout in case of rectangular shaped fuel cells, when used in square cross-sectional PEMFCs. The objective of this part of the study is to design a flow filed layout using the concept of ECSSFF for a square cross-sectional cell and evaluate its performance computationally. The outcome of this study would be very useful in designing commercial square shaped fuel cell stacks with an efficient flow field designs for larger power applications. Hence, this chapter addresses the final objective of the thesis work as presented in section 2.6 of Chapter 2.

7.1 Synthesis of ECSSFF layout for square type cell

The key concept of ECSSFF layout is to induce the cross flow to the U-bend portions of all the split serpentine channels. This helps in removing the accumulated water near the U-bends and replenish the reactants in the depleted regions. By ensuring this important concept/ feature, the ECSSFF layout has been extended to square cross-sectional cell with four split serpentine channels as shown in Figure 7.1(a). It can be clearly noticed that all the flooding prone areas are preferentially taken care by the respective feeder channels in this layout. This has been used as the cathode side flow field in the present study. The ECSSFF layout is firstly synthesized for a 50 cm^2 area and a detailed parametric study is conducted.

7.2 Description of cases and geometries considered

The current study presented here has been divided into four parts –

(1) Simulation and performance comparison of the square cross-sectional PEMFC having ECSSFF layout on cathode side against that with 5-path serpentine flow field (as shown in Figure 7.1(b)) reported by Iranzo et al. [121].

(2) Finding the best channel to rib width ratio for the proposed ECSSFF Layout.

(3) Parametric study on the square shaped PEMFC having ECSSFF design with optimized channel and rib dimensions on cathode side.

(4) Evaluation of the ECSSFF design for large area square cross-sectional fuel cells.

Table 7.1 Fuel cell component dimensions.

Dimension of the component		**Value in cm**
Thickness	Membrane	0.0175
	Cathode CL	0.0012
	Anode CL	0.0006
	GDL	0.042
	Bipolar Plate	0.2
Channel Height		0.1
Channel Width		0.1
Flow field Length		7.2
Flow field Width		7.1

In all the above studies, cathode channel is the proposed square ECSSFF layout and anode channel is parallel layout. The ECSSFF layout synthesized for square cross-sectional cell is applied firstly for a 50 cm^2 area PEM fuel cell and the performance is simulated. The performance of the square shaped cell with ECSSFF is also compared with the performance of the cell with a 5- path serpentine flow field (as shown in Figure 7.1(b)) for similar operating conditions. A 3-D geometry of PEMFC having bipolar plate with gas flow channel, GDL, CL and membrane is created in solid works® 2010. The dimensions of the fuel cell and channel and rib considered for the first part of the study are taken from the work of Iranzo et al. [121], which are tabulated in Table 7.1. The generated geometry is imported to ICEMCFD 17.2, for discretizing the geometry into small computational cells. The hexahedral cells, which do not form highly skewed cells are used to have stable and convergent numerical solution. Grid independence studies are carried out as discussed in the Chapter 3 and the final selected grid has 2 million cells. The generated geometry with the computational mesh is imported to ANSYS FLUENT®17.2 to solve for flow, electrochemistry and species balance equations using Fuel cell add-on module.

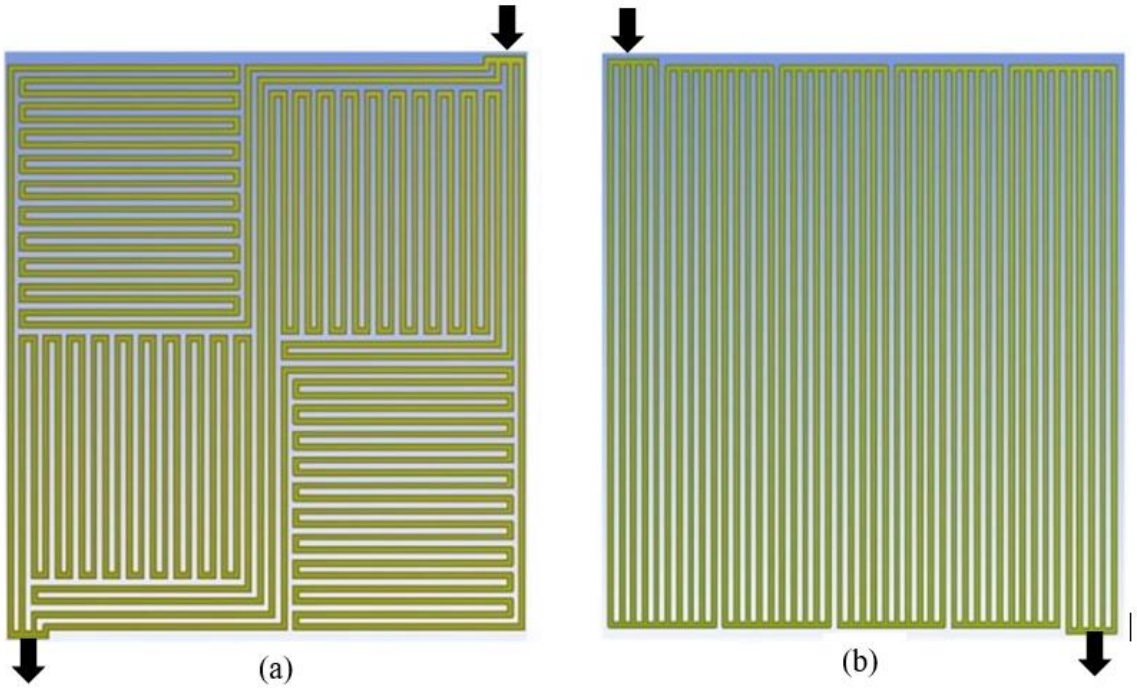

Figure 7.1 (a) ECSSFF layout for a square cross-sectional PEM fuel cell (b) Five -path serpentine flow design used in Iranzo et al. 2010 [121].

In the second part of the study, the effect of channel and rib widths on the cell performance is analyzed by varying the channel width while keeping the rib width constant at 1 mm. The best channel to rib width ratio is found with respect to maximum power density and peak power output. Later, a detailed parametric study including the effect of operating temperature, pressure, relative humidities and flow rates of the reactants on the cell performance with the synthesized ECSSFF with obtained best channel dimensions on cathode side is carried out. Finally, the effectiveness of the proposed ECSSFF layout is tested for higher active area square type cells by simulating the performance with different active areas of 50 cm^2, 100 cm^2, 150 cm^2 and 200 cm^2. The dimensions of the cell for these areas are listed in Table 7.2 and the thicknesses of the cell components used in these cells are same as listed in Table 7.1. The power output from the cells and the pressure drop incurred in the cells have been evaluated and a detailed performance comparison analysis is presented.

Table 7.2 Dimensions of the cell used for evaluation to higher active area cells.

Cell Area, cm^2	**Cell Length, cm**	**Cell Width, cm**
50	7.2	7.1
100	9.7	10.1
150	12.1	12.1
200	13.9	14.1

7.3 Operating conditions

In the present study, the flow rates of the reactant are based on the stoichiometric numbers, which are computed based on the reference current density of 1A/cm^2. Reactants are sent into the fuel cell in counter current flow as the distribution of current density and membrane water content is more uniform than co-current flow [104]. A complete parametric study is carried out by varying one operating parameter and fixing all the remaining parameters. The ranges of operating conditions used for the third part of the simulation study are shown in Table 7.3. Material properties

used in the present study are from Iranzo et al. [121] which are presented in Table 3.4 of Chapter 3. Same modelling methodology and simulation strategy as discussed in Chapter 3 have been followed for the current study also.

Table 7.3 Operating conditions in the present study.

Variable		**Units**	**Value**
Operating Temperature		^{o}C	50, 60, 70 and 80
Operating Pressure		kPa	100, 200, 300 and 400
Fuel Cell Current Density		A/cm^2	1
Anode Gas Flow rate		kg/s	1,1.5,2 and 2.5 times of stoichiometry
Cathode Gas Flow rate		kg/s	1,2,3 and 4 times of stoichiometry
RH of Inlet Gas	Anode	-	0%, 50%, 80% and 100%
	Cathode	-	0%, 50%, 80% and 100%

The modeling methodology has been validated using the PEMFC with 5-path serpentine channel flow field on cathode side and parallel flow field on the anode side and is already discussed in the section 3.6 of Chapter 3. In the present work, grid independent study is conducted as discussed in Chapter 3 by generating 5 different grid sizes (0.17 million, 1.25 million, 2.09 million, 4.83 million and 8.37 million elements) and the variation in current density with respect to grid size at 0.5 V is observed. It is found that, the % change in current density obtained is 1% when the grid size increases from 2.09 million to 4.83 million and hence to keep the requirement of computational hardware minimal, the mesh with 2.09 million elements is selected for further study. An iterative independence study is also carried out as discussed in Chapter 3 to fix the number of iterations for all cases to get the final value within 1% error. The variation in current density with number of iterations at 0.5 V is monitored and it is observed that, the % difference in current density is less than 1% beyond 3500 iterations. Hence for further studies, the number of iterations are fixed at 3500 to save time required for the simulations without affecting the accuracy of the results.

7.4 Performance comparison of the fuel cells with ECSSFF design and 5-path serpentine design

Performance of the square cross-sectional fuel cell with ECSSFF design (shown in Figure 7.1(a)) as cathode channel is simulated for the same operating conditions (RH 60%, Stoichiometric factors 1.5/3.0 for anode and cathode, Temperature 60 ^{o}C, Pressure 400 kPa) and is compared with the performance obtained with 5-path serpentine channel design. The polarization and power density curves comparing the performance of the two cells with square ECSSFF design and 5- path serpentine channel design are shown in Figure 7.2. It can be observed that the performance of both the fuel cells is similar till 0.7 V as the reactant consumption is less at higher voltages and hence the performance is not much effected by the type of flow design. Below the voltage of 0.7V, a steady increase in the difference in performance can be observed, with the cell having square ECSSFF design showing improved performance. 10% improvement in the current density at 0.3 V and 6.5% increase in the peak power density are noticed with the ECSSFF layout. These improvements are obtained with the channel and rib dimensions, which are same as that of the dimensions used for 5-path serpentine channel in Iranzo et al. [121]. More improvements in the performance may be possible by finding the best channel and rib dimensions for the ECSSFF layout and operating conditions. The results of the study on the effect of channel and rib widths ratio on the cell performance are presented in the next section.

Figure 7.3 shows the contour plot of oxygen concentration (mass fraction) on mid-plane of the cathode CL of the two simulated PEMFCs with ECSSFF and 5-path serpentine flow fields at the operating voltage of 0.4 V. It can be observed that, the reactant concentration is high and more uniform in most areas of catalyst layer in case of cell with square ECSSFF design, while the maximum reactant concentration can be observed only in the initial part of the channel, which gradually decreases towards the end of the channel in the case of 5-path serpentine design. The enhanced cross-flow feature of the square ECSSFF design improves the reactant concentration at the middle portions on the catalyst surface, as can be seen from Figure 7.3(a). The availability of higher reactant concentration on most parts of the catalyst surface enhances the conversion of the

reactant leading to higher power output. This causes the cell having Square ECSSFF to display better performance than the cell with 5-path serpentine (Figure 7.2).

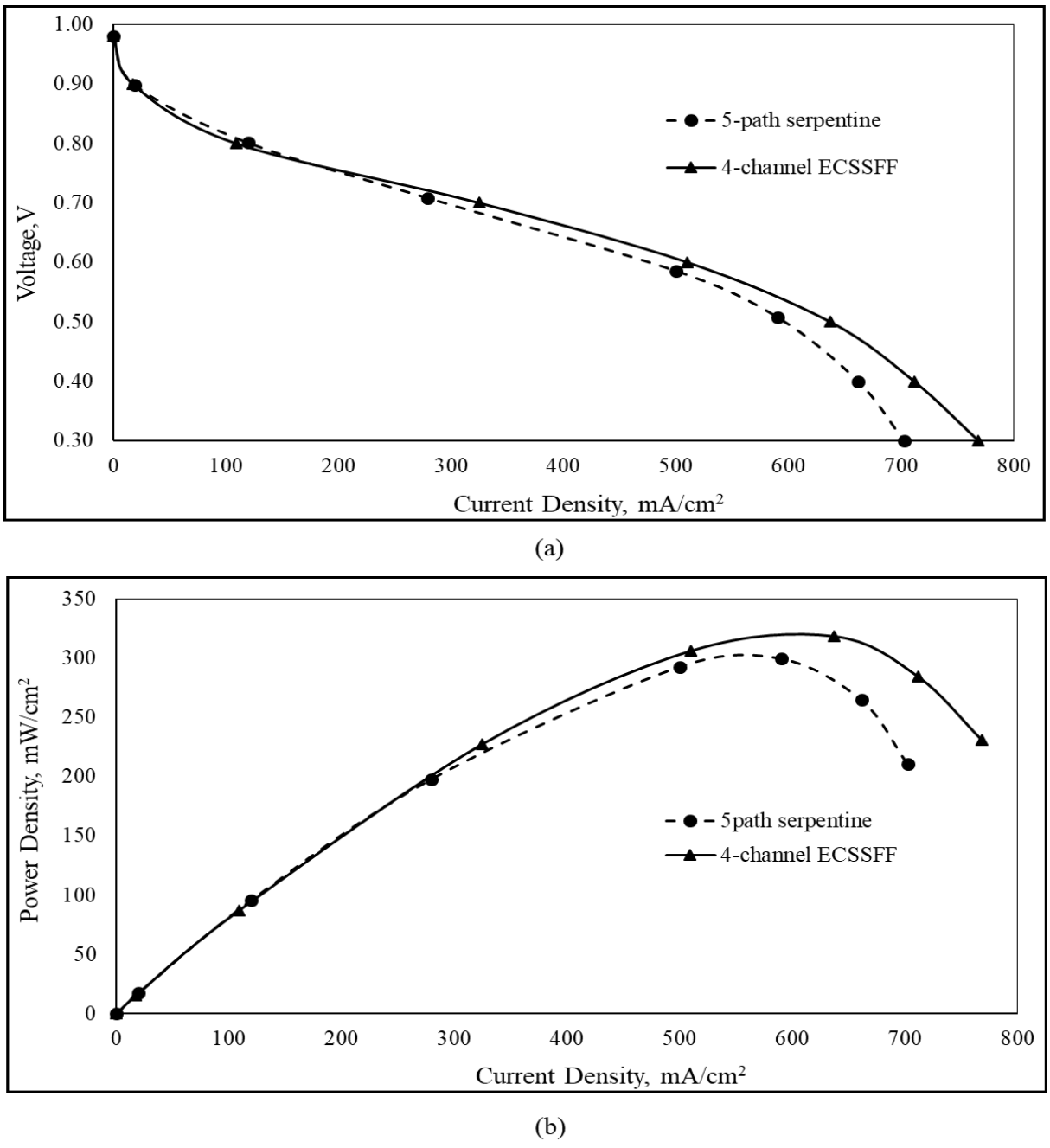

Figure 7.2 Comparison of (a) V-I curve and (b) P-I curve obtained with 4-channel ECSSFF and 5-path serpentine flow field.

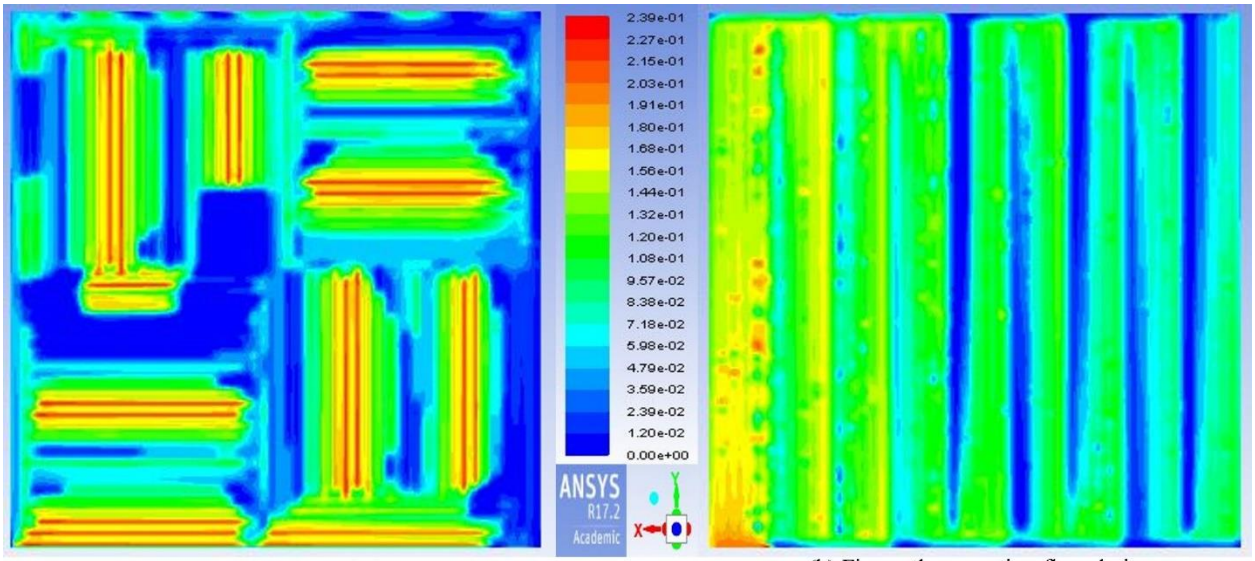

(a) Square ECSSFF design (b) Five-path serpentine flow design

Figure 7.3 Mass fraction of oxygen at mid-plane of cathode catalyst layer in the PEMFCs with (a) Square ECSSFF and (b) Five-path serpentine at V = 0.4V.

7.5 Effect of channel width to rib width ratio for square shaped ECSSFF design on cell performance

The ratio of channel width (CW) to rib width (RW) effects the pressure drop in the flow field. So to find the best cathode channel dimensions with least pressure drop, a study is carried out by varying CW while keeping the RW constant at 1 mm in the present study. The fuel cell is operated at RH 100%, Stoichiometric factors 1.5/3.0 for anode and cathode, Temperature 60 ^{o}C, Pressure 200 kPa. These conditions are varied as the individual parameter is studied. The polarization and power curves of the fuel cell with square ECSSFF design simulated for different ratios of CW to RW are presented in Figure 7.4(a). It can be noticed that the power output from the PEMFC is increasing with increase in CW to RW ratio from 0.5 to 1mm and then it is decreasing for CW to RW ratios from 1 to 2 mm.

The narrow channel width increases the gas velocity which leads to drying of the membrane because of which the average membrane water content is lower for narrow channels and increases as the channels get wider. This affects the proton conducting capacity of the membrane and increases ohmic losses for narrow channels. But as the channel width increases, the reactant gas

velocity decreases. At higher currents, water generation is more and need to be removed to avoid flooding in the catalyst, GDL and channels of the cell. The evacuation of water will be difficult for lower gas velocities and results in higher concentration polarization. High CW will also result in low contact area between rib and GDL, which adversely affects the electron transport.

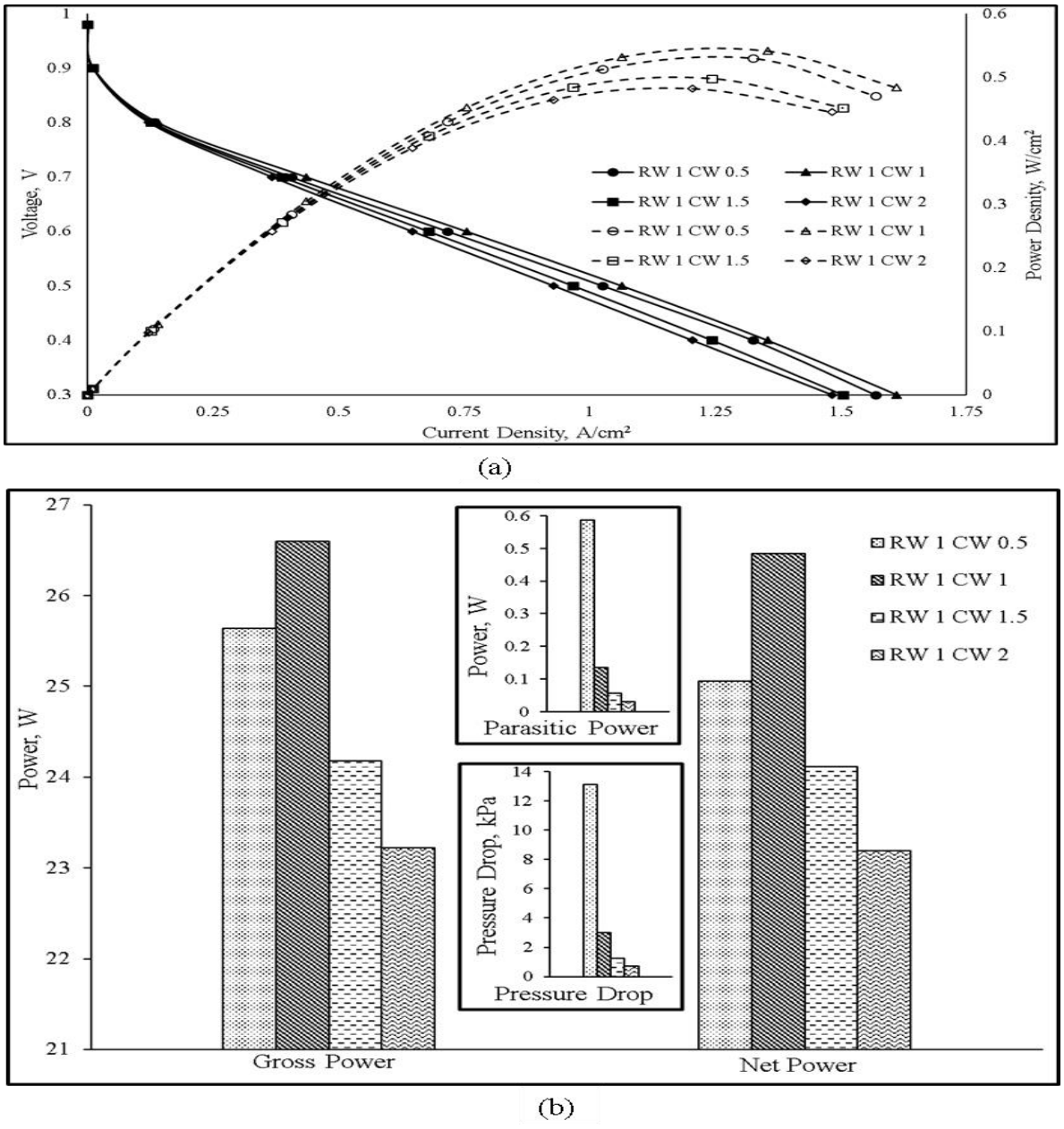

Figure 7.4 (a) Polarization and power curves (b) Gross, Net & Parasitic powers and Pressure drop at 0.5 V, for different Channel width to Rib width ratios.

From Figure 7.4(a), it can be observed that for the ECSSFF layout for square type cell, CW to RW ratio of 1 (CW=RW=1 mm) exhibited the best performance among all other channel widths considered for the design. The dimensions of the flow channel for the fuel cell should be selected in such a way that, the channels are neither too small which may cause local drying and hotspots on the membrane, nor too large which will substantially reduce the convective flow between channels [17]. The pressure drop across the channel is dependent on the channel width to rib width ratios. Figure 7.4(b) shows the gross power, net power, parasitic power and pressure drop at 0.5 V, for different CW to RW ratios. The method for finding the parasitic power loss due to pressure drop is same as discussed in section 3.2. At lower channel width of 0.5mm, the flow field offered highest pressure drop of 13 kPa. With the increase in CW, the pressure drop decreased to 0.7 kPa for CW of 2 mm. High pressure drop causes more parasitic power losses and hence reduces the net cell power output. Too low pressure drop is also not advantageous as there will be very low cross flow, which causes flooding of the cell. Hence, the gross power and net power are higher for CW of 1 mm compared to those with 1.5 mm and 2 mm, even though they offer less pressure drop compared to CW of 1 mm case. As a result, the CW by RW ratio of 1mm by 1mm is considered for further studies with the proposed ECSSFF layout, as this ratio resulted in best performance.

7.6 Parametric study on the performance of square shaped PEMFC having ECSSFF design

7.6.1 Effect of Reactant Flow rates

The performance of a fuel cell is very much dependent on the availability of reactants. To get maximum PEMFC performance, it is suggested that to have optimum reactant flow rates. As too little flow reduces the performance due to non-availability of the reactant for participating in reaction in some areas and too much flow will also lead to lower performance due to higher water evacuation leading to membrane dehydration, which increases ohmic losses. To analyse the effect of reactants stoichiometry, a systematic procedure is adopted. The performance of the fuel cell is simulated by varying the cathode stoichiometry (S_c) from1 to 4, with an increment of 1 at fixed anode stoichiometry (S_a) of 1. This is repeated for other anode stoichiometries – 1.5, 2 and 2.5.

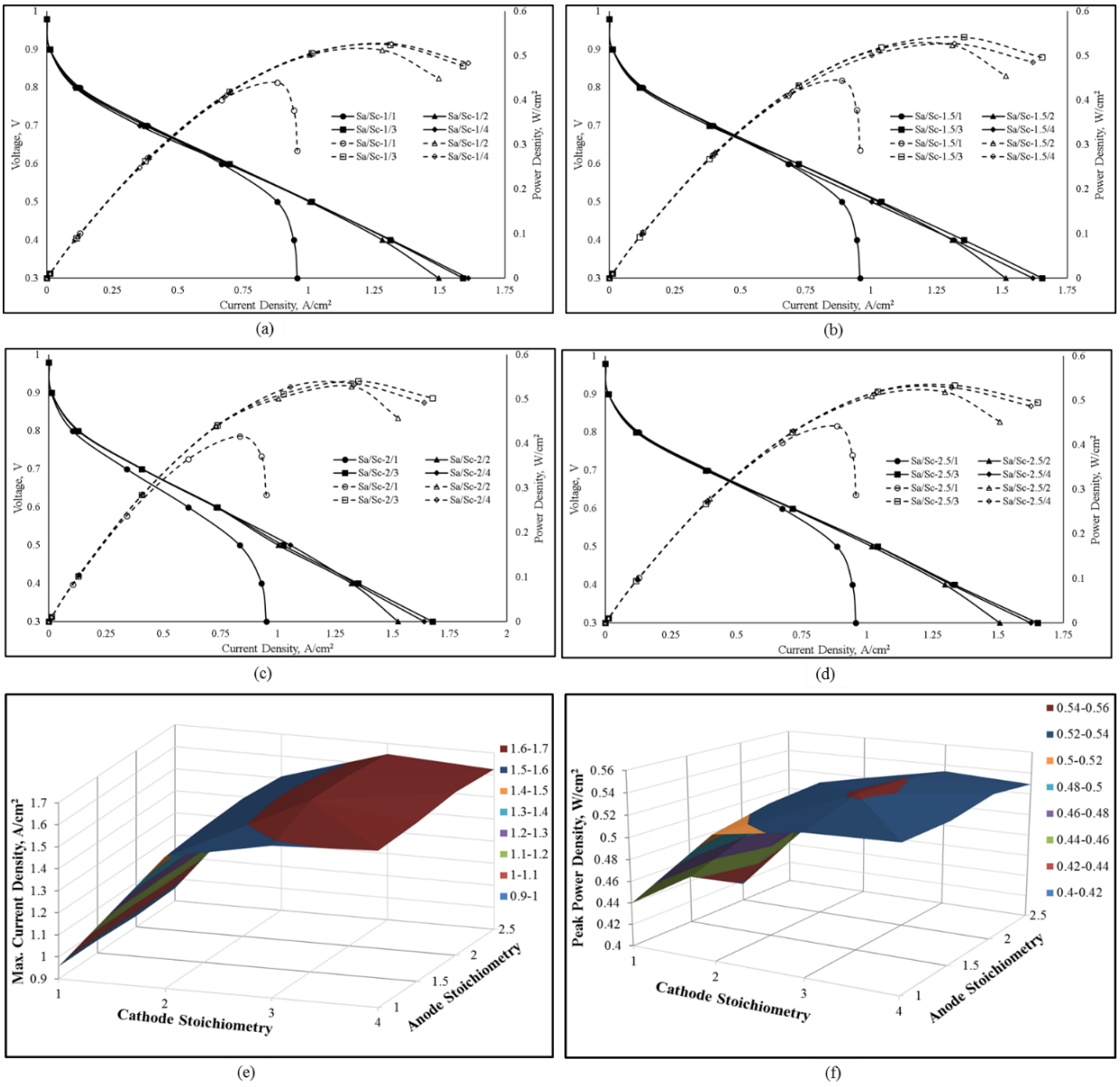

Figure 7.5 Polarization and power curves at different cathode stoichiometries (S_c) and anode stoichiometry (S_a) of (a) 1, (b) 1.5, (c) 2, (d) 2.5 and surface plots of (e) maximum current density at 0.3 V and (f) peak power density at various S_a and S_c.

Figure 7.5 shows the polarization and power curves at different anode and cathode stoichiometries, along with the maximum current and power densities (Figure 7.5(e) & (f)) generated at different S_a and S_c. It can be observed from Figures 7.5 (a) to (d) in general that the cell performance increases for any value of S_a with the increase in S_c because of supply of higher oxygen concentration. As the ORR is the limiting reaction in a PEMFC, with higher O_2

concentration, more conversion takes place, which results in improved power output. Higher air flow rates also improve the water evacuation in the cell. The performance improvement is noticed till S_c increases to 3, beyond that the performance started decreasing. This trend is observed because, very high values of S_c (>3) reduces the residence time of the reactant in the cell and causes drying of the membrane, which ultimately deteriorates the cell performance. Higher flow rates also increases the parasitic losses, which reduce the net power output [101]. Similarly, same was observed for hydrogen flow rate also, where the cell power output increased from S_a from 1 to 1.5 and then onwards, the performance decreased. The optimum set of stoichimetries for hydrogen and air can be clearly observed from the surface plots of maximum current density at 0.3 V and peak power density generated at different anode and cathode stoichiometries as shown in Figures 7.5 (e) & (f). It can be noticed from this study that the maximum power density and maximum current density are obtained at the optimum set of S_a = 1.5 and S_c = 3. Hence, the stoichiometry of 1.5 times for anode and 3 times for cathode is selected for further analysis. These results are in consistent with the studies of Badduri et. al [129] and Zhenzhong et. al[130].

7.6.2 Effect of Operating Temperature

The PEM fuel cell performance is dependent on the operating temperature as the diffusivity of gases, reaction kinetics and the membrane conductivity strongly depend on the temperature [97]. These parameters improve with the increase in operating temperature. The proton conductivity of the Nafion® is dependent on the hydration level of the membrane, which reduces with increase in the temperature due to reduced evaporation[95,136]. So, it is essential to run the PEMFC at an optimum temperature such that, the membrane will be fully hydrated and also conductivity will be high. In this work, the performance of the fuel cell is simulated for operating temperatures of 50 ^{o}C, 60 ^{o}C, 70 ^{o}C and 80 ^{o}C to find the optimum temperature.

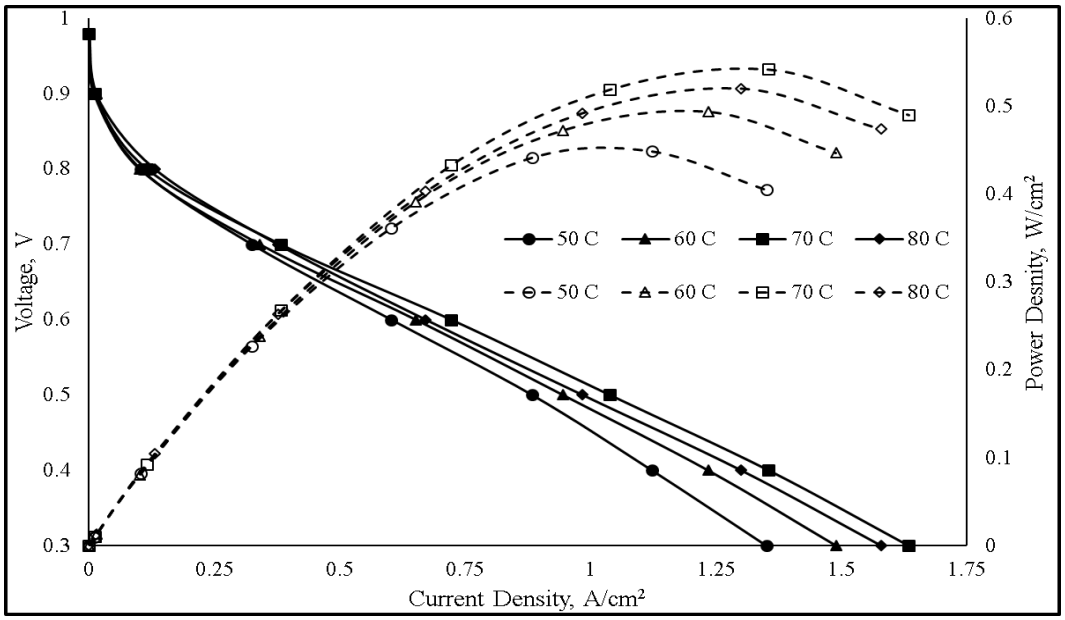

Figure 7.6 Polarization and Power curves for different operating temperature from 50 ^{o}C to 80 ^{o}C.

Figure 7.6 shows the power and polarization curves at various operating temperatures. It can be noticed that the performance of the cell increased till the temperature of 70 ^{o}C and then it reduced. The performance increase is due to increase in the gas diffusivity, membrane conductivity and reaction kinetics with temperature. The adverse effect on the cell performance with further increase in temperature beyond 70 ^{o}C is due to the reduced water content in the membrane owing to the reduction in condensation and/or increased rate of water evaporation. The trends of these results agree with the findings of yan et. al [99] and Badduri et. al[36]. So the operating temperature is fixed at 70 ^{o}C for the remaining cases.

7.6.3 Effect of Operating Pressure

From the literature it is observed that operating pressure have great effect on the fuel cell performance [137]. In general, when the operating pressure increases, the mole fractions of individual reactants increase, which lead to higher reactant concentration in the CL. This increase in pressure also helps in evacuation of water, which reduces the flooding probability. Hence, higher operating pressure increases the limiting current density and the overall power output of the

PEMFC. However, maintaining high pressure in the cell containing thin and porous structures is not that easy and pumping power for the reactant gases will also increase.

Figure 7.7 (a) displays the polarization and power curves of PEMFC when operated at pressures of 100 kPa, 200 kPa, 300 kPa and 400 kPa. It can be observed that the fuel cell performance improves as the operating pressure increases, which is in line with the findings of Carcadea et al. [17], Abdollahzadeh et al. [138] and other works [100,106,136,137]. In general, when air is used on cathode side, compressor is employed to pump air to the fuel cell. Han et al. [127] showed that the compressor consumes a large chunk of total system power consumption. Even though operating the PEMFC at higher pressures is advantageous, it has two important drawbacks which are - the pressure drop across the channel increases at elevated operating pressures and the high power consumption by compressor, which needs to send the reactants at high pressures. These increase the parasitic losses and consequently reduces the net power generated from the cell. It is important to take note of channel pressure drop and compressor power consumption before finalizing the operating pressure.

Figure 7.7 (b) shows the gross power, net power-1 and net power -2 at operating voltage of 0.5 V. Net power-1 is the output power after subtracting the parasitic power loss due to pressure drop across cathode channel from the gross power output. The method for finding the parasitic power loss due to pressure drop is same as discussed in section 3.5 of chapter 3. Net power -2 is the net power output of the fuel cell after subtracting the compressor power from net power -1. The power required for the compressor to pump air at higher pressures is calculated as suggested by Tirnovan and Giurgea [19] using equation (34).

From Figure 7.7 (b), it can be observed that the gross power output increases with increase in operating pressure even when the parasitic loss due to channel pressure drop is considered. But when the total parasitic loss including both the power loss due to pressure drop and compressor power are subtracted from the gross power produced, the net power output-2 started decreasing after the operating pressure of 200 kPa, which is consistent with the findings of Zhao et al. [139],

where peak power increased firstly and then decreased with further increase in pressure. From this analysis, the operating pressure of 200 kPa is fixed for the further studies.

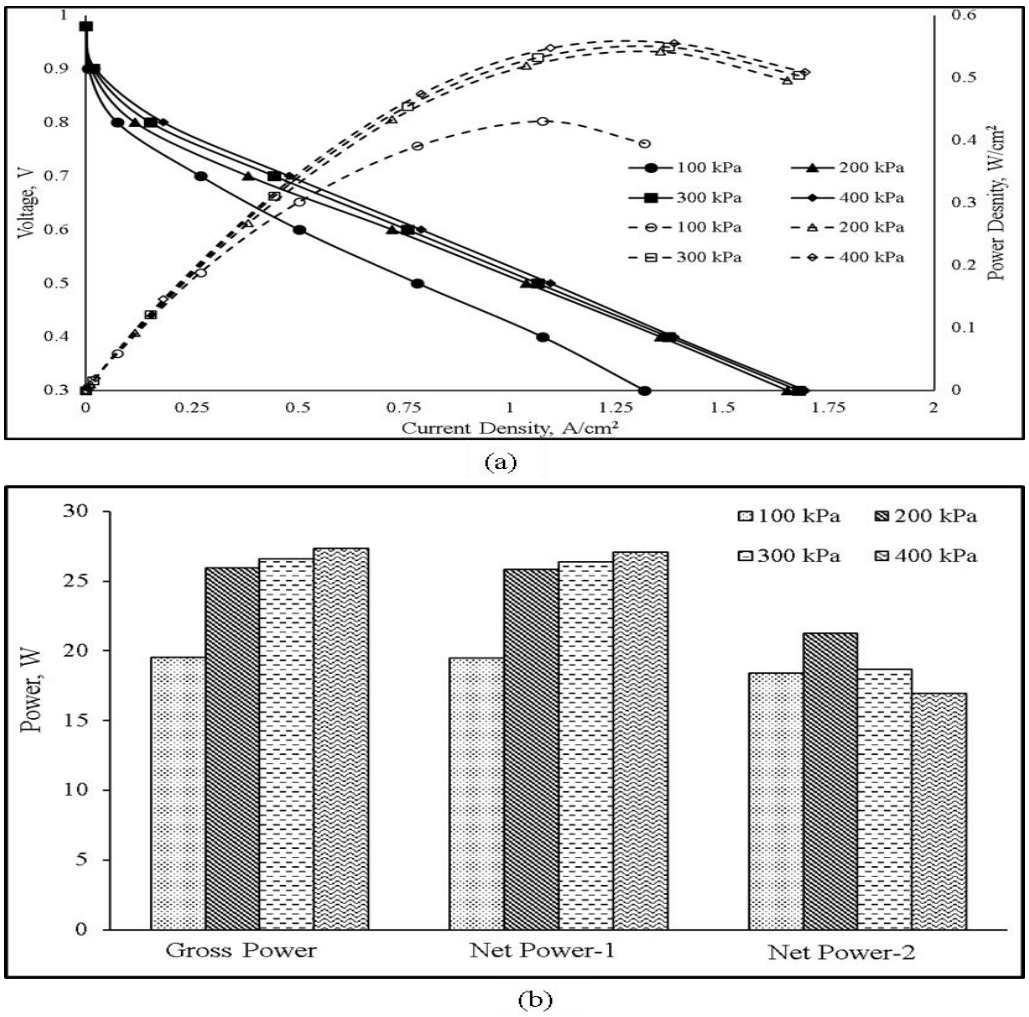

Figure 7.7 Effect of operating pressure on (a) Polarization and Power density plot (b) Gross Power, Net Power-1 (subtracting power losses due to pressure drop in channel from gross power) and Net Power-2 (subtracting compressor power from Net Power-1) at operating voltage of 0.5V.

7.6.4 Effect of Reactant Relative Humidities

The polymer membrane of a PEMFC should always be properly hydrated to facilitate the protons transport from anode to cathode. This can be maintained by sending humidified reactants to the fuel cell. Excessively humidified reactants (on both anode and cathode side) may result in

flooding of the cell, which unfavorably affects the cell performance [95]. In present parametric analysis, asymmetrical RH conditions have been applied by fixing RH_a at one value and varying RH_c at 0 %, 50 %, 80 % and 100 %. RH_a is also varied among 0 %, 50 %, 80 % and 100 %.

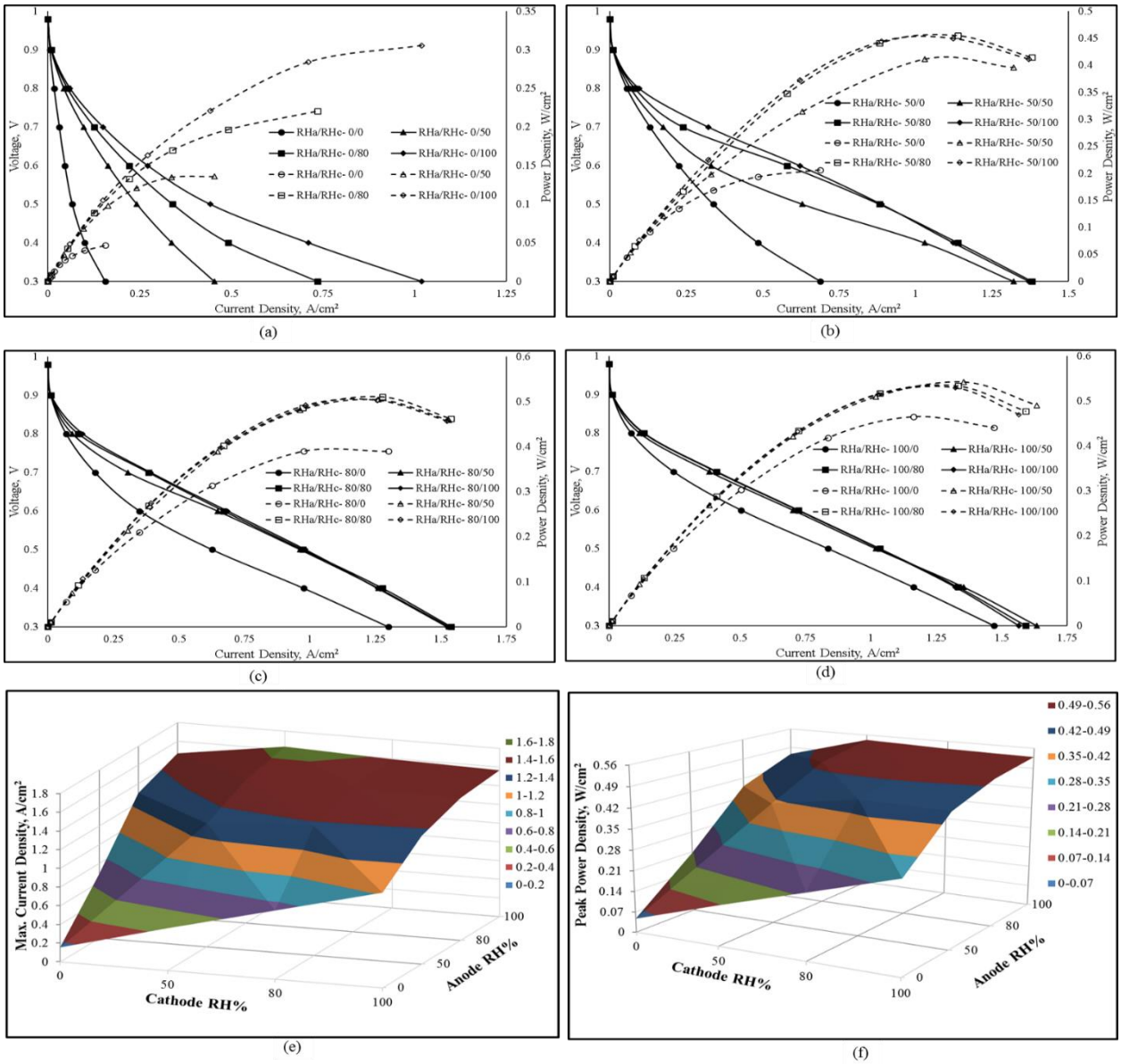

Figure 7.8 Polarization and Power curves at varies cathode Relative humidities (RH) at fixed anode RH (a) RHa-0%, (b) RHa-50%, (c) RHa-80% & (d) RHa-100% and (e) Maximum current density (A/cm^2) & (f) Maximum power density (W/cm^2) generated with increase in anode and cathode RH's.

Figure 7.8 (a to d) show the polarization and power curves of the PEMFC with ECSSFF design on cathode side at various anode side RH (RH_a) and cathode side RH (RH_c) conditions along with the maximum current and power densities (Figure 7.8 (e) & (f)) at 70^oC and 200 kPa. It can be observed from Figure 7.8 (a) that the maximum current density at 0.3 V is increasing with increase in RH_c as higher RH_c increases the membrane hydration, which reduces the ohmic losses, thereby improving the cell performance. Worst performance is observed when both the reactants are fed in dry condition, because of inadequate membrane hydration. With increase in the cathode RH, membrane hydration gets improved due to back diffusion of water to the anode side. Similar trend is observed for RH_a of 50 % and 80 % (Figure 7.8 (b) & (c)), but when RH_a is increased to 100 % (Figure 7.8 (d)), performance increased till RH_c of 50 % and then started decreasing. This behavior is observed mainly due to reduction of the back diffusion of water formed on cathode side to anode side, when fully humidified anode reactants are supplied. So the formed water stays on cathode side and if it is not evacuated properly, it leads to flooding of the CL, GDL and channels, reducing the fuel cell performance. Same conclusion can be drawn from Figures 7.8 (e) & (f), where the maximum current and power densities are plotted against the RH of anode and cathode sides. These densities increased with the increase in anode RH, but when cathode RH is increased, improvement is observed till RH_c of 50 % only, from there the increase in RH_c deteriorated the cell performance. These obtained results support the findings of Wang et. al [79], in which cell operated at RH_a 100 %, RH_c 50 % gave better performance after RH_c of 25 %. Works of Wong et al. [140] and Kahveci & Taymaz [89] also showed that, it is advantageous to use fully humidified anode side reactants with less humidified cathode side reactants for optimum PEM fuel cell performance. So the relative humidities of 50 % on cathode side and 100 % on anode side reactants are used for the further study.

7.7 Evaluation of the ECSSFF design for higher active area square cross-sectional fuel cells

PEM fuel cells are made of different sizes depending on the application and power requirement. So a comparative study of the fuel cell performance at different active areas is essential to find out whether the proposed ECSSFF layout is effective when used for large area

square cross-sectional cells. The active areas considered in the present study are 50 cm^2, 100 cm^2, 150 cm^2 and 200 cm^2 with the cell dimensions as shown in Table 7.2. The best combination of the operating conditions selected from the previous analysis are used in this comparison study.

The power and polarization curves of PEMFCs with different active areas having square ECSSFF channel design are shown in Figure 7.9. It can be observed that the performance (peak power as well as maximum current density) of the PEMFC is decreasing with the increase in active area. This is mainly because of the fact that shorter path lengths of channels in smaller area cells ensure uniform reactant distribution and better water removal, while the lengthy channels in case of large area cells cause uneven reactant distribution and accumulation of water resulting in reduction in the cell performance. Though there is a decrease in the performance for higher active area cells, the % drop in the performance is only 12% for increase in area from 50 cm^2 to its four times i.e., 200 cm^2 as can be observed from Figure 7.9 (b), which shows the variation of power density at 0.5 V with active area. The power density is dropped by 3.9 % when the active area is increased from 50 cm^2 to 100 cm^2 and is further reduced by 4.7% and 5.1%, when the area is increased from 100 to 150 cm^2 and 150 to 200 cm^2 respectively.

It was shown in our recent work [141] that the ECSSFF layout is effective for rectangular cross-sectional PEMFCs with less drop in power density with increase in active area. Figure 7.9 (c) shows a comparison between the effectiveness of ECSSFF layouts for rectangular and square cross-sectional cells at higher active areas. It can be seen that ECSSFF layout for square cross-sectional cells is also effective for higher active areas as the drop in power density is less with increase in area. Hence, the square cross-sectional ECSSFF layout is also an efficient flow field design to be considered for scaling up of the square shaped PEMFCs for large power production.

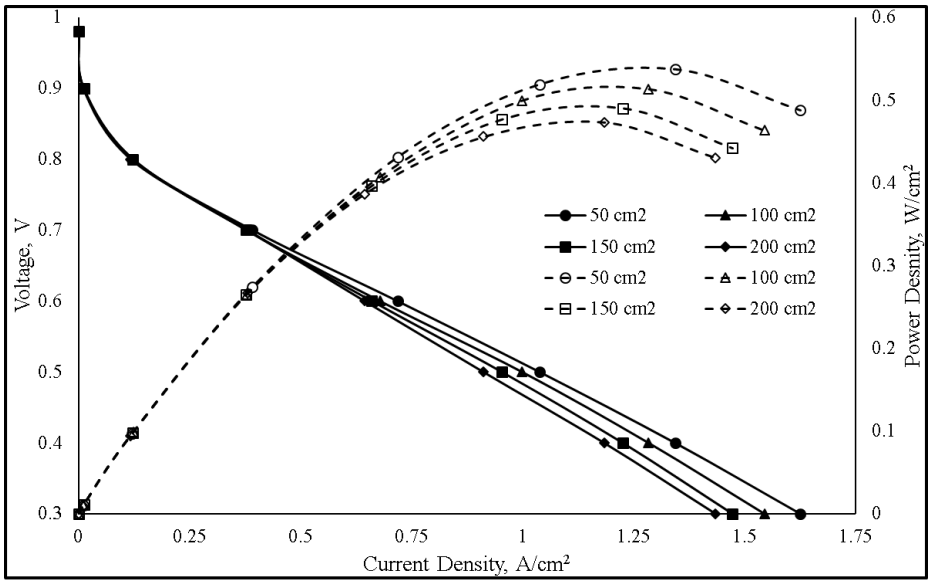

(a)

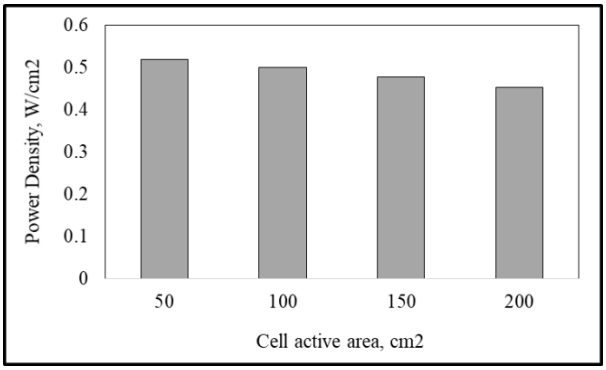

(b)

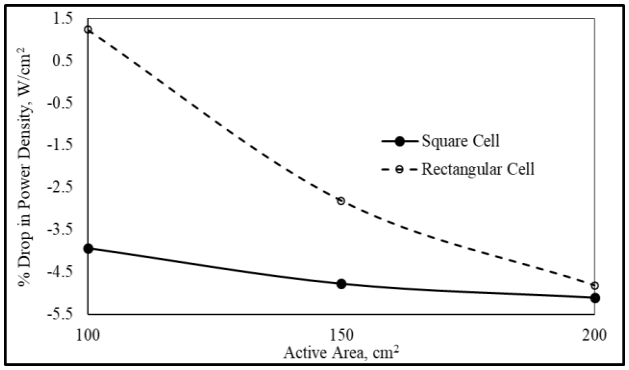

(c)

Figure 7.9 (a) Polarization and Power curves of different active area cells with optimum operating conditions and (b) Variation of power density at 0.5 V with increase in active areas (c) Comparison of drop in power density with increase in area between rectangular and square shaped cells with ECSSFF layout.

7.8 Summary

In the present study, detailed performance analysis of enhanced cross-flow split serpentine flow field layout for square cross-sectional PEM fuel cells was presented using complete 3-D, two phase CFD model. The concept of ECSSFF layout, which was shown to be effective for rectangular cross-sectional PEMFCs was extended to square shaped cells. The square cross-sectional PEMFC with the proposed ECSSFF layout was shown to be performing better than the cell with the 5-path

parallel serpentine flow field. A detailed parametric analysis was presented for the fuel cell with square ECSSFF systematically to find the optimum operating conditions for obtaining the maximum possible performance from the cell. Towards the end, the ECSSFF was also evaluated for higher active areas at the optimum operating conditions. Based on the present computational analysis, the following conclusions can be drawn:

- The optimal ratio of rib width to channel width was found to be 1:1, which displayed maximum performance.

- The asymmetric analysis of stoichiometry showed that, the anode stoichiometry of 1.5 times and cathode stoichiometry of 3 times gave the best performance.

- The optimum operating temperature and pressure were found to be 70 ^{o}C and 200 kPa after considering the power requirement by air compressor.

- The optimum set of relative humidities of the reactants were found to be 100% on anode side and 50% on cathode side.

- The ECSSFF design for square cross-sectional PEMFC was shown to be effective even for higher active areas.

Finally, from the present study, it can be concluded that Square ECSSFF design layout is a potential channel design for square type PEM fuel cell even at higher active areas.

Chapter 8

Overall Conclusions

8. Overall Conclusions

The conclusions drawn from the overall study and the scope for future work are presented in this chapter.

8.1 Overall Conclusions

A detailed performance analysis of enhanced cross-flow split serpentine flow field design for both rectangular and square cross-sectional PEMFCs using a full scale three-dimensional multiphase steady state computational fluid dynamic model was presented in this work. The study was conducted with air and pure hydrogen as reactants by using ECSSFF design on cathode side of the cell because of the sluggish oxygen reduction reaction kinetics and a parallel flow field was used on the anode side of the cell. The performance of rectangular cross-sectional PEMFC with 3-channel ECSSFF was simulated and compared against the performance obtained with single serpentine and parallel triple serpentine flow designs under similar conditions. The performance was evaluated in terms of their polarization curves and pressure drops. The effect of channel and rib width ratio for the flow fields on the cell performance was also studied. A detailed parametric study was also carried out by varying different operating conditions, viz, reactant flow rates, cell operating temperature, pressure and reactant humidities. The effectiveness of the rectangular as well as square cross-sectional ECSSFF designs were evaluated for higher active areas.

The key findings of the whole study presented in the previous chapters are summarized as follows:

- ECSSFF exhibited superior performance over TSFF under all operating conditions because of its inherent layout advantages of enhanced cross-flow in the flooding prone areas of U-bends in serpentine channels and oxygen replenishment in the oxygen lean areas of the cell.

- Parasitic losses are less in case of ECSSFF than TSFF due to less pressure drop, and hence, the net power output is high in the cell using ECSSFF on cathode side.

- The channel width and rib width dimensions of 2 mm and 1 mm for rectangular cross-sectional ECSSFF design is found to display the best cell performance.

- The performance displayed by rectangular ECSSFF design through IV and IP characteristics is on-par with that of SSFF design with almost 30 times lesser pressure drop. If the same pressure drop is maintained across both the flow fields, the fuel cell with ECSSFF does not show concentration polarization and the maximum current density offered is 100% more than that of SSFF.

- Cell temperature of 70 ^{o}C and 200 kPa pressure are found to be the best operating conditions for the cell having rectangular ECSSFF design with 100% humidified reactants.

- ECSSFF design has shown superior performance compared to SSFF by offering lower pressure drop even at high flow rates of the reactants. As less pressure drop increases the life span of the delicate polymer membrane and MEA in a PEM fuel cell, ECSSFF channel design is a better choice over SSFF for building fuel cell stacks.

- The average mass fraction of oxygen in the cathode gas diffusion layer and catalyst layer at higher active areas are higher for the cells with ECSSFF compared to those with TSFF, whereas the water mass fractions in those layers are lower in case of ECSSFF because of the induced cross- flow and better water evacuation capability.

- For all active areas considered in the study, the performance exhibited by the cells with ECSSFF in terms of offering higher current density, lower pressure drop (70% less) as well as higher net power is superior to that exhibited by the cells with TSFF.

- The drop in the net power output with increase in the cell active area in case of rectangular cross-sectional ECSSFF is 55% less compared to that with TSFF.

- The concept of ECSSFF layout developed for rectangular cross-sectional cells is extended to square shaped cells and the square cross-sectional PEMFC with the proposed ECSSFF layout having 4-channels has shown superior performance compared to the cell with the 5-path parallel serpentine flow field.

- The optimal ratio of rib width to channel width is found to be 1:1 for square shaped ECSSFF.

- From the asymmetric analysis of stoichiometry, it is observed that the anode stoichiometry of 1.5 times and cathode stoichiometry of 3 times gives the best performance.

- The optimum set of relative humidities of the reactants are found to be 100% on anode side and 50% on cathode side.

- The ECSSFF design for square cross-sectional PEMFC is shown to be effective even for higher active areas.

The key advantage of the proposed ECSSFF flow layout is the ability to produce higher currents for the same flow rate with lower pressure drop compared to single and parallel serpentine designs. This results in following benefits with respect to economics: (i) For the same cost of the system, fuel cell/stack with ECSSFF design offers higher currents compared to that with other serpentine designs. (ii) To draw the same current, the fuel cell/stack with ECSSFF design offers lower cost compared to that with other serpentine designs and (iii) because of lower pressure drop offered by the cell with ECSSFF, the life span of the delicate membrane increases, which will reduce the overall annual cost of the fuel cell/stack. Due to these advantages, the usage of ECSSFF layout in single or stack PEM fuel cell will be more economical.

This study established that the ECSSFF layout was more beneficial when a PEM fuel cell needs to be operated at higher current densities and was a potential flow field design to be considered for higher active area cells/stacks for large scale power production. The findings suggest that ECSSFF design brings in good improvement in the total net power output from large area cells/stack compared to the parallel serpentine flow field designs.

8.2 Scope for future work

The present work theoretically through extensive computational studies, establishes that ECSSFF channel layout is a promising design for application to PEM fuel cells compared to the respective parallel serpentine designs. However, the present work can be further continued as there is a good scope for future work on the following.

- A detailed experimental study using ECSSFF design on both rectangular and square cross-sectional PEM fuel cells can be conducted to realize the findings of the present work. This will help in understanding the effect of different parameters on the fuel cell performance with proposed channel design. The optimized channel to rib dimensions and other operating conditions can be verified experimentally. These experimental studies will help in finding the best configuration and conditions to run a single PEM fuel cell. The experimental study can also be extended to fuel cell stacks with optimized single cell configuration. Humidification of the reactant gases and maintaining the cell temperature are some of the important issues to be taken care in the experimentation. Uniform distribution of the reactant gases among different cells of the stack is another important issue to be considered. Proper air cooling or water cooling needs to be maintained to control the stack temperature while experimenting with the stacks.

- The ECSSFF layout has been extensively studied for low temperature PEM fuel cell applications in this study. When the PEM fuel cells are operated at high temperatures, the handling of reactants and products is easier as they are in gas phase. Present work has shown that the proposed layout has the ability to distribute the reactants evenly compared to single and/or parallel serpentine layout. So it will be interesting to study theoretically and experimentally PEM fuel cell with ECSSFF layout for high temperature PEM fuel cells. The main issue in the operation of high temperature fuel cells is to raise the temperature of the cell and maintain the temperature at a desired value. Proper thermal management is essential to ensure that the cell temperature is neither too low (which may lead to low cell efficiency) nor too high (which may damage the materials of the stack). The high heat generation rate in high temperature PEM fuel cells, especially at high current densities where it can exceed the total electric power output, poses a challenge to the thermal

management of high temperature fuel cell stacks. This issue needs to be properly taken care while extending the application of ECSSFF design to high temperature cells/stacks.

- Scope also exists for extending the application of ECSSFF design with necessary modifications to redox flow batteries. The reaction chemistries and handling of liquid electrolytes have to be handled carefully in redox flow batteries.

List of Publications based on the Thesis

International Journal Papers

1. Abdulla S, Patnaikuni VS, Detailed analysis of polymer electrolyte membrane fuel cell with enhanced cross-flow split serpentine flow field design. *International Journal of Energy Research*. 2019; 43: 2806–2820. https://doi.org/10.1002/er.4368.

2. Abdulla S, Patnaikuni VS, Performance evaluation of Enhanced Cross flow Split Serpentine Flow Field design for higher active area PEM fuel cells, *International Journal of Hydrogen Energy*. 2020; 45: 25970-25984. https://doi.org/10.1016/j.ijhydene.2020.01.199.

3. Abdulla S, Patnaikuni VS, Performance Comparison of PEM Fuel Cell with Enhanced Cross-Flow Split Serpentine and Single Serpentine Flow Field Designs, *Arabian Journal for Science and Engineering*, 2020; 45: 7691-7703. https://doi.org/10.1007/s13369-020-04803-0 .

4. Abdulla S, Patnaikuni VS, Parametric study of Enhanced Cross-Flow Split Serpentine Flow Field design in a square type polymer electrolyte membrane fuel cell, *Renewable Energy* (Under Review).

International Conference Papers

1. Abdulla Sheikh and P. V. Suresh, Performance analysis of PEM Fuel cell with Enhanced Cross-flow Split Serpentine Flow Field, 5th International Hydrogen and Fuel Cell Conference (IHFC - 2016), 11-13 December 2016 at Hyderabad.

2. Abdulla Sheikh and P. V. Suresh, Superiority of Enhanced Cross-Flow Split Serpentine Flow Field Design over Triple Serpentine Flow Field Design in PEM Fuel Cell, International Conference on Membrane Technology and its Applications (Mem Sep-2017), 21 – 23 February 2017 at National Institute of Technology, Tiruchirappalli.

3. Abdulla Sheikh, Venkata Suresh Patnaikuni and Murali Mohan Seepana, Superiority of Enhanced Cross-Flow Split Serpentine Flow Field Design over Four Serpentine Flow Field Design in PEM Fuel Cell, First International Conference on Energy and Environment: Global Challenges (ICEE-2018), 9 – 10 March 2018 at National Institute of Technology, Calicut.

4. Abdulla Sheikh and Venkata Suresh Patnaikuni, Performance Analysis of PEM Fuel Cell with ECSSFF design at Different Operating Conditions, International Conference on Advances and Challenges for Sustainable Ecosystems (ICACSE-2018), 6 – 8 December 2018 at National Institute of Technology, Tiruchirappalli.

5. Abdulla Sheikh and Venkata Suresh Patnaikuni, Performance Evaluation of Enhanced Cross-Flow Split Serpentine Flow Field Design for Large Area PEM Fuel Cells, 2nd International Conference on New Frontiers in Chemical, Energy and Environmental Engineering (INCEEE-2019) 15 – 16 February 2019 at National Institute of Technology, Warangal.

6. Abdulla Sheikh and Venkata Suresh Patnaikuni, Effect of reactants humidity on the performance of polymer electrode membrane fuel cell with enhanced cross-flow split serpentine flow field and triple serpentine flow field design, 11th International Exergy, Energy and Environment symposium (IEEES-11), 14 - 18 July 2019 at SRM Institute of Science & Technology, Chennai.

References

[1] UN DESA. World Population Prospects 2019: Highlights | Multimedia Library - United Nations Department of Economic and Social Affairs. United Nations 2019.

[2] Outlook BPE. BP Energy Outlook – 2019 Insights from the Evolving transition scenario – India India ' s share of total global primary energy demand is set to BP Energy Outlook – 2019 Insights from the Evolving transition scenario – India 2019.

[3] Ge SW and M. Everything You Need to Know About the Fastest-Growing Source of Global Emissions: Transport | World Resources Institute 2019. https://www.wri.org/blog/2019/10/everything-you-need-know-about-fastest-growing-source-global-emissions-transport (accessed April 12, 2020).

[4] History of Fuel Cells n.d. http://www.fuelcell.co.uk/history-of-fuel-cells/ (accessed September 25, 2020).

[5] Fuel Cell History - Fuel Cell Today n.d. http://www.fuelcelltoday.com/history (accessed November 17, 2019).

[6] Fuel Cells | Hydrogen n.d. https://hydrogeneurope.eu/fuel-cells (accessed October 2, 2020).

[7] Liu H, Li P, Juarez-Robles D, Wang K, Hernandez-Guerrero A. Experimental study and comparison of various designs of gas flow fields to PEM fuel cells and cell stack performance. Front Energy Res 2014;2:1–8. https://doi.org/10.3389/fenrg.2014.00002.

[8] Polarization Curves n.d. https://www.fuelcellstore.com/blog-section/polarization-curves (accessed July 3, 2020).

[9] DOE Technical Targets for Polymer Electrolyte Membrane Fuel Cell Components | Department of Energy n.d. https://www.energy.gov/eere/fuelcells/doe-technical-targets-polymer-electrolyte-membrane-fuel-cell-components (accessed April 12, 2020).

[10] Alaswad A, Baroutaji A, Achour H, Carton J, Al Makky A, Olabi AG. Developments in fuel cell technologies in the transport sector. Int J Hydrogen Energy 2016;41:16499–508.

https://doi.org/10.1016/j.ijhydene.2016.03.164.

[11] Woodman AS, Anderson EB, Jayne KD, Kimble MC. Development of corrosion-resistant coatings for fuel cell bipolar plates. Proc AESF SUR/FIN Annu Tech Conf 1999;6:21–4.

[12] Randrianarizafy B, Schott P, Chandesris M, Gerard M, Bultel Y. Design optimization of rib/channel patterns in a PEMFC through performance heterogeneities modelling. Int J Hydrogen Energy 2018;43:8907–26. https://doi.org/10.1016/j.ijhydene.2018.03.036.

[13] Arvay A, French J, Wang JC, Peng XH, Kannan AM. Nature inspired flow field designs for proton exchange membrane fuel cell. Int J Hydrogen Energy 2013;38:3717–26. https://doi.org/10.1016/j.ijhydene.2012.12.149.

[14] Akbari MH, Rismanchi B. Numerical investigation of flow field configuration and contact resistance for PEM fuel cell performance. Renew Energy 2008. https://doi.org/10.1016/j.renene.2007.10.009.

[15] Tiss F, Chouikh R, Guizani A. A numerical investigation of the effects of membrane swelling in polymer electrolyte fuel cells. Energy Convers Manag 2013;67:318–24. https://doi.org/10.1016/j.enconman.2012.12.006.

[16] Vazifeshenas Y, Sedighi K, Shakeri M. Numerical investigation of a novel compound flow-field for PEMFC performance improvement. Int J Hydrogen Energy 2015;40:15032–9. https://doi.org/10.1016/j.ijhydene.2015.08.077.

[17] Carcadea E, Varlam M, Ingham DB, Ismail MS, Patularu L, Marinoiu A, et al. The effects of cathode flow channel size and operating conditions on PEM fuel performance: A CFD modelling study and experimental demonstration. Int J Energy Res 2018;42:1–16. https://doi.org/10.1002/er.4068.

[18] Grigoriev SA, Kalinnikov AA, Kuleshov NV, Millet P. Numerical optimization of bipolar plates and gas diffusion electrodes for PBI-based PEM fuel cells. Int J Hydrogen Energy 2013;38:8557–67. https://doi.org/10.1016/j.ijhydene.2012.12.021.

[19] Tirnovan R, Giurgea S. Efficiency improvement of a PEMFC power source by optimization of the air management. Int J Hydrogen Energy 2012;37:7745–56.

https://doi.org/10.1016/j.ijhydene.2012.02.029.

[20] Rostami L, Mohamad Gholy Nejad P, Vatani A. A numerical investigation of serpentine flow channel with different bend sizes in polymer electrolyte membrane fuel cells. Energy 2016;97:400–10. https://doi.org/10.1016/j.energy.2015.10.132.

[21] Masuda H, Ito K, Oshima T, Sasaki K. Comparison between numerical simulation and visualization experiment on water behavior in single straight flow channel polymer electrolyte fuel cells. J Power Sources 2008;177:303–13. https://doi.org/10.1016/j.jpowsour.2007.11.069.

[22] Pei P, Chen H. Main factors affecting the lifetime of Proton Exchange Membrane fuel cells in vehicle applications: A review. Appl Energy 2014;125:60–75. https://doi.org/10.1016/j.apenergy.2014.03.048.

[23] Kerkoub Y, Benzaoui A, Haddad F, Ziari YK. Channel to rib width ratio influence with various flow field designs on performance of PEM fuel cell. Energy Convers Manag 2018;174:260–75. https://doi.org/10.1016/j.enconman.2018.08.041.

[24] Ghanbarian A, Kermani MJ, Scholta J, Abdollahzadeh M. Polymer electrolyte membrane fuel cell flow field design criteria – Application to parallel serpentine flow patterns. Energy Convers Manag 2018;166:281–96. https://doi.org/10.1016/j.enconman.2018.04.018.

[25] Wang C, Zhang Q, Shen S, Yan X, Zhu F, Cheng X, et al. The respective effect of under-rib convection and pressure drop of flow fields on the performance of PEM fuel cells. Sci Rep 2017;7:1–9. https://doi.org/10.1038/srep43447.

[26] Chowdhury MZ, Genc O, Toros S. Numerical optimization of channel to land width ratio for PEM fuel cell. Int J Hydrogen Energy 2018;43:10798–809. https://doi.org/10.1016/j.ijhydene.2017.12.149.

[27] Zeng X, Ge Y, Shen J, Zeng L, Liu Z, Liu W. The optimization of channels for a proton exchange membrane fuel cell applying genetic algorithm. Int J Heat Mass Transf 2017;105:81–9. https://doi.org/10.1016/j.ijheatmasstransfer.2016.09.068.

[28] Cooper NJ, Santamaria AD, Becton MK, Park JW. Investigation of the performance improvement in decreasing aspect ratio interdigitated flow field PEMFCs. Energy Convers Manag 2017;136:307–17. https://doi.org/10.1016/j.enconman.2017.01.005.

[29] Manso AP, Marzo FF, Barranco J, Garikano X, Garmendia Mujika M. Influence of geometric parameters of the flow fields on the performance of a PEM fuel cell. A review. Int J Hydrogen Energy 2012;37:15256–87. https://doi.org/10.1016/j.ijhydene.2012.07.076.

[30] Ferng YM, Su A. A three-dimensional full-cell CFD model used to investigate the effects of different flow channel designs on PEMFC performance. Int J Hydrogen Energy 2007;32:4466–76. https://doi.org/10.1016/j.ijhydene.2007.05.012.

[31] Henriques T, César B, Branco PJC. Increasing the efficiency of a portable PEM fuel cell by altering the cathode channel geometry: A numerical and experimental study. Appl Energy 2010;87:1400–9. https://doi.org/10.1016/j.apenergy.2009.09.001.

[32] Khazaee I, Ghazikhani M. Experimental Characterization and Correlation of a Triangular Channel Geometry PEM Fuel Cell at Different Operating Conditions. Arab J Sci Eng 2013;38:2521–31. https://doi.org/10.1007/s13369-013-0605-2.

[33] Wan Z, Quan W, Yang C, Yan H, Chen X, Huang T, et al. Optimal design of a novel M-like channel in bipolar plates of proton exchange membrane fuel cell based on minimum entropy generation. Energy Convers Manag 2020;205:112386. https://doi.org/10.1016/j.enconman.2019.112386.

[34] Kuo JK, Yen TH, Chen CK. Three-dimensional numerical analysis of PEM fuel cells with straight and wave-like gas flow fields channels. J Power Sources 2008;177:96–103. https://doi.org/10.1016/j.jpowsour.2007.11.065.

[35] Roshandel R, Arbabi F, Moghaddam GK. Simulation of an innovative flow-field design based on a bio inspired pattern for PEM fuel cells. Renew Energy 2012;41:86–95. https://doi.org/10.1016/j.renene.2011.10.008.

[36] Badduri SR, Srinivasulu GN, Rao SS. Influence of bio-inspired flow channel designs on the performance of a PEM fuel cell. Chinese J Chem Eng 2019.

https://doi.org/10.1016/j.cjche.2019.07.010.

[37] Tamerabet M, Hocine BM, Youcef S, Abdallah M. Unsteady three-dimensional numerical study of mass transfer in PEM fuel cell with spiral flow field. Int J Hydrogen Energy 2017;42:1237–51. https://doi.org/10.1016/j.ijhydene.2016.12.084.

[38] Atyabi SA, Afshari E. Three-dimensional multiphase model of proton exchange membrane fuel cell with honeycomb flow field at the cathode side. J Clean Prod 2019;214:738–48. https://doi.org/10.1016/j.jclepro.2018.12.293.

[39] Zhang C, Chen Y, Wu R, Shi M. Flow boiling in constructal tree-shaped minichannel network. Int J Heat Mass Transf 2011;54:202–9. https://doi.org/10.1016/j.ijheatmasstransfer.2010.09.051.

[40] Dong-Hui W, Lin-Zhi Y, Zhong-Yu P, Cong-Da L, Gang L, Qiao-Hui L. A novel intersectant flow field of metal bipolar plate for proton exchange membrane fuel cell. Int J Energy Res 2017;41:2184–93. https://doi.org/10.1002/er.3779.

[41] Damian-Ascencio CE, Saldaña-Robles A, Hernandez-Guerrero A, Cano-Andrade S. Numerical modeling of a proton exchange membrane fuel cell with tree-like flow field channels based on an entropy generation analysis. Energy 2017;133:306–16. https://doi.org/10.1016/j.energy.2017.05.139.

[42] Kang HC, Jum KM, Sohn YJ. Performance of unit PEM fuel cells with a leaf-vein-simulating flow field-patterned bipolar plate. Int J Hydrogen Energy 2019;44:24036–42. https://doi.org/10.1016/j.ijhydene.2019.07.120.

[43] El-Dosoky M, Ahmed M, Ashgriz N. Numerical simulation of condensate removal from gas channels of PEM fuel cells using corrugated walls. Int J Energy Res 2018;42:1664–76. https://doi.org/10.1002/er.3962.

[44] Zehtabiyan-Rezaie N, Arefian A, Kermani MJ, Noughabi AK, Abdollahzadeh M. Effect of flow field with converging and diverging channels on proton exchange membrane fuel cell performance. Energy Convers Manag 2017;152:31–44. https://doi.org/10.1016/j.enconman.2017.09.009.

[45] Xing L, Cai Q, Liu X, Liu C, Scott K, Yan Y. Anode partial flooding modelling of proton exchange membrane fuel cells: Optimisation of electrode properties and channel geometries. Chem Eng Sci 2016;146:88–103. https://doi.org/10.1016/j.ces.2016.02.029.

[46] Wang Y, Yue L, Wang S. New design of a cathode flow-field with a sub-channel to improve the polymer electrolyte membrane fuel cell performance. J Power Sources 2017;344:32–8. https://doi.org/10.1016/j.jpowsour.2017.01.075.

[47] Fan L, Niu Z, Zhang G, Jiao K. Optimization design of the cathode flow channel for proton exchange membrane fuel cells. Energy Convers Manag 2018;171:1813–21. https://doi.org/10.1016/j.enconman.2018.06.111.

[48] Dehsara M, Kermani MJ. Proton exchange membrane fuel cells performance enhancement using bipolar channel indentation. J Mech Sci Technol 2014;28:365–76. https://doi.org/10.1007/s12206-013-0983-0.

[49] Wang X, Qin Y, Wu S, Shangguan X, Zhang J, Yin Y. Numerical and experimental investigation of baffle plate arrangement on proton exchange membrane fuel cell performance. J Power Sources 2020;457:228034. https://doi.org/10.1016/j.jpowsour.2020.228034.

[50] Heidary H, Kermani MJ, Prasad AK, Advani SG, Dabir B. Numerical modelling of in-line and staggered blockages in parallel flowfield channels of PEM fuel cells. Int J Hydrogen Energy 2016;41:6885–93. https://doi.org/10.1016/j.ijhydene.2016.10.076.

[51] Perng SW, Wu HW. A three-dimensional numerical investigation of trapezoid baffles effect on non-isothermal reactant transport and cell net power in a PEMFC. Appl Energy 2015;143:81–95. https://doi.org/10.1016/j.apenergy.2014.12.059.

[52] Heidary H, Abbassi A, Kermani MJ. Enhanced heat transfer with corrugated flow channel in anode side of direct methanol fuel cells. Energy Convers Manag 2013;75:748–60. https://doi.org/10.1016/j.enconman.2013.08.040.

[53] Thitakamol V, Therdthianwong A, Therdthianwong S. Mid-baffle interdigitated flow fields for proton exchange membrane fuel cells. Int J Hydrogen Energy 2011;36:3614–22.

https://doi.org/10.1016/j.ijhydene.2010.12.060.

[54] Choi KS, Kim HM, Moon SM. Numerical studies on the geometrical characterization of serpentine flow-field for efficient PEMFC. Int J Hydrogen Energy 2011;36:1613–27. https://doi.org/10.1016/j.ijhydene.2010.10.073.

[55] Lim BH, Majlan EH, Daud WRW, Husaini T, Rosli MI. Effects of flow field design on water management and reactant distribution in PEMFC: A review. Ionics (Kiel) 2016;22:301–16. https://doi.org/10.1007/s11581-016-1644-y.

[56] Taccani R, Zuliani N. Effect of flow field design on performances of high temperature PEM fuel cells: Experimental analysis. Int J Hydrogen Energy 2011;36:10282–7. https://doi.org/10.1016/j.ijhydene.2010.10.026.

[57] Liu H, Li P, Juarez-robles D, Wang K, Hernandez-guerrero A. Experimental study and comparison of various designs of gas flow fields to PEM fuel cells and cell stack performance 2014;2:1–8. https://doi.org/10.3389/fenrg.2014.00002.

[58] Wang XD, Duan YY, Yan WM, Peng XF. Local transport phenomena and cell performance of PEM fuel cells with various serpentine flow field designs. J Power Sources 2008;175:397–407. https://doi.org/10.1016/j.jpowsour.2007.09.009.

[59] khazaee I, Sabadbafan H. Effect of humidity content and direction of the flow of reactant gases on water management in the 4-serpentine and 1-serpentine flow channel in a PEM (proton exchange membrane) fuel cell. Energy 2016;101:252–65. https://doi.org/10.1016/j.energy.2016.02.026.

[60] Kang DG, Shin DK, Kim S, Kim MS. Experimental study on the performance improvement of polymer electrolyte membrane fuel cell with dual air supply. Renew Energy 2019;141:669–77. https://doi.org/10.1016/j.renene.2019.04.029.

[61] Alizadeh E, Rahimi-Esbo M, Rahgoshay SM, Saadat SHM, Khorshidian M. Numerical and experimental investigation of cascade type serpentine flow field of reactant gases for improving performance of PEM fuel cell. Int J Hydrogen Energy 2017;42:14708–24. https://doi.org/10.1016/j.ijhydene.2017.04.212.

[62] Baz FB, Ookawara S, Ahmed M. Enhancing under-rib mass transport in proton exchange membrane fuel cells using new serpentine flow field designs. Int J Hydrogen Energy 2019;44:30644–62. https://doi.org/10.1016/j.ijhydene.2018.11.147.

[63] Han SH, Choi NH, Choi YD. Performance and flow characteristics of large-sized PEM fuel cell having branch channel. Int J Hydrogen Energy 2015;40:4819–29. https://doi.org/10.1016/j.ijhydene.2015.01.039.

[64] Li W, Zhang Q, Wang C, Yan X, Shen S, Xia G, et al. Experimental and numerical analysis of a three-dimensional flow field for PEMFCs. Appl Energy 2017;195:278–88. https://doi.org/10.1016/j.apenergy.2017.03.008.

[65] Limjeerajarus N, Santiprasertkul T. Novel hybrid serpentine-interdigitated flow field with multi-inlets and outlets of gas flow channels for PEFC applications. Int J Hydrogen Energy 2020;45:13601–11. https://doi.org/10.1016/j.ijhydene.2018.12.160.

[66] Rahimi-Esbo M, Ranjbar AA, Ramiar A, Alizadeh E, Aghaee M. Improving PEM fuel cell performance and effective water removal by using a novel gas flow field. Int J Hydrogen Energy 2016;41:3023–37. https://doi.org/10.1016/j.ijhydene.2015.11.001.

[67] Sreenivas J, Abhijit PD, Prathap H PV. Fuel cell with enhanced cross-flow serpentine flow fields. Indian Patent No: 301913, 2018.

[68] Suresh P V., Jayanti S, Deshpande AP, Haridoss P. An improved serpentine flow field with enhanced cross-flow for fuel cell applications. Int J Hydrogen Energy 2011;36:6067–72. https://doi.org/10.1016/j.ijhydene.2011.01.147.

[69] Arun Saco S, Thundil Karuppa Raj R, Karthikeyan P. A study on scaled up proton exchange membrane fuel cell with various flow channels for optimizing power output by effective water management using numerical technique. Energy 2016;113:558–73. https://doi.org/10.1016/j.energy.2016.07.079.

[70] Chowdhury MZ, Timurkutluk B. Transport phenomena of convergent and divergent serpentine flow fields for PEMFC. Energy 2018;161:104–17. https://doi.org/10.1016/j.energy.2018.07.143.

[71] Martins Belchor P, Camargo Forte MM, Ortiz Suman Carpenter DE. Parallel serpentine-baffle flow field design for water management in a proton exchange membrane fuel cell. Int J Hydrogen Energy 2012;37:11904–11. https://doi.org/10.1016/j.ijhydene.2012.05.091.

[72] Karthikeyan P, Vasanth RJ, Muthukumar M. Experimental investigation on uniform and zigzag positioned porous inserts on the rib surface of cathode flow channel for performance enhancement in PEMFC. Int J Hydrogen Energy 2015;40:4641–8. https://doi.org/10.1016/j.ijhydene.2015.01.175.

[73] Ebrahimzadeh AA, Khazaee I, Fasihfar A. Experimental and numerical investigation of obstacle effect on the performance of PEM fuel cell. Int J Heat Mass Transf 2019;141:891–904. https://doi.org/10.1016/j.ijheatmasstransfer.2019.07.034.

[74] Patnaikuni VS. An Improved flow field - gas diffusion layer architecture for enhanced cross-flow in PEM fuel cell applications. Indian Institute of Technology, Madras, India., 2011.

[75] Hsing IM, Futerko P. Two-dimensional simulation of water transport in polymer electrolyte fuel cells. Chem Eng Sci 2000;55:4209–18. https://doi.org/10.1016/S0009-2509(00)00066-X.

[76] Kim YB. Study on the effect of humidity and stoichiometry on the water saturation of PEM fuel cells. Int J Energy Res 2012;36:509–22. https://doi.org/10.1002/er.1845.

[77] Xing L, Cai Q, Xu C, Liu C, Scott K, Yan Y. Numerical study of the effect of relative humidity and stoichiometric flow ratio on PEM (proton exchange membrane) fuel cell performance with various channel lengths: An anode partial flooding modelling. Energy 2016;106:631–45. https://doi.org/10.1016/j.energy.2016.03.105.

[78] Zhang Z, Jia L, Wang X, Ba L. Effects of inlet humidification on PEM fuel cell dynamic behaviors. Int J Energy Res 2011;35:376–88. https://doi.org/10.1002/er.1692.

[79] Wang Y, Wang S, Liu S, Li H, Zhu K. Optimization of reactants relative humidity for high performance of polymer electrolyte membrane fuel cells with co-flow and counter-flow configurations. Energy Convers Manag 2020;205:112369.

https://doi.org/10.1016/j.enconman.2019.112369.

[80] Kim KH, Lee KY, Lee SY, Cho E, Lim TH, Kim HJ, et al. The effects of relative humidity on the performances of PEMFC MEAs with various Nafion® ionomer contents. Int J Hydrogen Energy 2010;35:13104–10. https://doi.org/10.1016/j.ijhydene.2010.04.082.

[81] Iranzo A, Boillat P, Biesdorf J, Salva A. Investigation of the liquid water distributions in a 50 cm2 PEM fuel cell: Effects of reactants relative humidity, current density, and cathode stoichiometry. Energy 2015;82:914–21. https://doi.org/10.1016/j.energy.2015.01.101.

[82] Neyerlin KC, Gasteiger HA, Mittelsteadt CK, Jorne J, Gu W. Effect of Relative Humidity on Oxygen Reduction Kinetics in a PEMFC 2005. https://doi.org/10.1149/1.1897368.

[83] Wang X-D, Duan Y-Y, Yan W-M, Weng F-B. Effect of humidity of reactants on the cell performance of PEM fuel cells with parallel and interdigitated flow field designs. J Power Sources 2008;176:247–58. https://doi.org/10.1016/j.jpowsour.2007.10.065.

[84] Kulikovsky AA. Quasi-3D Modeling of Water Transport in Polymer Electrolyte Fuel Cells. J Electrochem Soc 2003;150:A1432. https://doi.org/10.1149/1.1611489.

[85] Lee CI, Chu H Sen. Effects of cathode humidification on the gas-liquid interface location in a PEM fuel cell. J Power Sources 2006;161:949–56. https://doi.org/10.1016/j.jpowsour.2006.05.012.

[86] Hu M, Zhu X, Wang M, Gu A, Yu L. Three dimensional, two phase flow mathematical model for PEM fuel cell: Part II. Analysis and discussion of the internal transport mechanisms. Energy Convers Manag 2004;45:1883–916. https://doi.org/10.1016/j.enconman.2003.09.023.

[87] Jang JH, Yan WM, Li HY, Chou YC. Humidity of reactant fuel on the cell performance of PEM fuel cell with baffle-blocked flow field designs. J Power Sources 2006;159:468–77. https://doi.org/10.1016/j.jpowsour.2005.07.096.

[88] Kahveci EE, Taymaz I. Effect of Humidification of the Reactant Gases in the Proton Exchange Membrane Fuel Cell. J Clean Energy Technol 2015;3:356–9. https://doi.org/10.7763/jocet.2015.v3.223.

[89] Kahveci EE, Taymaz I. Assessment of single-serpentine PEM fuel cell model developed by computational fluid dynamics. Fuel 2018;217:51–8. https://doi.org/10.1016/j.fuel.2017.12.073.

[90] Sun H, Zhang G, Guo LJ, Dehua S, Liu H. Effects of humidification temperatures on local current characteristics in a PEM fuel cell. J Power Sources 2007;168:400–7. https://doi.org/10.1016/j.jpowsour.2007.03.022.

[91] Chen C-C, Shaw D, Hsueh K-L. Optimization of the electrodes humidification temperature and clamping pressure to achieve uniform current density in a commercial-sized proton exchange membrane fuel cell. Int J Hydrogen Energy 2017;42:3185–96. https://doi.org/10.1016/j.ijhydene.2016.09.178.

[92] Zhang D, Cai Q, Gu S. Three-dimensional lattice-Boltzmann model for liquid water transport and oxygen diffusion in cathode of polymer electrolyte membrane fuel cell with electrochemical reaction. Electrochim Acta 2018;262:282–96. https://doi.org/10.1016/j.electacta.2017.12.189.

[93] Molaeimanesh GR, Shojaeefard MH, Moqaddari MR. Effects of electrode compression on the water droplet removal from proton exchange membrane fuel cells. Korean J Chem Eng 2019;36:136–45. https://doi.org/10.1007/s11814-018-0157-y.

[94] Suresh P V., Jayanti S. Peclet number analysis of cross-flow in porous gas diffusion layer of polymer electrolyte membrane fuel cell (PEMFC). Environ Sci Pollut Res 2016;23:20120–30. https://doi.org/10.1007/s11356-016-6629-x.

[95] Ozen DN, Timurkutluk B, Altinisik K. Effects of operation temperature and reactant gas humidity levels on performance of PEM fuel cells. Renew Sustain Energy Rev 2016;59:1298–306. https://doi.org/10.1016/j.rser.2016.01.040.

[96] Song C, Tang Y, Zhang JL, Zhang J, Wang H, Shen J, et al. PEM fuel cell reaction kinetics in the temperature range of 23-120 °C. Electrochim Acta 2007;52:2552–61. https://doi.org/10.1016/j.electacta.2006.09.008.

[97] Coppo M, Siegel NP, Spakovsky MR vo. On the influence of temperature on PEM fuel

cell operation. J Power Sources 2006;159:560–9. https://doi.org/10.1016/j.jpowsour.2005.09.069.

[98] Santarelli MG, Torchio MF. Experimental analysis of the effects of the operating variables on the performance of a single PEMFC. Energy Convers Manag 2007;48:40–51. https://doi.org/10.1016/j.enconman.2006.05.013.

[99] Yan Q, Toghiani H, Causey H. Steady state and dynamic performance of proton exchange membrane fuel cells (PEMFCs) under various operating conditions and load changes. J Power Sources 2006;161:492–502. https://doi.org/10.1016/j.jpowsour.2006.03.077.

[100] Li Y, Zhou Z, Liu X, Wu WT. Modeling of PEM fuel cell with thin MEA under low humidity operating condition. Appl Energy 2019;242:1513–27. https://doi.org/10.1016/j.apenergy.2019.03.189.

[101] Zhang J, Li H, Shi Z, Zhang J. Effects of hardware design and operation conditions on PEM fuel cell water flooding. Int J Green Energy 2010;7:461–74. https://doi.org/10.1080/15435075.2010.515185.

[102] Khazaee I, Ghazikhani M. Numerical Simulation and Experimental Comparison of Channel Geometry on Performance of a PEM Fuel Cell. Arab J Sci Eng 2012;37:2297–309. https://doi.org/10.1007/s13369-012-0312-4.

[103] Wang XD, Yan WM, Duan YY, Weng FB, Jung G Bin, Lee CY. Numerical study on channel size effect for proton exchange membrane fuel cell with serpentine flow field. Energy Convers Manag 2010;51:959–68. https://doi.org/10.1016/j.enconman.2009.11.037.

[104] Morin A, Xu F, Gebel G, Diat O. Influence of PEMFC gas flow configuration on performance and water distribution studied by SANS: Evidence of the effect of gravity. Int J Hydrogen Energy 2011;36:3096–109. https://doi.org/10.1016/j.ijhydene.2010.11.070.

[105] Yuan W, Tang Y, Pan M, Li Z, Tang B. Model prediction of effects of operating parameters on proton exchange membrane fuel cell performance. Renew Energy 2010;35:656–66. https://doi.org/10.1016/j.renene.2009.08.017.

[106] Benmouiza K, Cheknane A. Analysis of proton exchange membrane fuel cells voltage

drops for different operating parameters. Int J Hydrogen Energy 2018;43:3512–9. https://doi.org/10.1016/j.ijhydene.2017.06.082.

[107] Wang L, Husar A, Zhou T, Liu H. A parametric study of PEM fuel cell performances. Int J Hydrogen Energy 2003;28:1263–72. https://doi.org/10.1016/S0360-3199(02)00284-7.

[108] Awan A, Saleem M, Basit A. Simulation of Proton Exchange Membrane Fuel Cell by using ANSYS Fluent. IOP Conf Ser Mater Sci Eng 2018;414:012045. https://doi.org/10.1088/1757-899X/414/1/012045.

[109] Han I, Park S, Chung C. Modeling and operation optimization of a proton exchange membrane fuel cell system for maximum efficiency. Energy Convers Manag 2016;113:52–65. https://doi.org/10.1016/j.enconman.2016.01.045.

[110] Shimpalee S, Greenway S, Van Zee JW. The impact of channel path length on PEMFC flow-field design. J Power Sources 2006;160:398–406. https://doi.org/10.1016/j.jpowsour.2006.01.099.

[111] Wang XD, Zhang XX, Yan WM, Lee DJ, Su A. Determination of the optimal active area for proton exchange membrane fuel cells with parallel, interdigitated or serpentine designs. Int J Hydrogen Energy 2009;34:3823–32. https://doi.org/10.1016/j.ijhydene.2008.12.049.

[112] Li X, Sabir I, Park J. A flow channel design procedure for PEM fuel cells with effective water removal. J Power Sources 2007;163:933–42. https://doi.org/10.1016/j.jpowsour.2006.10.015.

[113] Shimpalee S, Greenway S, Spuckler D, Van Zee JW. Predicting water and current distributions in a commercial-size PEMFC. J Power Sources 2004;135:79–87. https://doi.org/10.1016/j.jpowsour.2004.03.059.

[114] Li X, Sabir I. Review of bipolar plates in PEM fuel cells: Flow-field designs. Int J Hydrogen Energy 2005;30:359–71. https://doi.org/10.1016/j.ijhydene.2004.09.019.

[115] Um S, Wang C-Y, Chen KS. Computational Fluid Dynamics Modeling of Proton Exchange Membrane Fuel Cells. J Electrochem Soc 2000;147:4485. https://doi.org/10.1149/1.1394090.

[116] Bockris JO, Reddy AKN G-AM. Modern Electrochemistry 2A. Kluwer Academic Publishers; 2002. https://doi.org/10.1007/b113922.

[117] Springer TE, Zawodzinski TA, Gottesfeld S. Polymer Electrolyte Fuel Cell Model. J Electrochem Soc 1991;138:2334–42. https://doi.org/10.1149/1.2085971.

[118] Soc JE, The A, Society E, Springer TE, Zawodzinski TA, Gottesfeld S. Polymer Electrolyte Fuel Cell Model 1993;138:2334–42.

[119] Versteeg HK, Malalasekera W, Orsi G, Ferziger JH, Date AW, Anderson JD. An Introduction to Computational Fluid Dynamics - The Finite Volume Method. Pearson education; 1995. https://doi.org/10.2514/1.22547.

[120] Sierra JM, Moreira J, Sebastian PJ. Numerical analysis of the effect of different gas feeding modes in a proton exchange membrane fuel cell with serpentine flow-field. J Power Sources 2011;196:5070–6. https://doi.org/10.1016/j.jpowsour.2011.01.079.

[121] Iranzo A, Muñoz M, Rosa F, Pino J. Numerical model for the performance prediction of a PEM fuel cell. Model results and experimental validation. Int J Hydrogen Energy 2010;35:11533–50. https://doi.org/10.1016/j.ijhydene.2010.04.129.

[122] Ansys Inc. ANSYS Fluent Fuel Cell Modules Manual, Release 15.0 2013;15317:2019.

[123] Limjeerajarus N, Charoen-amornkitt P. Effect of different flow field designs and number of channels on performance of a small PEFC. Int J Hydrogen Energy 2015;40:7144–58. https://doi.org/10.1016/j.ijhydene.2015.04.007.

[124] Arvay A, Ahmed A, Peng XH, Kannan AM. Convergence criteria establishment for 3D simulation of proton exchange membrane fuel cell. Int J Hydrogen Energy 2012;37:2482–9. https://doi.org/10.1016/j.ijhydene.2011.11.005.

[125] Iranzo A, Muñoz M, Pino J, Rosa F. Update on numerical model for the performance prediction of a PEM Fuel Cell. Int J Hydrogen Energy 2011. https://doi.org/10.1016/j.ijhydene.2011.04.102.

[126] Limjeerajarus N, Charoen-Amornkitt P. Effect of different flow field designs and number of channels on performance of a small PEFC. Int J Hydrogen Energy 2015;40:7144–58.

https://doi.org/10.1016/j.ijhydene.2015.04.007.

[127] Han IS, Park SK, Chung CB. Modeling and operation optimization of a proton exchange membrane fuel cell system for maximum efficiency. Energy Convers Manag 2016;113:52–65. https://doi.org/10.1016/j.enconman.2016.01.045.

[128] Takalloo PK, Nia ES, Ghazikhani M. Numerical and experimental investigation on effects of inlet humidity and fuel flow rate and oxidant on the performance on polymer fuel cell. Energy Convers Manag 2016;114:290–302. https://doi.org/10.1016/j.enconman.2016.01.075.

[129] Badduri SR, Srinivasulu GN, Rao SS. Experimental analysis of PEM fuel cell performance using lung channel design bipolar plate. Int J Green Energy 2019;16:1591–601. https://doi.org/10.1080/15435075.2019.1677238.

[130] ZHONG Z, CHEN J, PENG R. Design and Performance Analysis of Micro Proton Exchange Membrane Fuel Cells. Chinese J Chem Eng 2009;17:298–303. https://doi.org/10.1016/S1004-9541(08)60208-6.

[131] Zhang J, Tang Y, Song C, Xia Z, Li H, Wang H, et al. PEM fuel cell relative humidity (RH) and its effect on performance at high temperatures. Electrochim Acta 2008;53:5315–21. https://doi.org/10.1016/j.electacta.2008.02.074.

[132] Zinko T, Pianko-Oprych P, Jaworski Z. Three-dimensional computational fluid dynamics modelling of a proton exchange membrane fuel cell with a serpentine micro-channel design. Chem Process Eng - Inz Chem i Proces 2018;39:143–54. https://doi.org/10.24425/119105.

[133] Ozden E, Tari I. Proton exchange membrane fuel cell degradation: A parametric analysis using Computational Fluid Dynamics. J Power Sources 2016;304:64–73. https://doi.org/10.1016/j.jpowsour.2015.11.042.

[134] Liu X, Guo H, Ye F, Ma CF. Flow dynamic characteristics in flow field of proton exchange membrane fuel cells. Int J Hydrogen Energy 2008;33:1040–51. https://doi.org/10.1016/j.ijhydene.2007.11.018.

[135] Karthikeyan P, Velmurugan P, George AJ, Ram Kumar R, Vasanth RJ. Experimental investigation on scaling and stacking up of proton exchange membrane fuel cells. Int J Hydrogen Energy 2014;39:11186–95. https://doi.org/10.1016/j.ijhydene.2014.05.086.

[136] Kazim A, Forges P, Liu HT. Effects of cathode operating conditions on performance of a PEM fuel cell with interdigitated flow fields. Int J Energy Res 2003;27:401–14. https://doi.org/10.1002/er.884.

[137] Iranzo A, Salva JA. Effect of Anode/Cathode Operating Pressures on the Liquid Water Content and Performance of a PEM Fuel Cell. Fuel Cells 2018;18:742–7. https://doi.org/10.1002/fuce.201800076.

[138] Abdollahzadeh M, Pascoa JC, Ranjbar AA, Esmaili Q. Analysis of PEM (Polymer Electrolyte Membrane) fuel cell cathode two-dimensional modeling. Energy 2014;68:478–94. https://doi.org/10.1016/j.energy.2014.01.075.

[139] Zhao P, Wang J, Gao L, Dai Y. Parametric analysis of a hybrid power system using organic Rankine cycle to recover waste heat from proton exchange membrane fuel cell. Int J Hydrogen Energy 2012;37:3382–91. https://doi.org/10.1016/j.ijhydene.2011.11.081.

[140] Wong KH, Loo KH, Lai YM, Tan SC, Tse CK. A theoretical study of inlet relative humidity control in PEM fuel cell. Int J Hydrogen Energy 2011;36:11871–85. https://doi.org/10.1016/j.ijhydene.2011.06.017.

[141] Abdulla S, Patnaikuni VS. Performance evaluation of Enhanced Cross flow Split Serpentine Flow Field design for higher active area PEM fuel cells. Int J Hydrogen Energy 2020:1–15. https://doi.org/10.1016/j.ijhydene.2020.01.199.

Resume

Name: **Abdulla Sheikh**

Gender: Male

Nationality: Indian

Academic profile:

Pursuing **Ph.D** (Department of Chemical Engineering) form National Institute of Technology, Warangal, Telangana, India.

M.Tech: Energy Engineering from National Institute of Technology, Tiruchirappalli, Tamil Nadu, India, (2014).

B.Tech: Chemical Engineering from Andhra University, Visakhapatnam, Andhra Pradesh, India, (2011).

Awards and Honors:

- Represented school in Short-put at zonal games in IXth class.
- Stood school first in Xth class.
- Placement Coordinator for my department during M-Tech.
- Secured best paper for our work titled," Superiority of Enhanced Cross-Flow Split Serpentine Flow Field Design over Triple Serpentine Flow Field Design in PEM Fuel Cell", International Conference on Membrane Technology and its Applications (Mem Sep-2017), February 21st - 23rd , 2017 National Institute of Technology, Tiruchirappalli.